Doctoral school of the University of Torino

PhD programme in Chemical and Materials Sciences XXXV cycle

Optimization of charge strategies and *post-mortem* characterization of Li ion cells for automotive applications

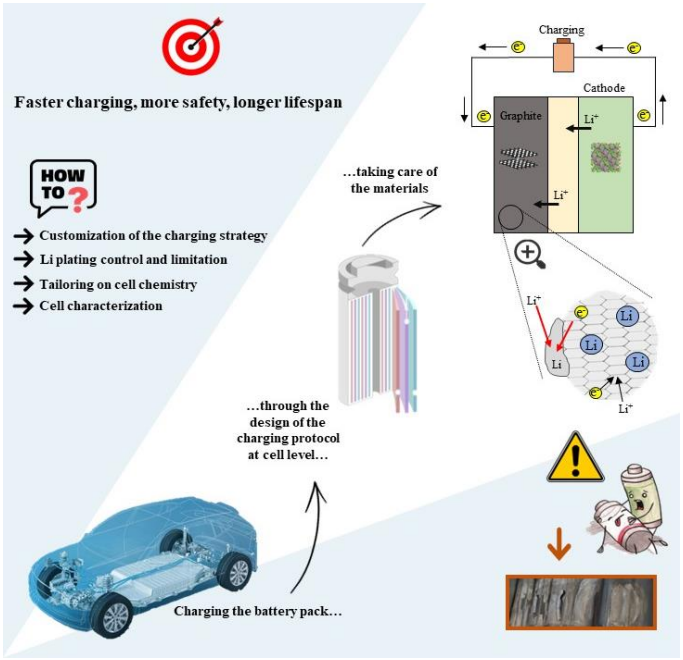

Matteo DOTOLI

Academic supervisor: Prof. Carlo Nervi;

Industrial supervisor: Mauro Francesco Sgroi, PhD

Doctoral school of the University of Torino

PhD programme in Chemical and Materials Sciences XXXV cycle

Optimization of charge strategies and *post-mortem* characterization of Li ion cells for automotive applications

Candidate: **Matteo Dotoli**

Academic supervisor: **Prof. Carlo Nervi**

Industrial supervisor: **Mauro Francesco Sgroi, PhD**

Jury members: **Prof. Silvia Bodoardo**

Politecnico di Torino

Dipartimento Scienza Applicata e Tecnologia (DISAT)

Martin Petit, PhD

IFP, Energies Nouvelles – Direction Physico-chimie et Mécanique appliquées

Prof. Marcello Baricco

Università degli Studi di Torino

Department of Chemistry

Head of the Doctoral School: **Prof. Alberto Rizzuti**

PhD Programme Coordinator: **Prof. Bartolomeo Civalleri**

Summary

List of Figures

Preface

This dissertation entitled “Optimization of charge strategies and post-mortem characterization of Li ion cells for automotive applications” has been submitted to the Doctoral School of the University of Torino to fulfil the requirements for obtaining the PhD degree in Chemical and Material Science. The results presented in this dissertation were obtained in the last 3 years as a PhD student of the XXXV cycle (from November 2019 to January 2023) working within a collaboration between Centro Ricerche Fiat S.c.P.A, under the supervision of Mauro Francesco Sgroi, PhD and the Department of Chemistry and NIS centre at the University of Turin, under the supervision of Prof. Carlo Nervi.

PhD courses, schools, seminars, workshops, and conferences attended, publications, oral presentation presented during these 3 years are reported in a short bullet point overview.

Chapter 1 first introduces the automotive context and the aim of the work, closely related to the optimization of charging strategies. **Chapter 2** develops some basic knowledge on the field of energy storage and the market needs, with some basic information about the electrochemistry to understand Li ion cells. Inputs about the most common trend about R&D on materials are provided. **Chapter 3** summaries information about the aging of Li ion cells and **Chapter 4** gives input about the methodologies commonly used to characterise batteries. In **Chapter 5** the *ante-mortem* analysis is showed, to keep information about the cell sample used for all the activities. **Chapter 6** describes the results coming from the implementation of two different methods to setup a DCFC strategy for charging the cells. **In Chapter 7** the results obtained from the electrical characterization performed after the cycle aging campaign on the samples, together with a deep *post-mortem* analysis represents a big portion of the activity. **Conclusions and outlook** summarised the main findings and provide inputs for the future.

List of activities

Papers

- Dotoli, M.; Milo, E.; Giuliano, M.; Rocca, R.; Nervi, C.; Baricco, M.; Ercole, M.; Sgroi, M.F. Detection of Lithium Plating in Li-Ion Cell Anodes Using Realistic Automotive Fast-Charge Profiles. Batteries 2021, 7, 46. https://doi.org/10.3390/batteries7030046.
- M. F. Sgroi, M. Dotoli, M. Giuliano, G. Nicol, F. Parussa and R. Rocca, "Smart batteries: requirements of the automotive world," 2021 IEEE International Workshop on Metrology for Automotive (MetroAutomotive), 2021, pp. 42-47, doi:10.1109/MetroAutomotive50197.2021.9502851.
- Ahniyaza, I. de Meatza, A. Kvasha, O. Garcia-Calvo, I. Ahmed, M. Francesco Sgroi, M. Giuliano, M. Dotoli, M.A. Dumitrescu, M. Jahn, N. Zhang, “Progress in solid-state high voltage lithium-ion battery electrolytes”, Advances in Applied Energy, Volume 4, 2021, 100070, ISSN 2666-7924, https://doi.org/10.1016/j.adapen.2021.100070.
- Dotoli, M.; Rocca, R.; Giuliano, M.; Nicol, G.; Parussa, F.; Baricco, M.; Ferrari, A.M.; Nervi, C.; Sgroi, M.F. A Review of Mechanical and Chemical Sensors for Automotive Li-Ion Battery Systems. Sensors 2022, 22, 1763. https://doi.org/10.3390/s22051763.
- Dotoli, M., Rocca, R., Giuliano, M., Sgroi, M. et al., “Physical-Chemical Characterization of Cycle Aged Commercial Cells of Automotive Interest,” SAE Technical Paper 2022-01-0276, 2022, doi:10.4271/2022-01-0276.
- Dotoli, M.; Milo, E.; Giuliano, M.; Tiozzo, A.; Baricco, M.; Nervi, C.; Ercole, M.; Sgroi, M.F. Development of an Innovative Procedure for Lithium Plating Limitation and Characterization of 18650 Cycle Aged Cells for DCFC Automotive Applications. Batteries 2022, 8, 88. https://doi.org/10.3390/batteries8080088.
- Ferrarotti, A.; Ghiggini, E.V.; Rocca, R.; Dotoli, M.; Scaglione, F.; Errigo, C.; Marchiaro, G.; Baricco, M. Simulation of Corrosion Phenomena in Automotive

Components: A Case Study. Materials 2023, 16, 5368. https://doi.org/10.3390/ma16155368

- Arianna Tiozzo, Matteo Dotoli, Georgia Kastrinaki , Marcello Baricco, Emmanouil Daskalos , Mattia Giuliano, George Karagiannakis, Carlo Nervi, Giovanna Nicol, Dimitrios Zarvalis, Mauro Sgroi, DCFC strategies for automotive Li-ion cells: non disruptive electrochemical analysis and post-mortem Raman characterization (submitted to TRA conference 2024).

Projects participation

- H2020 Spider
- H2020 Si-Drive
- H2020 Teesmat
- H2020 Solidify
- H2020 Magenta
- H2020 Upgrade

Talks

- Annual Metallurgy Group Lab. Meeting, Italy, Vaie (TO),
- IWES 2021 - First Italian workshop on energy storage (26 February 2021)
- Seminar at Unito (July 2021)
- 2nd year PhD presentations, Turin, University of Turin, Department of Chemistry, Italy (September 2021)

PhD Courses and Schools Attended

- "Optimization and computation of thermodynamic proprieties and phase diagrams", Marcello Baricco, University of Turin, Department of Chemistry.
- "Vitreous state", Livio Battezzati, University of Turin, Department of Chemistry.
- Solid State NMR: Basics and applications", Roberto Gobetto, Michele Remo Chierotti, University of Turin, Department of Chemistry.
- "Electrochemical energy storage and conversion systems", Mauro Sgroi, University of Turin, Department of Chemistry.
- "Engine Exhaust After-treatment Systems", Mauro Sgroi, University of Turin, Department of Chemistry.
- "Introduction to Scientific programming (in Python)", Alessandro Erba, University of Turin, Department of Chemistry.
- "Raman Day", University of Turin, Department of Chemistry.
- Machine Learning Meets Chemistry, (Torino, Italia), 17/02/2019 (14.30-17:30) -18/02 (9:30-13).
- "English for scientific academic purpose, J. Robinson (University of Turin)
- ENGINE2021 (Grenoble, France), 15-19/02/2021 - Online mode
- Crystallography School 2021 (Torino, Italia), 21/06-9/07/2021 - Online mode
- Inomat Winter School 15-18 december 2021
- TEESMAT H2020 Eu Project final meeting (4th July) + A new approach to efficient battery characterization event (5th July) at Grenoble (FR).

Seminars

- "Le Batterie Per Veicoli Elettrici (Ed Altri Mezzi Di Trasporto): Produzione, Uso, Invecchiamento, Durata, Riutilizzo, Riciclo", Torino 26/11/2019 (Energy Center – Fondazione Telios)

- “Workshop sulla ricerca bibliografica – 2019”, Polo di scienze della natura (Torino, 27/11 – 3/12/2019) – 8 ore
- Lithium-ion cells: components and production, Battery 2030+ (30/03/2021)
- IWES 2021 - First Italian workshop on energy storage, 24-26/02/2021
- Young scientist event, 1st June 2022 (Battery 2030+ event at Politecnico di Torino)

1 - The automotive company perspective and the goal of the work

Chapter 1 contains the introduction to the project with some links to the e-mobility market trends. The context is introduced and the main goals of the project are presented at the end of the chapter.

1.1 Introduction

This project born to answer to an applied research problem. Since in 2019, when the project started, most of the automotive players were used to consider the core element composing the battery pack (Li ion cell) as a "buy" product, it was important to gain knowledge about the products purchased by the suppliers.

Within this framework this PhD project was developed in collaboration between a research entity (Centro Ricerche Fiat S.c.P.A) and the engineering department of the former FCA company (now Stellantis), both part of same corporate.

In fact, nowadays LIBS are produced by a relatively small number of players, all over the world. Big historical companies, such as Samsung, LG, CATL, Panasonic, together with newborn players as Northvolt and ACC are moving in a growing market, offering solutions for answering to the automotive demand, which for sure will cover a very high percentage of the needs, in terms of MWh stored.

Market guidelines are today set on the production of the so-called Gen3 cells[1], generally composed by a liquid organic electrolyte, graphite anode (sometimes blended with little amount of silicon) and metal oxides as cathodes, where the choice in this case is strongly guided by the application of the cell. It is in fact common to find cells with LFP (lithium iron phosphate) cathodes where the cost is limited (i.e. city cars or stationary applications), on the contrary NMC/NCA (nickel, manganese and cobalt in the first case; nickel, cobalt and aluminium in the

second) cathodes are more widespread where the cost and requirements of the application grows. One example could be the sizing of a premium car battery pack.
If high energy density is required, LFP must be excluded in favour of NMC811 (~150 Wh/Kg vs ~200-250 Wh/Kg), which means a lighter vehicle with higher range autonomy.
On the contrary, if safety is the driving force, for sure LFP guarantees an easier risk management than NMC based cells.

1.2 Cell formats and requirements

From the cell format point of view, if limited to the Gen3 state of the art cells, the market offers three types of Li ion cells formats, as reported by the Fraunhofer institute[2] :

- Cylindrical (18650, 21700 etc. their design and stability are easily scalable for mass production),
- Pouch (their main feature lies in their lightweight thanks to their safety barrier envelope),
- Prismatic (characterized by their packaging capacity thanks to their configuration by stacked "layers")

Usually, the automotive player needs to properly define the kind of cell for the appropriate application. Since the e-mobility trend is facing a sudden change, fleets are now mainly composed by internal combustion engine (ICE) vehicles, hybrid (MHEV, PHEV, HEV) and full electric (BEV) vehicles. If from one side ICE vehicles will disappear within 15-20 years, hybrid and full electric ones will dominate the scene for the next decades. It is then crucial to properly design the battery pack, to satisfy the specific need. Talking about hybrid cars, it is in fact common to use high-power cells, which must deliver energy very quickly, often as support for the ICE acceleration and for guaranteeing small kilometres ranges, with no need of very long-range demand. On the opposite side, full electric vehicles need to be designed to have long range autonomy, so they are often equipped with high-energy cells. Table 1 below shows the main features of high power and high energy cells.

Table 1 – High energy vs High power cells

Component	High-energy cell (HE)	High-power cell (HP)
Electrodes	Thick (high mass loading), low porosity, low amount of conductive carbon and medium/large particle size	Thin (low mass loading), high porosity, high amount of conductive carbon and small/medium particle size
Current collector	Thin and coated (adhesion increase)	Thick and coated (contact resistance reduction)
Separator	Thin	
Electrolyte	High safety	High safety and conductivity

1.3 The automotive industry perspective

Since usually automotive companies are not Li ion cell producers, except for some examples (i.e. Tesla), they need to buy Li ion cells as a product, after the definition of specifications.

As already mentioned, recently the biggest players in this field are actively trying to create joint ventures or associated companies (Verkor for Renault, PowerCo for Volkswagen, ACC for Stellantis, Mercedes and Total etc.) to push and have more control over the core product of the future fleets, the Li ion cell itself. The building up of the so-called gigafactories will probably be the game changer, permitting to OEMs to customise the product to be mounted on their battery packs according to the desired specification, also reducing costs.

From what seen from the automotive industry perspective, today this is a tough task to be pursuit. Often the choice of the cell is done by purchasing already existing products from

companies such as LG, Samsung, Panasonic etc, with product not perfectly designed for a specific vehicle or platform.

In this framework it is crucial to play with the boundary conditions where the battery cell must be used, by considering it as a sort of “black box”.

The present work operates in this context, with the aim of optimizing the cycle life and the performance of one kind Gen3 Li ion cell, chosen by Stellantis for one specific vehicle of the fleet.

1.4 The aim of the work

First, within a deep collaboration among departments inside the company (Engineering, R&D, Material labs), it was decided to divide the whole activity into three main phases:

1) Identification of the cell, according to format and specification;
2) Electrical and physical-chemical characterization of the selected Li ion cell;
3) Cycle aging at different discharging, DoD% and Temperature conditions (at module level);
4) Focus on the charging step: tuning of the charging profile, cycle aging and post-mortem characterization (at cell level).

If the first points were fundamental to collect preliminary information about the system used, the third provided precious hints to better define operative voltage limitations to enhance performances, exercise temperature etc.

Given that, the last point, which represents the core of this PhD work, was deeply focused on the optimization strategy to charge the battery pack limiting the degradation mechanisms occurring inside the Li ion cell during the operations.

In order to reach in this aim it was decided to concentrate on the charging step design. Two parallel activities were conducted. From one side, an extensive cycle aging campaign where the charging step was considered as a constant, was performed. For this activity the focus was on temperature, DoD% and discharging profile, which were varied to age cells in different conditions. This activity, which was not the core of this PhD project, provided useful

information. All the testing campaign was performed with modules composed by five cells in parallel.

To step forward, the core of the present work was instead focused on the attempt of proposing alternative charging profiles, to optimize the charging time but preserving the health of the cell. As previously mentioned, since most of the automotive companies often do not build their Li ion cells it is crucial to optimize the life cycle of the product, to guarantee safety and long-term life for the client. Within this framework, it was decided to maintain DoD%, T and discharging profiles as constants, varying only the charging strategy.

This chapter presented an overview about the e-mobility market, with focus on the cell as a product to be studied in deep. The main objectives of this PhD project are presented, taking care of:

- Safety improvement (tailor of the charging step);
- Time profit (push on high C rate within the admitted limits);
- Long term life improvement.

All the activity developed on the charging step was performed at the cell level.

2. Fundamentals of lithium energy storage systems[3,4]

Chapter 2 contains general information about Li ion battery cells, starting from a high-level analysis of the topic, going to some technical aspects useful to understand which are the fundamental elements inside a cell and which are the concepts behind a battery cell.
Some information related to the most diffused materials for state-of-the-art and next-gen cells are briefly described with hints on theoretical aspects, to let the reader some background information that can be dig deeper in literature. The chapter ended with the presentation of a roadmap, to visualize the technological trends for the next years.

2.1 Context and introduction

New renewable sources are always more and more studied and developed, trying to slow the rise of greenhouse gases and pollutants in the atmosphere.
During the past in fact, fossil fuels have represented a fundamental energy source for humans' daily life. Oil dominated the energy market for decades, with tremendous risks for the climate and consequent global warming effects. Among the applications, private and public transports, which play a predominant part in this game, were strongly linked to oil demand.
Indeed, nowadays fossil fuels-based transportation suffer from several tremendous issues, e.g., CO_2 emissions increase, but also non-renewable resources depletion and unstable demand for oil. It is then necessary to drastically find alternative energy sources. During the last years, lots of efforts have been made to give people more consciousness about preserving the environment. If from one side there is the absolute need to shift towards green solutions, from the other we are still facing some critical points.

1. Energy availability is today limited worldwide, for emerging countries.
2. Renewable energy sources compete with oil and coal from the cost and availability point of view.

Recently, governments are pushing with a promise to reach carbon neutrality by 2050, going towards "green" renewable energy sources. It is then necessary to drastically find alternative energy systems. The replacement of the Internal Combustion Engine (ICE) with Electric, Hybrid Electric and Plug-in Hybrid Electric Vehicles (EVs, HEVs. and PHEVs) seems to track the route towards a sustainable mobility[5,6].

Among them, wind and solar energies are the most widespread. Unfortunately, they suffer from intrinsic instability, strongly depending on the climate conditions, rather than the positioning where they are located on the planet.

It is then important to store the produced energy into the so-called grid energy storage devices. Market in this field is rapidly growing, with an expected 33% annual growth until 2030, to reach almost 5 TWh, according to McKingsey & company[7].

In a wide panorama with new emerging energy storage approaches[8–11] to guide the ecological transition, lithium-ion batteries are considered among the most promising and mature technologies for large-scale applications[12], with an increasing interest coming from the main players in the automotive field, together with numerous other applications (micro mobility, stationary grids, etc.).

Lithium-ion cells, showing significant energy (150-200 Wh/Kg) and power (300-1500 W/Kg) density, along with affordable durability, cover a key role to trace this route[13,14].

Given the well-established compromise between technology readiness and maturity, cost, and performances, Li ion batteries seem to be the best choice for scaling up the e-mobility market.

Carmakers are always more and more pushed by governments to switch their fleets from Internal Combustion Engines (ICEs) to hybrid and electric powertrains, with strict deadlines[15,16] and tough carbon neutrality targets by 2050.

In this framework Europe is moving, trying to force the building up of several Gigafactories, widespread all over the countries, with Germany, France, England, and Scandinavian countries to lead the European battery taskforce to become independent from the Asian market. From an organizational perspective, the last decades have seen the birth of well-established organizations such as BEPA (Batteries European Partnership Association), EERA (European

Energy Research Alliance), EBA (European battery alliance) etc. These associations work into a European framework, trying to lead the reinforcement of Europe in the Li-ion battery production field, promoting innovation, funding and collaboration among members to succeed in becoming a competitive with respect to extra European markets.

Within this framework it is fundamental to increase the production of the "state of the art" Li ion cells, together with pushing the efforts into the research field, optimizing the product from several points of view.

Looking the topic from the most "demanding client" point of view, it is worth noticing that nowadays, the use of an electric vehicle is still strongly limited by high costs for the purchase of an electric vehicle and the increase of the energy price are still limiting the growth of e-vehicles around Europe.

Together with this, "range anxiety"[17] can also affects the widespread of e-mobility. The drivers' main concern is related to the kilometric range of the vehicle, limited by the usable energy of batteries if compared to those using fossil fuels, and to the charging time, significantly higher than the time required for refuelling. These limitations limited the usability of the vehicle, forcing people to change the paradigm of car transportations, transforming the way of travelling for long trips.

Shortening the charge time will mitigate the current limiting factor on the time consumed for the charging of LIBs, enlarging the widespread use of battery electric vehicles (BEVs).

Since the range autonomy is closely linked to the cell chemistry, which defines the energy density, the specific energy, and the total price of the battery system, it is fundamental to research innovative materials able to store higher quantities of energy, also having a close look at safety concerns.

The power density is then influenced not only by the chemistry, but other factors such as manufacturing parameters (anodic thickness, porosity, anode/cathode mass loading ratio) highly influence the power capability of the cell. In this context, many efforts have been made for the development of innovative materials for Li-ion batteries[18], including cathodes for high operating voltage[19] and high-capacity anodes[20].

One of the predominant themes in this field is linked to the improvement of the cell performances. The goal is to try to reach higher and higher power and energy densities, with longer lifetime also. It is well known that even the normal usage of the cell promotes degradation mechanisms inside the active materials, with loss in performance and durability.

The degradation mechanisms, occurring both in cycling and calendar aging conditions[21], can influence active (anode and cathode) and non-active (electrolyte, binder, separator, current collectors, etc.) components of the Li-ion battery cell.

Because of this, physical-chemical degradation, structural integrity loss, and electrolyte chemical decomposition can occur.

The optimization of the cell chemistry, along with factors related to manufacturing variables, are not sufficient to properly take advantage of a specific cell. To optimize the cycle life, it is necessary to tailor the charging step, while also optimizing the fast-charging procedure, which is essential for the everyday usage of a battery. This kind of optimization is for sure not easy and for each kind of cell a specific protocol must be developed. One of the main topics the researchers are dealing with is related to the implementation of optimized fast charging profiles, to decrease charging time and to limit the cell degradation, maintaining performance and reducing the capacity fade[22]. An optimized fast charge profile can help to decrease the charging time, without degrading the cell performance and reducing the cycle life. One of the main reasons for battery capacity fade is linked to the lithium plating phenomenon. This work investigates two methodologies, i.e., three-electrode cell measurement and internal resistance evolution during charging, for detecting the lithium plating conditions. From this preliminary analysis, it was possible to develop new Multi-Stage Constant-Current profiles, designed to improve the performance in terms of charging time and cells capacity retention with respect to a reference profile. Five new profiles, equivalent in terms of energy throughput, were tested and compared to a double step reference charging profile. The results coming from the new profiles demonstrate an improvement in terms of charging time and/or cycling life, showing the reliability of the implemented methodology in preventing/limiting lithium plating[23]. An overall study on the aging of the tested materials were also provided.

2.2 Li ion batteries, basic information and fundamentals[4,24,25]

Rechargeable lithium-ion batteries (LIBs) are systems based on reversible electrochemical reactions, able to transform chemical energy into usable electrical energy, and vice versa by storing it.

"State-of-the-art" Li-ion batteries are used in portable electronics, e-mobility applications, and energy storage systems. Respect with other storage technologies they have several advantages, including high energy density (up to 300 Wh kg^{-1} at the cell level, compared to 20 ÷ 40 Wh kg^{-1} for lead-acid batteries which still dominate the market of rechargeable batteries), long cycle life, low self-discharge, and low maintenance.

Some of the key developments in Li-ion batteries include:

- Anode materials: researchers are focused on improving the anodic capacity and stability, with a shift from graphite towards silicon or lithium metal anodes.
- Cathode materials: Li-ion batteries with high nickel content cathodes, such as NMC (Nickel, Cobalt, Manganese), are becoming more and more popular, due to their high energy density.
- Electrolytes: based on lithium salts dissolved in flammable organic solvents, for example in diethyl carbonate (DEC) or carbonate mixtures. The trend is going towards improved electrolytes to enhance safety and stability, as well as increase the operating temperature range.
- Form factors: Li-ion batteries are also being developed in flexible and foldable form factors to enable new applications.
- Recycling and sustainability: efforts are being made to improve the sustainability and recyclability of Li-ion batteries, reducing their environmental impact and increasing their economic viability.

Coming back to the traditional LIBS, they have a structure composed of three main layers:

- Cathode (it provides the Li ions during the charge);

- Electrolyte (it usually can be liquid or solid, if liquid it impregnates the separator and permits the ion exchange between the electrodes);
- Anode (it provides the Li ions during the discharge).

As visible in Figure 1, during the charging phase Li ions migrate from the cathode (de-intercalation) to the anode structure (intercalation), passing through the electrolyte which acts as a bridge for the ions, creating an internal circuit. To avoid short circuits inside the cell, it is necessary to use a membrane, known as a separator, to electrically isolate anode and cathode. Meanwhile, looking at the external circuit, during the charging step, electrons pass from the cathode to the anode with the help of a power source. Here electricity is converted into chemical energy, stored inside the electrochemical cell, available to be used as required.

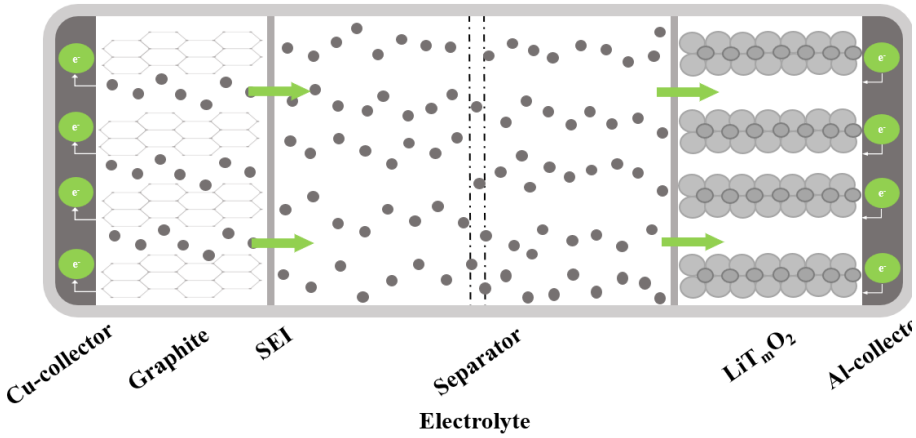

Figure 1 - Intercalation/deintercalation process on a Li ion cell

Currently Li-ion batteries suffer from some limitations. Main concerns are related to safety, which worsen when fast charging is applied (because of the heat generation and Li plating) and to the relatively limited abundance of the so-called critical raw materials distribution which composes the cell. It is expected they will soon become critical or source of dramatic price fluctuations (e.g., cobalt and lithium).

2.3 Basic concepts of electrochemistry for batteries

When designing a Li ion cell, the coupling of the electrode materials is usually made by taking into consideration two key properties, listed here:

- Theoretical capacity (Q):

$$Q = xF/M_{Whost}$$

Where F is the Faraday constant and $M_{w\ host}$ is the molecular mass of the hosting material (1 g of material is taken into consideration).

- Redox potential:

$$Ox + xe^- + xLi^+ \rightarrow Red$$

$$xLi \rightarrow xLi^+ + xe^-$$

$$Ox + xLi \rightarrow Red$$

$$E^0\ vs\ Li^+/Li = \frac{-\Delta G}{nF}$$

Where E_0 is the redox standard potential and G is Gibbs free energy.

These two properties were usually displayed by the help of the so-called Ragone Plot (Figure 2), which correlates the redox potential (vs Li^+/Li) in function of the theoretical capacity, of the materials[26]. This instrument represents a very common tool to combine electropositive (cathodes) and electronegative (anodes) materials. The coupling of these materials creates the so-called electromotive force ΔE^0, usually known as "Li ion cell voltage", often known as open circuit voltage, (OCV). The final goal to ensure a cell with desired performances is to push ΔE, which means a wider working range for the cell. To do this, it is important to find anodic materials that work with a low operative voltage, cathodic materials that work with high operative voltage as well as electrolytes with a proper electrochemical stability. Together with this, it is also fundamental to research materials able to deliver high theoretical capacities, to maximize the amount of usable charge in the cell.

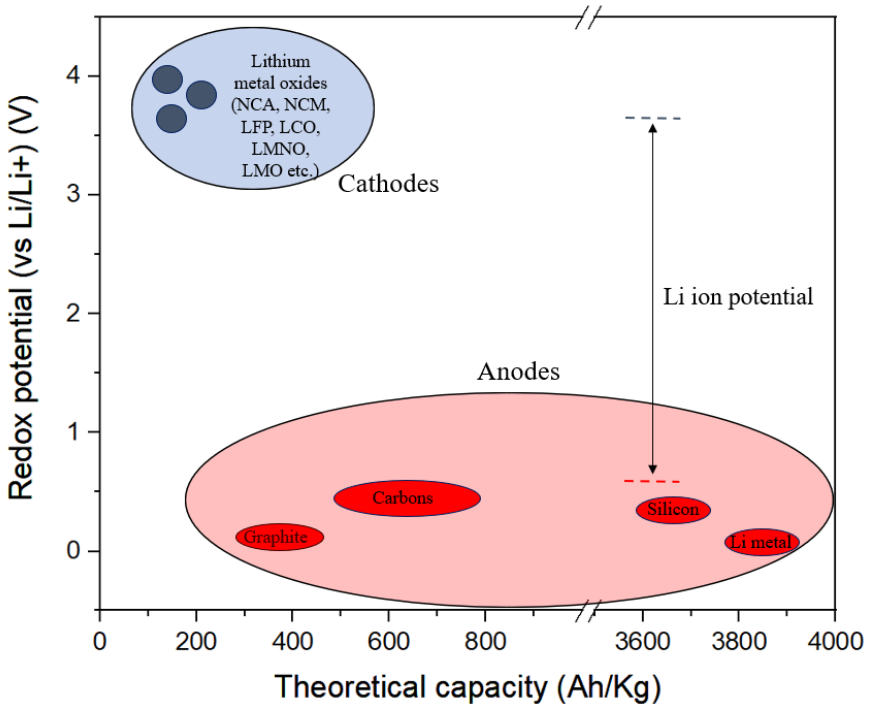

Figure 2 - Ragone plot for Li ion cells materials

It is known that the interaction of Li ions between the electrodes and electrolyte during charging and discharging processes causes constant decomposition and the occurrence of side reactions, with consumption of active Li and electrolytes, sometimes resulting in gas evolution.

These side reactions cause the initial irreversible loss of cell capacity, fostering electrochemical performance deterioration and safety hazards.

The polymeric separator undergoes an oxidizing environment from the cathode side, together with a reducing environment on the anode side electrode. For this reason, the separator needs to be stable in these harsh conditions, during the whole lifecycle of the cell, even at high temperatures. It is worth mentioning that the OCV (or V_{oc}) is determined by the difference of electrical potential between two terminals of a device, when disconnected from the circuit and in the absence of external load and current flow.

From an electrochemical perspective, it is formally defined as the difference between the cathodic (μ_c) and anodic (μ_a) intrinsic electrochemical potential, normalized by the number of electrons.

$$V_{oc} = \frac{\mu_a - \mu_c}{e}$$

According to literature, V_{oc} is to be limited by the "electrochemical stability window" of the electrolyte or by the top of the anion-p bands of the cathode. To our knowledge, the concept of "voltage stability window" of the electrolyte still need to be fully clarified.

From one side, Goodenough et al[27] stated that the "voltage stability window" of a liquid electrolyte is the energy gap between the lowest unoccupied molecular orbital (LUMO) and the highest occupied molecular orbital (HOMO), from the other, Peljo et al.[28] proposed that the concepts of HOMO and LUMO, derived from approximated electronic structure theory of isolated molecules, are not correlated to the redox reaction occurring at the electrodes and should be avoided when dealing with the electrolyte electrochemical stability. Following this approach, it is more correct to use respectively, the concepts of potentials of electrolyte reduction, at electronegative potentials and electrolyte oxidation, at electropositive potentials.

2.4 Materials for "State of the art" Li ion cells.

2.4.1 Cathodes

Since 1990s, researchers made great efforts in developing new materials, trying to overcome the energy density limitations, along with improving safety. From the cathode point of view we assisted to the passage from the layered oxides ($LiCoO_2$), to spinels ($LiMn_2O_4$) and polyanions ($LiFePO_4$)[29].

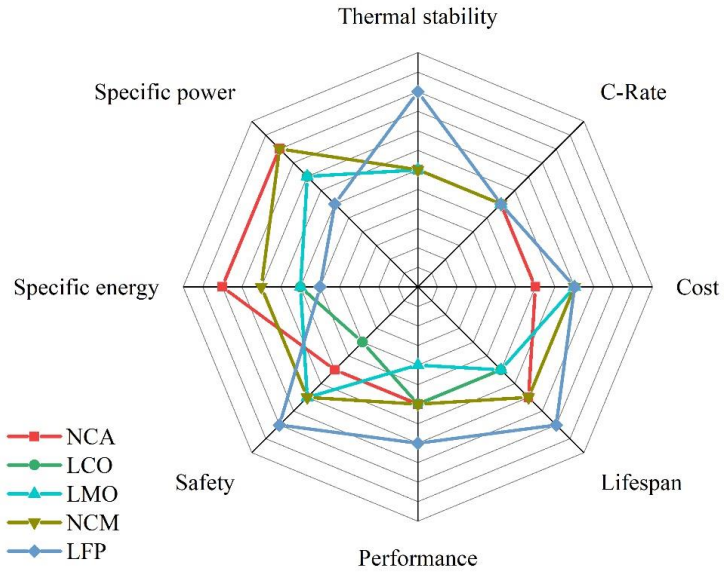

Figure 3 - Radar plot for mapping cathodes main features

Figure 3 shows the main features of the most common cathode materials[30]. Looking the "start of the art" production often LFP cathodes are used for industrial applications, stationary services and sometimes on cheaper vehicles. They present high thermal stability and safety, but low energy density.

Looking at other cathode materials, the past few years saw the shift from materials such as $LiCoO_2$ (LCO), to mixed oxides such as $LiNi_{0.8}Co_{0.15}Al_{0.05}O_2$ (NCA) and $LiNi_xMn_yCo_zO_2$ (NMC). Even if LCO, NCA and NMC present similarities, from a crystallographic point of view (layered structure) LCO was able to deliver almost 140 mAh/g as theoretical capacity, which is significantly lower with respect to NMC, which can exchange more than 200 mAh/g during charge-discharge processes. NCA, which present theoretical capacities around 200 mAh/g, very close to NMC, has some drawbacks related to safety[31].

High nickel content cathodes are becoming more and more popular in the manufacturing of Li ion cells for automotive purposes, due to their high energy density and long cycle life, along with the wider voltage window, with respect to LCO.

At lower TRLs we are assisting also to the widespread use of $LiNi_{0.5}Mn_{1.4}O_4$ (LMNO)[32]. It has a spinel crystal structure, with lower theoretical capacity if compared to NMC chemistries. Anyway, it can exchange 1 equivalent of lithium (full delithiation) reaching a higher redox potential (4.75V vs Li). Even if promising, some drawbacks related to electrolyte oxidation and degradation are limiting its usage. Another interesting material is the so-called lithium rich layered oxide, $Li_{1+y}M_{1-y}O_2$ (LRLO)[33], where M is a transition metal. This material has a layered structure and can deliver up to more than 300 mAh/g, with a redox potential that reach 4.6 V vs Li/Li^+. Also in this case, some drawbacks still need to be solved, because of degradations and oxygen release occurring when working at high voltages.

Overall, research into new cathode materials for Li-ion batteries is challenging and full of opportunities, with the goal of improving energy density, stability, and safety, while reducing costs and environmental impact.

2.4.2 Anodes

From the anode[34] point of view, graphite is the most widespread material on the "state of the art" Li ion cells, with new materials which slowly substituting the pure graphite.

Recent developments included Silicon-based anodes[35].Since Silicon has a higher capacity than graphite, composite anodes made from a mixture of different materials are being developed to take advantage of the strengths of each material while minimizing their limitations. The most common formulations are blends of graphite with a little amount of silicon inside, below the 10% w. The final goal should be the use of pure silicon at the anode side, but it tends to expand and contract during charging and discharging, leading to capacity loss and degradation over time. Efforts are being made to stabilize silicon anodes and increase their cycle life[36].

Among other classes of materials lithium metal[37] has a very high capacity but is highly reactive, which can lead to safety concerns. Recent efforts have been focused on improving the stability of lithium metal anodes and increasing their cycle life.

Among the most common approaches we can cite the possibility to create 3D scaffolds for the copper current collector, to increase the area and reducing the local current densities, limiting

hazardous Li dendrites. Artificial protection layers and optimization of the electrolyte systems are other common strategies under developement[38].

Graphene[39] is also emerging because of its high conductivity and mechanical strength.

Among the new classes we can cite also anodes with nanoscale architectures, such as nanotubes or nanowires[40], are being explored as a way to improve the capacity, rate performance and stability of Li-ion batteries.

2.4.3 Electrolytes[41]

Electrolytes for Li ion cells are non-active components, with excellent stability against anode and cathode surfaces.

The ideal electrolyte should have:

- a good ionic conductivity and electronic insulation,
- It should have a wide electrochemical window,
- It should also be inert to cell components (separators, electrode substrates, cell packaging materials),
- It should have a good thermal stability, for liquid electrolytes both the melting and boiling points should be outside the operation temperatures, Moreover, it should be liquid in a wide temperature range[42].
- It must have low toxicity, good safety levels, sustainability, and low cost.

Electrolytes for RT Li cells can be classified as follow:

1) Non-aqueous electrolytes (Li salt solubilized in an organic solvent or solvent mixture such as DMC, EC, DEC, PC);
2) Ionic liquids (ILs) consisting of an organic salt doped with a fraction of the Li salt equivalent.
3) Polymer electrolytes including gel polymer and solid polymer.
4) Hybrid electrolytes.

Among the most common lithium salts for state-of-the-art application, we can cite $LiPF_6$, $LiBF_4$, LiBOB etc.

Li ion cells with liquid electrolyte typically use various types of separators to separate the positive and negative electrodes, preventing internal short circuits while allowing the flow of lithium ions. The most common separator materials used in lithium-ion cells are polyethylene and polypropylene, often coated with ceramic materials, to enhance safety and performance.
If from one side it is important to define and improve specifications for the "state of the art" electrolytes, from the other, researchers in this field are working to develop:

- High-voltage electrolytes[43]: Recent studies are focusing on electrolytes with high voltage stability, for higher energy density and faster charging capabilities.
- Non-flammable electrolytes[44]: Literature reports development of electrolyte materials with focus on safety enhancement and thermal runaway reduction.
- Room temperature ionic liquids (RTILs)[45]: Ionic liquids, used in a large number of applications, are finding space also in the Li ion battery field. This new type of electrolyte offers high conductivity and stability, as well as a wide operating temperature range.
- Dual-salt electrolytes[46,47]: Dual-salt electrolytes, based on a mixture of two salts, are starting to be considered to improve the safety and stability of Li-ion batteries, as well as increase the operating temperature range.
- Additives and dopants: Additives and dopants, such as silicon and sulphur, are being added to electrolytes to improve the performance and stability of Li-ion batteries.

2.5 Next generation Li ion cells[47]

2.5.1 Solid state batteries: introduction to the technology[9]

During the last decade researchers are strongly pushing to enhance the development of solid-state batteries (SSBs). They can be classified as the next generation of Li-ion batteries, with a rechargeable "nature", that should replace the traditional LIBS, with liquid or gel electrolytes, with a solid membrane.
Solid state batteries should offer several advantages over Li-ion batteries, including:

- Improved safety: the use of solid electrolytes limits the risk of leakage and thermal runaway, making solid-state batteries intrinsically safer to be used and stored.
- Better stability: solid-state electrolytes are more stable than liquid or gel electrolytes, leading to improved cycle life and reduced capacity fade over time.
- Wider operating temperature range: solid-state electrolytes can be designed to operate at a wider temperature range than liquid or gel electrolytes, improving performance and safety in harsh conditions.
- Thinner form factor: The use of solid electrolytes allows the production of batteries with a thinner form factor. Conductivity of new solid electrolytes are becoming more and more comparable to liquid electrolytes.

2.5.2 Solid state batteries: How are they made?

A solid-state battery is typically composed by three main components: the anode, cathode, and solid electrolyte.

- Anode: The anode is the negative electrode in the battery, it is typically made of a lithium-based material such as lithium metal or a lithium alloy.
  Sometimes when talking about SSBs, anode less (or anode free) batteries are cited[50]. These are systems where lithium is not inserted into the cell during the manufacturing process, but it is formed during the discharging step.
- Cathode: The cathode is the positive electrode in the battery, and it can be made of a variety of materials, including transition metal oxides, sulphides, and phosphates.
- Solid electrolyte: The solid electrolyte is the component that separates the anode and cathode, allowing the ionic conduction between the electrodes.

In a solid-state battery, the anode, cathode, and solid electrolyte are typically stacked together and sealed within a battery case, forming a complete cell.

When dealing with SSBs the electrolyte covers a key role, with huge efforts in this field.

Among the most studied, inorganic, and organic classes of materials are under investigation.

Some common inorganic materials include:

- Oxide based: (e.g., Garnet type $Li_7La_3Zr_2O_{12}$ (LLZO), NASICON, LISICON, Perovskite type);
- Sulphide based.

Oxide-based ceramic electrolytes usually have good chemical stability and are compatible with high-energy cathode materials. However, the ion conductivity is lower than for sulphide-based electrolytes.

On the contrary, sulphide-based electrolytes generally have a higher ionic conductivity but are more chemically unstable, because of incompatibilities with Li metal.

Among the inorganic materials the most interesting are the polymers.

- Polymers: Polymer-based electrolytes, such as those based on polyethylene oxide (PEO) or polypropylene oxide (PPO), offer good flexibility and scalability, but may have lower ionic conductivity compared to ceramics.

The choice of the electrolyte material will depend on the specific requirements of the solid-state battery, including factors such as voltage, energy density, safety, and cost. Research is ongoing to develop new and improved catholyte materials that can further improve the performance and safety of solid-state batteries.

2.5.3 Post Li ion batteries [51–53]

At lower TRLs technologies, the so-called post Li-ion batteries, are a new generation of battery technologies that aim to overcome the limitations of traditional systems both in terms of energy density, safety, stability, and sustainability.

Some of the most promising post-Li-ion cells include:

- Sodium-ion batteries (SIBs);
- Magnesium-ion batteries (MIBs);
- Aluminium-ion batteries (AIBs);
- Zinc-air batteries.
- Lithium-air batteries.
- Lithium-sulphur batteries (Li-S).

This is an active area of research, with the goal of developing a more sustainable and high-performing battery technology for various applications, including electric vehicles, grid storage, and portable electronics. Figure 4 below shows an overview of the cell technologies[54,55] with indication on the generation and a timeline for research and hypothetical industrial production.

This chapter contains basic information about the energy storage field, with the aim of providing the reader some fundamental concepts to proceed with the lecture and a very high-level treatment about research & development trends for the next years.

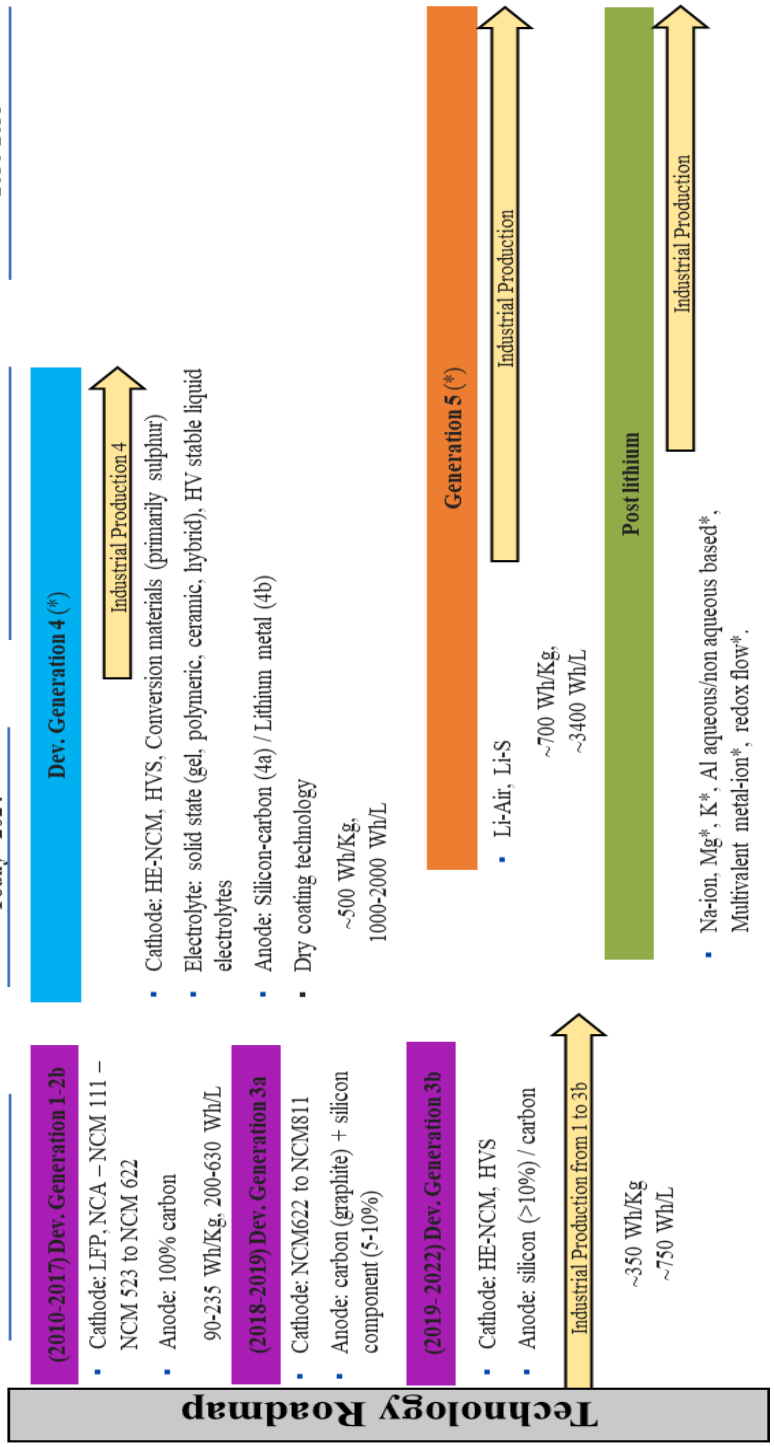

Figure 4 - Technology roadpmaps for batteries R&D and production

3 - Aging of LIBs

Chapter 3 contains general information about Li ion battery cells degradation, introducing the concept of "cell aging", starting from a high-level discussion of the topic, going to more detailed aspects at material level. Literature here is used as a support for the discussion.
Lithium plating concept is introduced here because of the importance of the theme, in relation to the thesis topics.

3.1 Introduction to aging mechanisms[56–63]

When dealing with Li ion batteries it is inevitable the occurrence of the known concepts of capacity and power fade. Starting from a very high-level evaluation, literature[64] presents these two phenomena as deleterious for the cycle life of the battery cell.

When talking about capacity fade, scientists mean the long-term decreasing capacity trend due to cycling. It is mainly attributed to the irreversible loss of active lithium along with the loss of contact for electrode materials during prolonged life cycling.

For power fade, the main cause is linked to the increase of the internal resistance, because of passive layers' formation, together with cracking of particles, with consequent loss of performances.

With this in mind, it is of primary importance to take care of cell degradation, usually known as "aging". It is a gradual process that occurs, at material level, during the life of the cell, leading to a decline (loss of reversible capacity and performance worsening).

Since Li ion cells are very complex systems where several detrimental side reactions can take place simultaneously during their lifetime, the concurrent occurring of these phenomena results a very tough task to be addressed. This is clearly visible in Figure 5, where a plenty of linked and concomitant degradation effects are summarized for emphasising the complexity in treating the topic of cell degradation.

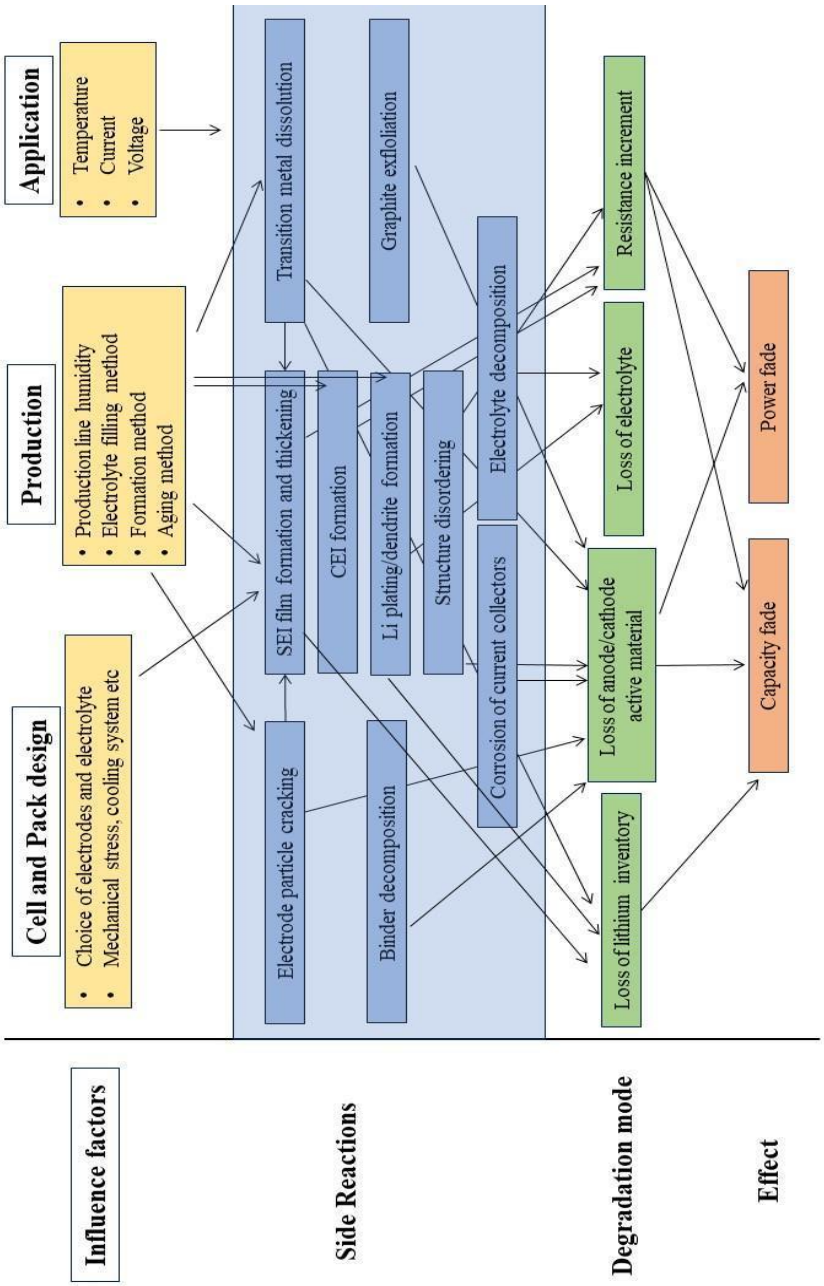

Figure 5 - Aging phenomena overview

More in detail, stated that lithium-ion cells suffer from inevitable degradation, the design of the cell (and the battery pack configuration), the production variables and the type of application must be tuned carefully, since they could strongly influence the life of the cell.

Among the main influence factors such an important role is taken by the choice of the materials and the coupling among them, the high depth of discharge (DoD), high charging-rates and low temperatures.Literature[65] reports a significant variety of aging effects' causes, with electrochemical, thermal and mechanical origins.

Among them, the loss of lithium inventory (LLI) seems to be one of the most important. During normal cycling conditions, the formation of a continuous solid electrolyte interphase at the anode (SEI) and at the cathode also (CEI), caused by the occurrence of parasitic reactions, is directly linked to this LLI, with permanent decrease of the cell capacity (capacity fade).

Irreversible loss of lithium is directly related either to the lithium plating phenomenon, when Li^+ ions leave the cathode towards the anode, in severe current and temperature conditions.

From a mechanical and structural point of view, the loss of active material (LAM) is mainly caused by the current collector contact loss.

Electrode powders are usually deposited into current collectors using binder materials. These structures permit the ionic and electronic conduction between the two sides of the cell system.

Mechanical failures (typically cracking of particles) during cycle aging, exposes new electrode surfaces to the electrolyte. The presence of new "dead" material, which does not participate actively in the redox reactions, brings the system to the formation of new SEI/CEI.

When the liquid electrolyte inside the cell works outside its electrochemical stability window, it goes towards reduction at the anode interphase, increasing the thickness and composition evolution of the passive layer (SEI), with strong correlation with LAM also. This brings to a general increase of the ohmic resistance increase (ORI) with consequent power fade.

Ideally, a SEI composed by Li_2CO_3 and LiF, once formed, would protect the remaining electrolyte from further reduction and degradation, permitting Li ions to be transported from cathode to anode and vice versa.

Real applications show that the volume expansion and contraction of the anode (pure graphite or graphite-based blends) during cycling cause the breakdown of the SEI layer, with a new active surface exposed to the electrolyte, with further consumption of Li ions and capacity decay.

Summarizing, the concurrency of these phenomena contributes to the general aging of the cell, accelerating the loss of performances and resulting in a complex system to be analysed, from the research point of view.

During cell aging, liquid electrolyte suffers also from several side reactions, which reduce transport properties such as t^+, the transference number, and the ion conductivity, promoting other failure mechanisms and, thus, aging.

3.2 SEI: Concept and basic information[66–68]

This paragraph aims to provide very basic information about the concept of SEI, since it is considered the core element for the "good functioning" of a traditional Li ion cell.

When dealing with batteries it is fundamental to mention the existence of the SEI, which is the acronym for "solid electrolyte interphase". It is a thin passivation layer (~50 nm) of material that forms on the surface of the anode in a lithium-ion cell since the very first cycles to the entire cycle life. Its formation mechanism is today observed with high attention. Literature reports the formation of the SEI layer as a natural process, occurring over time as the lithium-ion cell operates, with gas development as by product of the degradation reactions[69]. In this framework some researchers are starting to push the creation of artificial SEI[70,71], to have a control on the passivation layer, guiding the very first phases of a battery, with thew aim of prolonging life and guaranteeing safety.

It was seen in fact that the development of the natural SEI seems to be critical for the performances and stability of the cell itself. The SEI presence helps in fact to prevent further electrolyte decomposition.

During the manufacturing process, after the cell assembly, one key step of the whole process is the cell formation. It consists in performing a low current charge-discharge protocol, to activate the cell, promoting the formation of the SEI.

Electrodes and electrolyte start to be directly in contact. The interphase reactions between them promote the formation of insoluble inorganic components, due to the degradation reaction of the electrolyte formulation on the electrode surface. The product species act as a passivation layer, improving the cycle life and stability of the cell, as well as its safety.

However, SEI formation can also cause negative effects on the performance and overall life of a lithium-ion cell. During the cycle life it can increase thickness over time, along with forming also new SEI. It often occurs because of cracking of electrode particles, which expose new "fresh" surface available to be passivated by the remaining electrolyte. This is the cause for continuous linear trend capacity fade. In order to minimize the negative effects of the SEI, improving safety and performances of the lithium-ion cell, it is important to optimise the design and manufacture the product (both electrode and electrolyte formulation) and to optimize the operating conditions (charging path, voltage operative windows etc.)

Recently research[72] is involved to develop new electrolyte additives and materials to mitigate the formation of the SEI, improving its performance and stability. As mentioned above, there are several ways to improve the SEI formulation:

- Electrolyte optimization: one of the key points to improve the SEI formation is to carefully select and optimize the composition of the electrolyte, guaranteeing more stability and longer cycle life to the cell. This can be obtained by adding various electrolyte additives, such as surfactants, to improve the compatibility between the electrolyte and the electrodes, or by modifying the electrolyte to reduce its reactivity with the electrodes.
- Electrode optimization[73,74]: Another approach consists in optimizing the electrode composition and microstructure, to better control the SEI formation. This is feasible by new electrode materials implementation, such as graphene or silicon, or by the optimization of the electrode surface treatment.

- Operating conditions[75]: The optimization of the operating conditions (T, Voltage, SoC% Windows) allows to improve and reduce the SEI formation. It was observed how a good charge-discharge profile can preserve the cell from fast degradation, which is caused, among other aging phenomena, by severe SEI formation. A good control on temperature and voltage of the battery, together with avoiding extreme cycling conditions (overcharging or over discharging), can preserve the cell from continuous unstable SEI formation/disruption.

Focusing the attention on the electrolyte optimization point of view, researchers[72] are trying to optimize electrolyte formulations by addition of:

- Fluoroethylene carbonate (FEC): it is used to improve the SEI stability by reducing the formation of lithium dendrites, which can penetrate the SEI and cause short circuits.
- Vinylene carbonate (VC): it is used to improve the stability of the SEI by reducing the formation of lithium dendrites and by increasing the electrolyte thermal stability.

3.3 Aging trends and principal influencing factors[56,76]

Once defined the concept of SEI with some hints about how to control and improve its formation, it is worth to consider the panorama of phenomena contributing to the loss of performances during the lifetime of the cell, which are always linked to the SEI birth and growth.

From a macroscopic point of view it is common to divide between linear and non-linear trend aging[76].

3.3.1 Linear aging

For linear aging trend researchers refer to a gradual decrease in cell's performance and capacity over time. It can be described as a straight line on the SoH% vs N° of cycles plot, where the performance and capacity of the battery cell decreases in a linear fashion with time. In other words, a linear aging trend is indicative of constant rate capacity fade over time, with loss of

battery's performance and capacity at a steady rhythm. This kind of aging is usually predictable and can be estimated based on the battery's initial performance and capacity.
In general, linear aging trends are easier to be modelled and predicted than non-linear aging trends, thus they are often used as a benchmark for cell performance and degradation.
The most important factors contributing to aging, associated with a linear aging trend, include:

1. Electrochemical processes: the degradation of electrodes and electrolyte lead to capacity fade and loss of performance over time. This can include processes such as corrosion, side reactions, and formation of solid-electrolyte interphase (SEI) on the electrodes.
2. Mechanical stress[77]: Li ion cells are subject to mechanical stress from repeated expansion and contraction during charge and discharge cycles, which can cause damage to the electrodes and electrolyte over time.
3. Operating temperature: High temperatures can accelerate the degradation of the cell components, leading to a faster rate of capacity fade.
4. Operating conditions: Li ion cells subjected to high currents and long discharge times will experience a faster rate of capacity fade than cells that are operated under more favourable conditions.
5. Battery design: The design of the battery, including the choice of electrodes, electrolyte, and separator, can have a significant impact on the rate of capacity fade. For example, using a high-capacity anode material can slow the rate of capacity fade, while using a low-quality separator can accelerate the rate of degradation.

Because of the strong interdependency of many factors contributing to the aging of Li ion cells, it is important to try collecting and divide information in categories.

3.3.2 Non-linear aging mechanisms[78,79]

If from one side linear aging is easy to be predicted, non-linear aging occurs when the rate of capacity fade changes over time, because of the starting of severe phenomena. Literature[80] reports as “knee point” (Figure 6), the sudden change in the slope in the plot SoH% vs n° cycles.

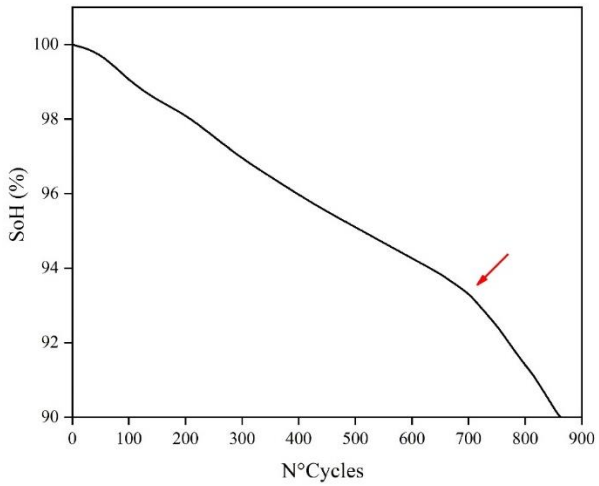

Figure 6 - Knee point as Li plating onset during cycle aging

Several factors contribute to non-linear aging:

- Imbalanced charging: If imbalanced charging occurs, where one electrode is charged more than the other, it can cause a non-uniform degradation of the electrodes and electrolyte, leading to a non-linear aging trend.
- Overcharging: Overcharging a cell can lead to a faster rate of degradation and can cause a non-linear aging trend as the rate of degradation changes over time.
- Electrode degradation: The electrodes degradation can be a complex process, resulting in a non-linear aging trend as the rate of degradation can change over time (Li plating).
- Operating temperature: High temperatures can accelerate the degradation of the battery components, leading to a faster rate of capacity fade. However, the rate of degradation can change over time as the battery ages and the temperature changes.

- Battery design: The design of the battery, including the choice of electrodes, electrolyte, and separator, can have a significant impact on the rate of capacity fade. A poorly designed battery may experience a non-linear aging trend as the rate of degradation changes over time.

Non-linear aging is a complex process that can be influenced by several factors. By understanding the causes of non-linear aging, it is possible to design and operate batteries to minimize the rate of degradation, and to extend the service life of the battery.
The optimization of the operational charging/discharging procedure will be of importance for the purpose of the present work.

3.4 Loss of Li inventory[56,60,81–84]

Formally, literature indicates the loss of lithium inventory (LLI) among the most effective aging phenomena concurring to the loss of performances inside a Li ion cell. With LLI, we intend the reduction in the amount of lithium available in the electrode over time. This can occur due to several different factors, including the formation of solid electrolyte interphase (SEI) layers, lithium plating and cracking of the active material particles. LLI can play a detrimental impact on the performance and overall life of a lithium-ion cell, it in fact reduces the amount of lithium available for electrochemical reactions with propension to capacity fade and reduction of rate performance. Additionally, it can also increase the risk of safety issues (i.e., thermal runaway) by altering the balance of lithium in the cell.

3.5 Loss of active material[81,85]

Another class of degradation phenomena that can bring to linear aging is grouped under the so-called “loss of active material (LAM)”. It refers to the reduction in the amount of active material in the electrode of a lithium-ion battery over time. The origin of this phenomenon is relative to mechanical degradation, cracking of the active material particles, and corrosion of the active material. LAM can play a negative impact on the performance and cyclability of a Li ion cell, reducing the amount of active material available for electrochemical reactions, causing capacity

fade and reduced rate performance, together with LLI. LAM can occur both at the anode and cathode sides. When talking about loss of active material it is important to cite the occurrence of particle cracking. It refers to the breaking or fragmentation of the particles within a material, during the cycling life. It is often observed from the cathode side, where transition metal oxides ($LiMO_x$) agglomerates tend to be fractured. The disruption of the original pattern causes negative effects on the overall performance of the cell.

It can occur:

- New surface availability which brings to new CEI formation and thus further loss of lithium,
- Worsening of the electric contact and of ion transport,
- Loss of mechanical stability.

Cracking of particles can be caused by several factors, including thermal expansion and contraction, mechanical stress, chemical reactions, and high current application.

Generally, it can be said that a linear aging trend in capacity fade is influenced by a simultaneous and complex interplay of factors, and the rate of degradation can vary greatly depending on the specific operating conditions and design of the battery.

By understanding the factors that contribute to the linear aging trend, it is fundamental to carefully design, manufacture and use the cell (within the proper limitation) as well as researching new materials/additives to promote a better SEI formation.

3.6 Lithium plating[56,59,81,86–90]

Given the scope of this work, lithium plating deserves a special mention. It is one of the main route causes for Li-ion cell fast degradation, occurring when lithium ions are deposited on the anode surface instead of being intercalated into the electrode material. This can lead to a change in the electrochemical behaviour of the battery, with dangerous effects related to safety issues also. The onset of non-linear aging caused by Li plating is graphically described (Figure 6) with the incoming of the “knee point” (inflection point) in the curve of State of Health (SoH) vs N° cycles.

Li plating occurs mainly during fast charging; thus, it is important to know that the most common parameters influencing the formation of Li plating (and dendrites) are:

- High current rates: If the applied C-Rate is too high, the Li^+ diffusion inside the anodic material (diffusion through Solid Electrolyte Interface and active material) has a slow kinetic with respect to applied current. This can bring to a high-level cell polarization.
- Charge at low temperature: When the exercise temperature decreases, the kinetics of the reactions slow down and the Li^+ diffusion resistance inside the anodic material increases. The intercalation process worsens, entering in competition with the Li plating.

From a general perspective, Li plating takes place in a non-uniform localized way. The electrode internal resistance inhomogeneity influences the formation of the plated area.

Inhomogeneity of the active material distribution and SEI thickness could cause localized increase of internal resistance.Looking at the entire electrode inside the cell, we can expect to have a temperature gradient. The current collector portions closer to the cell tabs for example should be at higher temperatures with respect to the rest of the current collector, because of the higher current density received. Moreover, in a battery pack, other external sources of temperature gradient are related to the heating/cooling system, where the lower side of the cell is usually heated or cooled. From an electrochemical point of view the competition between intercalation and plating is explained by the following reactions:

$$x\mathrm{Li}^+ + \mathrm{Li}_\delta\mathrm{C}_6 + x\mathrm{e}^- \rightarrow \mathrm{Li}_{\delta+x}\mathrm{C}_6$$

$$y\mathrm{Li}^+ + y\mathrm{e}^- \rightarrow y\mathrm{Li}$$

When charging, the total current is divided into intercalation current and Li plating current. Usually, when the cell is discharged, with high number of crystallographic sites available for Li intercalation, the lithiation of the graphite is predominant with respect to plating reaction on the graphite surface. When charging proceed, the vacancy sites for Li intercalation decrease and the limited solid-state diffusion in graphite cause the gradual reduction of the charge current for Li intercalation. Simultaneously, the Li plating current increases. The transport rate of Li^+

from electrolyte exceeds the Li-intercalation rate, causing the accumulation of more Li ions on the surface. This forces the anode potential to below 0 V, which is the potential where Li starts to plate on graphite. When lithium plating occurs, a portion of the deposited lithium undergoes the following reactions:

$$\varepsilon Li + Li_{\delta+x}C_6 \rightarrow Li_{\delta+x+\varepsilon}C_6$$

$$Electrolyte + Li \rightarrow Electrolyte–Li$$

The first is related to the reinsertion into the graphite anode during the tapering charging or resting time, the second is indicative of the reaction with the electrolyte.

If formed, the plated lithium can be passivated and exfoliate. The exfoliation can cause a loss of electrical contact with the anode surface, with consequent reduction in performance, due to the diminishing of the usable lithium. Here we can assist to the concomitant loss of electrical performances and to the interaction of the exfoliated lithium, which is active to react with the electrolyte, promoting parasitic reactions.

As reported in literature[89] part of the lithium plating could be reversible. During the discharge, the plated lithium which do not react with the electrolyte is supposed to be partially recovered if it maintained the electrical contact with anode matrix. A typical effect of the reduction of the usable lithium ions is the reduction of the capacity at high cell voltage.

If from one side a portion of Li plating is reversible and can be restored as active lithium, part of this Li plating is irreversible, often named as “dead lithium”. An important point regarding the irreversible lithium plating is linked to safety. The deposited dead lithium during the cycle aging increases the roughness of the electrode, leading to the formation of dendrites, especially in case of overcharging[91]. Dendrites can grow and pierce the separator, creating a dangerous short circuit inside the cell, with a possible thermal runaway and explosion. To minimize the occurrence of lithium plating, it is important to carefully control the operating conditions of the cell, including the charging and discharging currents, temperatures, and storage times. An appropriate tuning of the charging phase, as visible in the next chapters, will decrease the

occurrence of Li plating, extending the service life of the and to minimizing the rate of capacity fade.

This chapter provided some basic information about cell aging, presented as inevitable phenomenon to be considered when lifetime cycling is performed. Fundamental concepts are treated, from macroscopic to material level, to gain knowledge for the following portions of the manuscript. Li plating was treated in detail, since it is considered the main responsible for non-linear aging of Li ion cells, closely correlated with the concept of fast charging.

4 - Methods (fast charging strategies, charging profile definition and aging detection techniques for LIBs)[60]

Chapter 4 contains all the information related to methodologies, with the details for executing the analyses also. Theoretical information about Li plating detection methods are treated as first topic, in order to let the reader to know how to approach the study of the phenomenon from an experimental point of view. Some information about how to charge a Li ion cell, with focus on fast charging concept and strategies are provided. The choice among the charging possibilities was presented and the methodologies implemented for the aim of the work are here described.

This chapter also presents the list of experimental methodologies used for an extensive *ante* and *post-mortem* analysis on the samples.

4.1 Li plating detection methods

Since Li plating formation could cause severe operational damages, up to the catastrophic short circuit, caused by the formation of dendrites, it is fundamental to understand how to set the operative conditions to be applied when charging, to preserve the cells from severe degradation. It is then necessary to set the limits during charging, before lithium plating can occur, for several SoC values. Literature[56,86,87,90–93] proposed several methods, specifically adapted to the field of application.

Metallic lithium reference electrode

One of the most used approaches to have the control on the lithium plating occurrence when designing a charging profile is to take care of the anodic potential. It was seen how the plating reaction on the anode surface can take place if the anodic potential becomes negative with respect to Li metal electrode. This method is often adopted at the cell level, usually working with laboratory scale setup. The assembling of a cell with the materials of interest, using a

metallic lithium reference electrode, permits to investigate the anodic potential behaviour. Useful data can be obtained from:

- OCV of the two half-cells (cathode vs Li; anode vs Li);
- The half-cell internal resistance;
- Cells behaviour under charging at several C-rates;
- Cells behaviour under charging with specific charging profile;

Voltage relaxation

Another method used to detect Li plating presence is the so-called "voltage relaxation". This methodology is suitable for detecting Li plating during (and after) charging steps. When charging is stopped, it is possible to notice the presence of lithium plating by observing the voltage behaviour during the relaxation period (seconds). If no lithium plating occurs, the cell voltage drops exponentially when no current is passing (red line in Figure 7). If, on the contrary, a certain amount of lithium was plated during the charge, a non-exponential trend is visible during the resting phase.

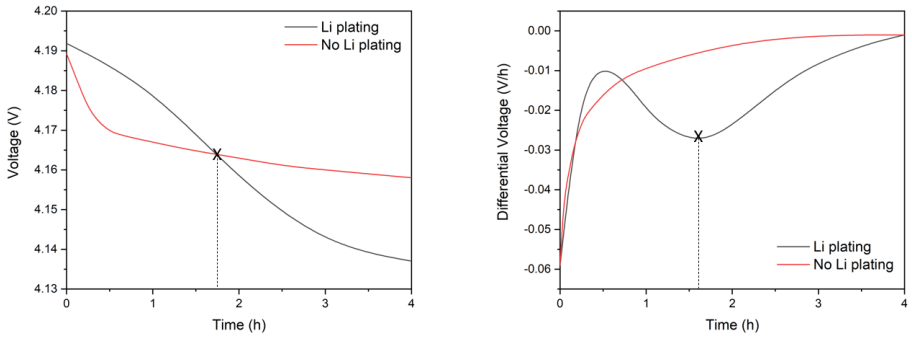

Figure 7 - Voltage vs Time (left), Differential voltage (dV/dt) vs time (right)

In fact, during the relaxation time, with a slower kinetics, the reversible portion of the plated lithium continues to intercalate leading to an increase in the concentration of the LiC_6 structure. In this framework, the implementation of differential voltage analysis (DVA) reveals to be a useful tool to well investigate voltage evolution during the rest phase. The local minimum

signed with (X) in Figure 7 individuates the end of the plated lithium intercalation and the beginning of the normal relaxation.
Literature reported a verification of this behaviour by comparing electrical and diffraction methods. Thanks to the observation of LiC_6 and LiC_{12} concentrations, performed with neutron diffraction, it was possible to confirm what was observed by electrical meauserements[94].
This method is useful to locate reversible Li plating, however it is not possible to totally exclude the occurrence of lithium plating even when the exponential voltage trend seems to be predominant.

Differential voltage analysis during discharge

During discharge, it is also possible to localize the occurring of lithium plating, by analysing the derivative of the voltage as a function of the capacity (dV/dQ). This method is known as differential voltage analysis (DVA). As demostrated[95], the initial phase of the curve is the most interesting portion when a low C-rate discharge was applied after a fast charge. When lithium plating occurs, in many cases it is present an inflection at the beginning of the discharge, as represented in Figure 8 (black line). A portion of the reversible Li plating could in fact intercalate into the graphite structure just after the end of the fast charging step.

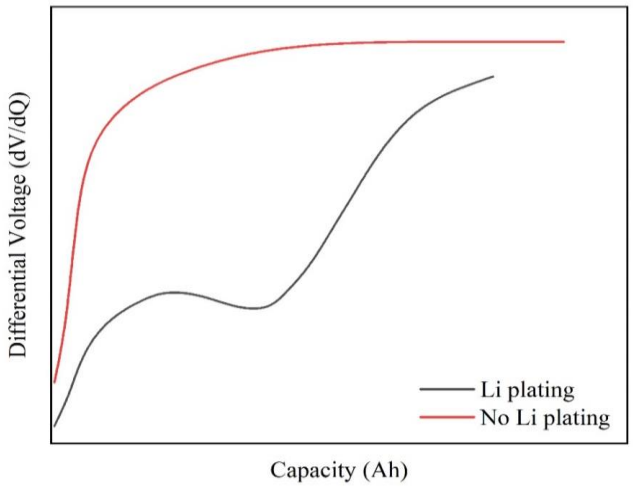

Figure 8 - dV/dQ vs capacity

Thickness increase

Another method for evaluating the presence of lithium plating consists in measuring the cell thickness, typically applied when dealing with pouch cells, because of the softness of the external case. On the contrary, since cylindrical and prismatic cells' jellyrolls are closed in a thick aluminium rigid case, this approach is less common and difficult to be implemented.

4.2 The charging strategy approach

To limit the formation of lithium plating and lithium dendrites' growth the development of an appropriate charging protocol can be the right strategy to prolong the cycling lifetime. Together with this, high speed charging and safety must be guaranteed. Literature[96] presents several protocols, proposed for Li-ion batteries purposes.

4.2.1 Constant Current – Constant Voltage (CCCV)

CCCV charging method results among the most widespread charging protocols. It can be easily implemented into BMS (battery management system) software. This procedure is composed of

a first constant current step, where a specific amount of charge passes into the cell, with a consequent change of the voltage, up to the so-called “cut off” voltage (Figure 9). When the voltage set point is reached, there is a switch in the electric parameters’ control, from the CC to the constant voltage CV step. The CV phase ends when the current drops down to a defined value. During this last step the aim is to complete the charge, minimizing the concentration gradient in the electrode materials (higher material loading creates higher thickness of the electrodes and thus higher concentration gradients). It can be observed how during the CV phase the charging current gradually decreases while the SoC slowly increases, with respect to the CC phase.

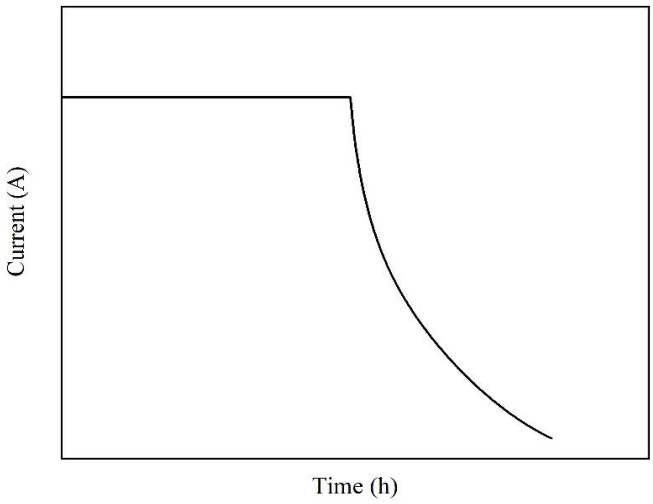

Figure 9 - CCCV charging curve

4.2.2 Multistage constant current (MCC) protocols

Multistage Constant Current (MCC) protocols are among the oldest approaches designed specifically for fast charging. The present approach consists of two or more CC steps, with current decreasing when shifting from one step to the other. Each step is set with a certain current value to be maintained up to a well-determined cut-off voltage. As this value is reached the next step starts, with a lower current value. Decreasing the current should avoid the anode

potential to become negative (vs Li metal potential). This is in fact a crucial point, which can be considered the starting event for the lithium plating phenomenon. Optionally, the latest part of the charging can be done using CV phase, this is known in literature as Multistage constant current – Constant voltage (Figure 10). It was evidenced[97] how this methodology reveals to be a valid alternative to CCCV charging. The implemented protocol guaranteed similar charging time, demonstrating that the MCC-CV protocol is also able to improve the cell capacity retention. Often researchers[98] used a cell with a Li metal reference in order to monitor the anodic potential and define an optimal MCC profile (two CC steps). Also, in this case the comparison with a reference CC-CV profile demonstrated an improved in the capacity retention for the MCC profile.

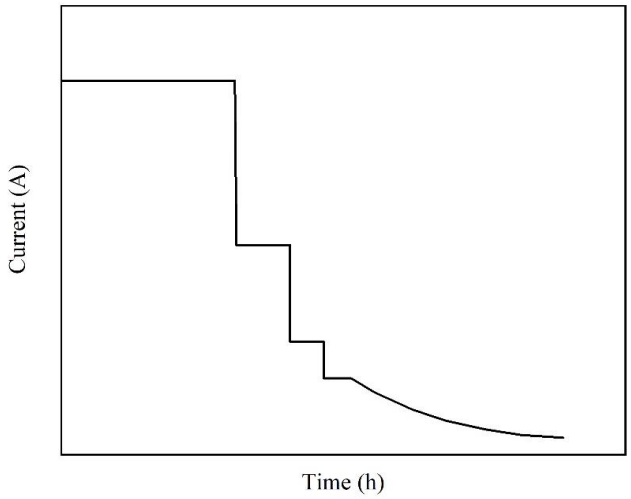

Figure 10 Multi-stage constant current charging profile

4.2.3 CC-CVNP

The CC-CVNP charging protocol consists in a constant current profile divided in a specific number of steps, interspersed by a negative pulsed current (Figure 11). Often a rest before the negative pulse can be included. The CC phase ends when the cut-off cell voltage is reached, the CV charging starts (as in the case of normal CC-CV protocol). The presence of the negative

pulses (current) is supposed to be useful for reducing the concentration gradients inside the electrode. Literature[99] reports the positive effects of this protocol by comparing CC-CVNP with CC and CCCV protocols, concluding that CC–CVNP leads to better results with respect to CCCV protocol. A comparison between CC-CV, MCC-CV, CC-CVNP, MCC-CVNP in several configurations was investigated[100]. MCC-CV and CC-CVNP demonstrated to be effective in reducing battery degradation and charging time.

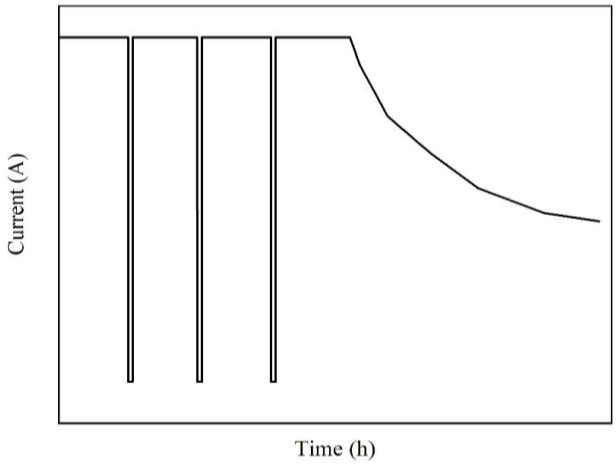

Figure 11 Constant-current with negative pulse charging profile

4.2.4 Pulse charging protocols

Another common approach for fast charging Li ion cells is the Pulse charging (Figure 12). This protocol consists of a series of constant current charging steps, with rest phases among the pulses. With this method it is possible to reduce the risk of having local anode negative potential (to avoid lithium plating) and improving the charging efficiency through a reduction of cell polarization. It was demonstrated[21] that the main factor to be taken in account for the pulse charge are pulse duration and the mean value of the charging current. However, no advantage with respect to a CCCV protocol have been identified. Other attempts[101] highlighted a reduction of the SEI growth using pulse charge protocols.

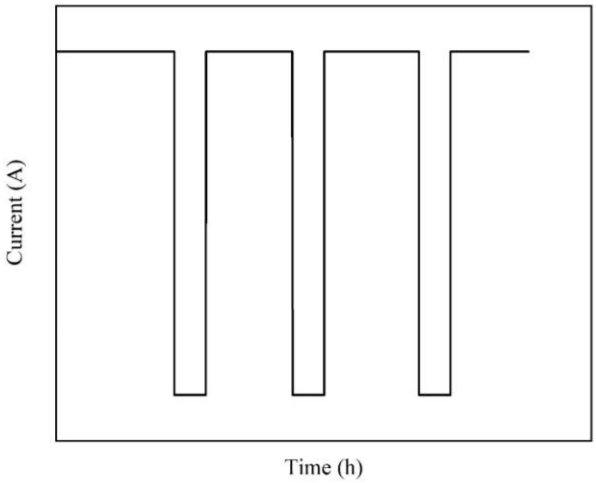

Figure 12 - Pulse current charging profile

4.2.5 Boost-charging

The Boost charging protocol[102] has an initial step characterized by a very high current value (Figure 13). When the anode is delithiated it is possible to accelerate the Li ion intercalation by the imposition of high currents, forcing the ion to move from cathode to anode. This step can be followed by a classical CCCV. Boost Charging with CV step resembles an MCC-CV protocol, with an initial short step characterized by a very high current. In alternative it can be followed by CV-CC-CV.

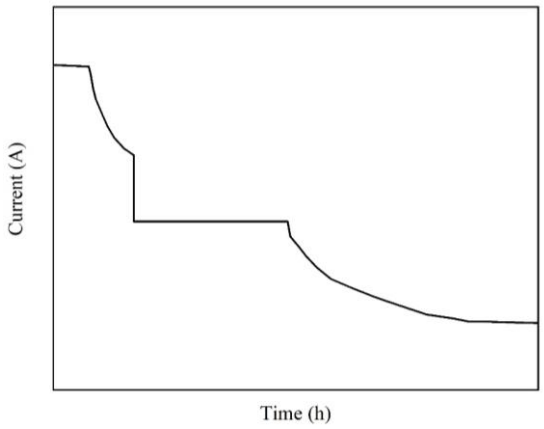

Figure 13 - Boost-charging current profile

4.2.6 Continuously Variable current profile & Variable voltage profile

Continuously Variable current profile (Figure 14) and Variable voltage profile (Figure 15), often abbreviated with VCP, is a fast charging method where a continuous current profile variation (or a large number of steps) occurs, trying to adapt it to the specific cell. Normally the cell impedance is high for SoC values close to 0% with a fast decrease increasing the SoC. Starting from a certain SoC value, the impedance trend goes towards higher values, because of the lack of available intercalation sites, in the partially lithiated graphite. The impedance behaviour permits to extrapolate a profile able to optimize the charging efficiency, reducing the heat generation. By evaluating the anode potential with respect to a lithium metal reference, it is also possible to limit the risk of lithium plating. Scientists[103] applied a VCP consisting of a series of step with a certain current value every 5% of SoC. The profile was developed to maintain constant the dissipated power. The studied profile resulted a valuable alternative to CC-CV protocol.

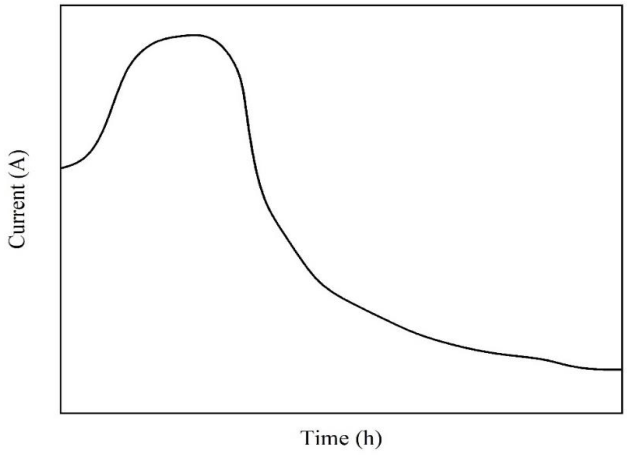

Figure 14 - Continuously variable current profiles

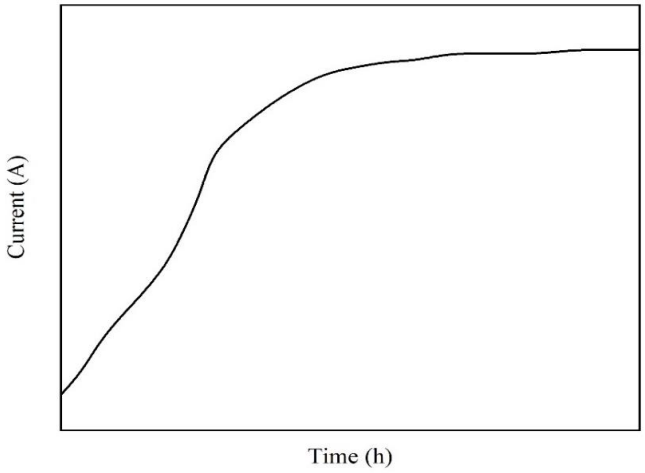

Figure 15 - Continuously variable voltage profile

Similarly, it is also possible to apply variable voltage profiles. Here the advantages are related to the fact that with cells aging it is necessary to redefine the current profile or, in alternative, it is necessary to define a derating function that takes in account the SoH of the cell. The variable voltage profile is, on the contrary, independent from cells SoH and it is strictly related to the cell chemistry.

4.2.7 Constant Temperature - Constant Voltage (CT-CV)

In the case of constant temperature profile the current profile is defined in order to keep the cell temperature constant[104]. The result of the first part of this kind of protocol can be similar to a MCC in which the current is a function of cells temperature, or it can result in a continuous variable current. The CT phase is followed by CV phase during which the cells temperature decrease, exactly as in the case of the normal CC-CV protocol.

4.3 DCFC profile design introduction

Since today e-mobility market main limitation are related to the price of the vehicle together with range anxiety and long charging times, the implementation of an optimized fast-charging profile can be helpful to decrease the time needed for a complete charge, without degrading the cell performances and prolonging the cycle life of the battery pack. Automotive producers consider that a fast-charging procedure is appropriate when the 80% of usable energy can be restored in 30–65 min, as reported in Table 2.

Table 2 - Electric vehicles battery pack datasheet

Electric Vehicle	Battery Pack Energy [kWh]	Peak Power [kWh]	Charging Time up to SoC equal to 80% (min)
Peugeot 208	50	100	30
Fiat 500	42	85	35
Renault Zoe 2	50	50	65
Honda E	35.5	50	31
Kia Niro	64	100	60
VW ID3	45 58	100	27 35

Among the wide panorama of charging approaches, for the aim of this work the Multistage Constant Current charging (MCC) approach was chosen. To our knowledge[116] it represents a

proper trade-off between efficiency and easy implementation in the battery management system (BMS).

One of the main goals of my PhD project consisted in finding the operating conditions able to avoid or reduce Li plating during fast charge. For this reason, two methodologies, useful to design custom DCFC protocols, specifically tailored on the cell object of study, were adopted:

1) Method 1) Evaluation of the anode electrode potential as a function of time, measured in a three-electrode cell (against a Li/Li^+ pseudo-reference electrode);
2) Method 2) Evaluation of the evolution of the internal resistance (DCIR) of the full cell as a function of time, during the charge process.

The two methodologies were tested and compared, to understand the feasibility and the reproducibility of the second approach. In fact, it permits faster and easier evaluation of the Li plating evolution, it can be applied to the full cells (cylindrical, pouch, prismatic format etc.) with no need of cell dismantling, avoiding testing the materials in a three-electrode lab scale cell.

4.4 Method 1) Laboratory-scale cell preparation

Before proceeding with the three-electrode cell preparation, the electrodes foils were cut into pieces and washed with dimethyl carbonate (DMC), in order to remove the Li salt residues on the active material surface, to limit the corrosion effects on the current collectors.

Figure 16 - El Cell basket to assemble 3-electrodes cell.

18 mm diameter disk electrodes were used to assemble a laboratory test cell (supplied by EL-Cell ®), as in Figure 16. This specific setup permits the use of an optional lithium metal ring, useful to work in three electrodes' conditions.

Figure 17 - El Cell® lab scale cell (PATCell)

The same setup could be reproduced with other setups (Swagelok, T cells, etc.). Since the electrodes on the original cylindrical cell were coated on both layers of the current collectors, for this specific aim it was necessary. to scratch one of the two active material sides, to allow the proper electric contact inside the EL-Cell setup (Figure 17), among electrodes and their respective plungers. EL-Cell® setup in fact can guarantee the closure of the electric circuit using two metal pieces, the upper and lower plungers, in our case made of stainless steel.

Since the adhesion of silicon-graphite blend on the current collector is not very good, to remove the unwanted coated side it was sufficient to use a blade, passing up-and-down gently on the surface, until the current collector was reached, only from one side.

The cathodic coating, because of the strong adhesion due to the PVDF binder, presents high resistance to the scratching. To avoid ruining the whole electrode, it was decided to use a rotating tool with a sandpaper on the top, for guaranteeing the removal of all the undesired cathodic powder.

The scratching of one coated side exposed copper and aluminium current collectors to the plunger, without influencing the mass loading ratio between cathode and anode materials, reproducing the original conditions. For this specific work, the EL-Cell configuration was preferred over a more traditional coin cell setup; it allows an easier dismantling of the cells for further post-mortem analysis of the tested materials, and it permitted to work with a pseudo reference lithium foil electrode.

To reproduce the original configuration, the laboratory-scale cell was filled with the same electrolyte (EC/DMC (1:1) and 1M $LiPF_6$), impregnated on an FS-5P double layered commercial separator. The samples were assembled in an MBraun Argon filled Glove Box and tested with a Basytec CTS Lab battery station. Once built, the cell needs to be formed.

The cell formation protocol consisted of 5 cycles at a current rate equal to C/10, and the cell capacity (mAh) was estimated as follow: CC-CV charge C/5 up to 4.2 V (CV step with an exit condition I < C/40); CC discharge at expected C/2 down to 2.75 V.

To monitor the lithium plating phenomenon occurring at the anode, the lab-scale setup was connected to the battery station by using an additional sensing cable, for controlling the anodic potential (U_{an}) versus lithium reference electrode. As already known from literature[105], when U_{an} becomes negative (vs. Li/Li^+), lithium plating is occurring. When charging, if the anodic potential reaches negative values, lithium ions are preferentially reduced and plated on the anode surface instead of intercalating inside graphite layers.

4.5 Method 1) Evaluation of Electrode Potential Measured in a Three-Electrode Cell against a Li/Li^+

The first method used to find the correct limitations when designing the charging profile is based on a three-electrode lab scale cell setup.

In order to build a complete experimental matrix at different C-rates, it was decided to apply a CC charging step, performed at several C-Rates. The main goal consisted in monitoring the anodic potential (U_{an}), checking when it would reach zero, marked as the ending condition before promoting plating.

Among the large panorama of possibilities for DCFC approaches, this work focused the attention on the Multistage Constant Current (MCC) method, considered a good trade-off between easy implementation on BMS and efficiency.

Since the main goal of this activity was focused on projecting new customized charging profiles, specific for a determined cell, this methodology permits to tailor each single step of the charge.

To design each single step of a multi-step charging profile, once decided, the C-Rate of the specific step was selected, and the full-cell voltage measured at the end of the charging phase (related to the selected C-Rate). The specific measured value was considered the cut-off voltage for the n-step.

4.6 Method 2) Evaluation of the evolution of IR as function of time during the charging process.

Together with the first method, described in 4.5 Method 1) Evaluation of Electrode Potential Measured in a Three-Electrode Cell against a Li/Li^+ this second approach is supposed to be complementary to the previous, with the difference of being applicable at the full cell level, with advantages in terms of speed and easier implementation.

It consists in executing a pulsed charge on the full 18650 cell. To perform this test a BasyTec XCTS battery testing station coupled with an Angelatoni climatic chamber set at 25°C, were used.

Since the aim of this methodology is to measure the cell DCIR to understand if lithium plating is occurring, it was decided to use a 3 seconds relaxation time to measure the resistance.

Using the current interrupt method, every single charge step increases the SoC of 2.5%. Cell internal resistance was measured among the steps, during the rest, as visible in Figure 18.

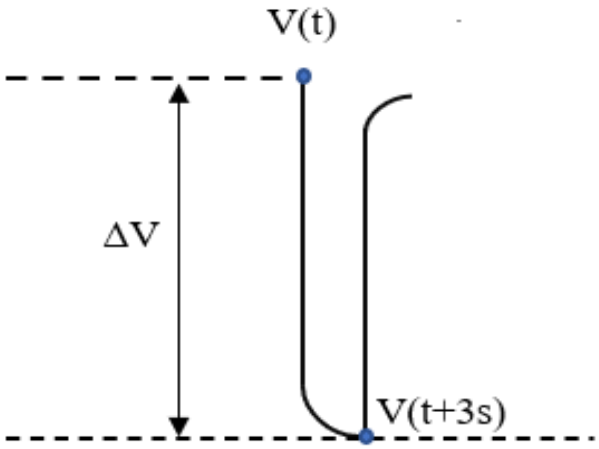

Figure 18 - Voltage response during the resting step

The current interrupt method was performed at fixed C rates (0.5C, 0.75C, 1C, 1.25C, 1.5C, 1.75C, 2C), with an interval of 0.25C among the steps.

Since the very slow current rate, the internal resistance obtained at 0.1C was considered a reference value, assuming the total absence of lithium plating at beginning of life (BOL) cell conditions.

As reported in literature[106,107], the internal resistance measured with the pulsed charge method seems to be a valid procedure to obtain information about the impedance evolution inside the cell, looking for lithium plating occurrence. As discussed, in case of lithium deposition, we assist to the competition between two phenomena:

- Intercalation of Li^+ among the graphite layers (in normal condition during charge): $xLi^+ + Li_\delta C_6 + xe^- \rightarrow Li_{\delta+x}C_6$
- Li reduction and deposition on the anode surface ($yLi^+ + ye^- \rightarrow yLi$)

It is possible to model the competition between intercalation and plating by using a simple electric model (Figure 19). When Li plating takes place, we must add a further resistance in parallel (competition). Since the equivalent resistance (R_{eq}) of two resistances in parallel is: $\frac{R\ int \cdot R\ pl}{R\ int + R\ pl}$ it is expected to assist to a decrease in terms of resistance, when Li plating takes place.

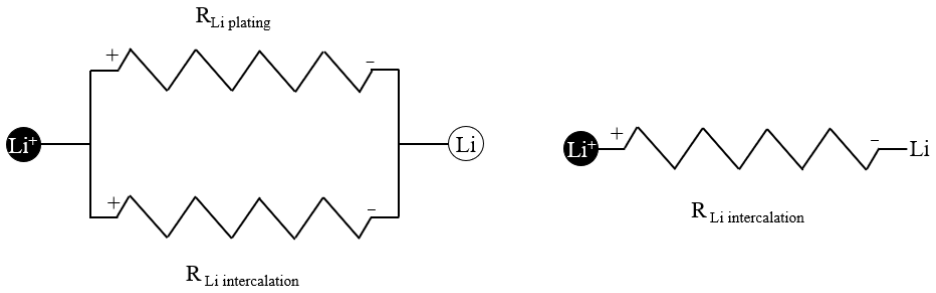

Figure 19 - Electric analogy for intercalation and plating competition

The current interrupt method applied provides information about the cut-off voltage we need to select, to avoid Li plating.

In general, cell thickness can change during charge and discharge processes. As indicated in literature[93], the comparison between thickness variation observed when low C-rate charge and high C-rate charge are applied, shows how higher C-rates generates greater increase in thickness, attributable to the deposition of metallic lithium on the anode surface. Another confirmation of the Li plating phenomenon is linked to the reduction in thickness of the cell when no current passes. As mentioned, this initial thickness increase, followed by a rapid decrease can be associated to the intercalation of plated Li among graphite layers during the rest phase.

4.7 Introduction to methods for characterization of Li-ion cells

When dealing with battery cells, the rise of aging mechanisms is well known, thus it is important to collect information about the properties decay, to better tune materials and operational limits. As a preliminary overview we can consider that a complete characterization can be achieved with the help of several morphological, chemical/electrochemical, and physical methodologies. Since these processes take place simultaneously, the identification of the single phenomenon with its contribution to the general aging is a very tough task. Scientists are used to match electrochemical techniques with an extensive post-mortem analysis[108–110]. The first category can be suitable and versatile for on-board applications, also implemented in the BMS for a continuous check during the cycle life, furthermore this class of techniques can have the advantage of being non-invasive. Incremental capacity analysis (ICA)[92,111] and internal resistance evaluation[86] are among the most diffused. Talking about the traditional "*post-mortem*" analysis there is a plenty of approaches to catch information about aging. Among morphological techniques, the scanning electron microscopy (SEM) is among the most widespread, because of its valid trade-off between cost of the analysis/time of execution and information obtained. It can be for instance a useful tool to highlight the evolution of cracking particles, morphology distribution, graphite flakes structure, SEI growth and eventual lithium plating presence[112]. TEM is also used for very high-level research, providing lots of information related also to crystallography, even if limited because of its time and cost consuming nature.

This technique can be often coupled with the energy dispersive X-ray spectroscopy (EDX), this can provide surface composition and distribution information[95].X-ray fluorescence (XRF) measurements can inform with a quantitative analysis of the superficial composition of both anode and cathode electrodes[113]. To collect information about metallic fraction inside the electrodes, when dealing with Li ion batteries, it is often performed with Inductively Coupled Plasma Optical Emission Spectroscopy (ICP-OES), which is useful for the quantitative elemental analysis. Literature[114] reports the combination of these techniques as the best strategy to validate the right elemental composition and morphological properties of both cathode and anode materials. From the electrolyte perspective, the analysis can be done with the help of several analytical techniques. Gas chromatography coupled with mass spectroscopy (GC-MS) seems to be among the most used. If from one side, GC-MS gives information about solvent composition, on the other High Pressure Ionic chromatography (HPIC) was applied for the determination of the anions of the Li salts inside the electrolyte.

4.8 Non destructive (electrical testing)

One of the first approaches to collect information about the SoH of a Li ion cell (or battery) is to start with an electrical non disruptive characterization. Often users measure capacity of the cell (Ah) and internal resistance (mOhm) to have information about the cell. To better understand phenomena occurring during the aging a plenty of techniques are used.

Here experimental information will be given, theoretical aspects, when less common methodologies will be treated, will be reported as appendix at the end of the manuscript.

The present work will show electrochemical results obtained by using the following instruments:

- BioLogic HCP 1005 (Battery cycling station + EIS);
- BasyTec XCTS (12 channels);
- BasyTec CTS Lab (8 channels);
- Arbin LBT 5V-250A (8 channels + Gamry EIS module).

4.8.1 Capacity fade method[115]

The so-called “capacity fading” method is one of the most used methods to measure the aging of Li-ion batteries as their decline in capacity over time. It is based on measuring the decrease in the cell ability to store and deliver energy, which is an indicator of the cell aging. It consists in carefully monitoring the aging trend after a certain number of charge-discharge cycles. Operatively the energy during the discharge cycle is used as reference. Often quite slow C-rates are used to permit the cell to dispense its actual energy properly. Once measured, it is compared to its initial capacity. The difference between the initial capacity and the current capacity is defined as the capacity fade, which is expressed as a percentage of the initial capacity.
Generally, this method can be used to monitor the cell performance over time and to determine when the battery needs to be replaced or recharged.

4.8.2 ACIR and electrochemical impedance spectroscopy (EIS)[116,117]

For the scope of the present work, PEIS was performed on the 18650 cylindrical cell by using a BioLogic HCP 1005, applying the following conditions:

- Ambient temperature (25°C);
- 50% SoC% (3.625 V);
- 10 mV for AC excitation signal;
- 10 kHz to 10 mHz as frequencies range.

ACIR (at 1 KhZ) was measured by a single point measurement. More information about the theoretical aspects are available in the appendix.

4.8.3 – DCIR[118,119]

For the aim of the work a current pulse able to charge the 18650 cylindrical cell of the 2.5% SoC was performed, followed by a 3s rest step (Figure 20), the equipment used was a BasyTec XCTS. The cells were stored inside a climatic chamber at 25°C ± 0.1°C.

The intensity of the charge step will depend on the C rate selected for the specific test; the duration of the pulse is controlled by the charging capacity (expressed as 2.5% SoC increment).

More information about the theoretical aspects is available in the appendix.

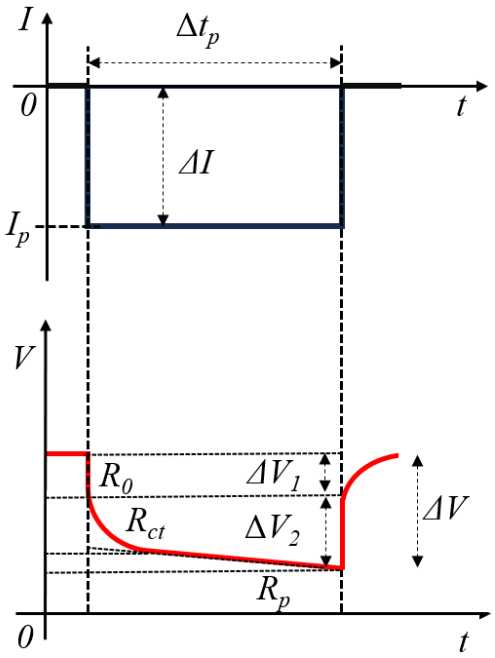

Figure 20 - DCIR measurement (current and voltage responses)[119]

4.8.4 Incremental capacity analysis[120–122]

Incremental capacity analysis was performed both on 18650 cylindrical cell and on three-electrode lab scale cell, using portion of materials sampled from the dismantling of the original cell.

This method can be executed by calculating the derivative of the capacity (dQ) with respect to the voltage (dV). It is the mathematical elaboration of a slow charge-discharge cycle (C/50) between 2.5 and 4.2 Volt, for the scope of this work. The selected C-rate was chosen to evaluate the phenomena occurring inside the cell in quasi-stationary conditions.

Incremental capacity analysis was displayed by plotting dQ/dV vs V.
More information about the theoretical aspects are available in the appendix.

4.9 Destructive (physical-chemical testing)

To better understand the aging behaviour, different techniques are usually adopted to complete the so-called *Post-mortem* analysis.

4.9.1 XRPD analysis

XRD Patterns were recorded with a Bragg-Brentano flat geometry, using a Cu-Kα radiation (λ = 1.5406 Å; 40 kV, 15 mA) at 0.02° interval in the range 5° < 2θ < 90° using a scanning velocity of 1°/min.
Cathode and anode active materials were tested in multiple conditions (material powders and electrodes).

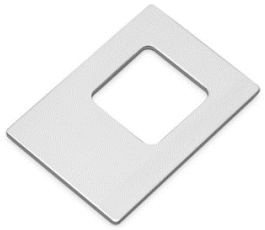

Figure 21 - Sample holder for XRPD

Figure 22 - Sample holder for XRPD for inert ambient analysis

Samples powders were scratched from the electrode foil and analysed after a thermal treatment at 350°C, in order to remove the presence of the binder, the standard full scale sample holder was used (Figure 21).
For the analysis of the calendered samples they were selected directly from the electrode foils in the original format and characterized in inert atmosphere, employing a specific XRD sample holder with a Kapton window (Figure 22).
The analysis was performed in both situations (powder samples obtained by machining a significant amount of material) and electrodes (analysing only the surface conditions) to emphasize eventual significant differences.

A Rietveld refinement was performed on XRD patterns using PDF software in the $15° < 2\theta < 90°$ range, considering a system composed by NMC811, together with a small fraction of carbon phase, associated to the conductive agent present in the electrode formulation. A trigonal structure (s.g.: R-3m, 166) was assumed for the NMC 811 phase as a model for the refinement.

4.9.2 SEM/EDX

For the morphological analysis SEM/EDX measurements were performed by using a Zeiss Sigma Scanning Electron Microscope (Oberkochen, Germany).

The anode images were collected by means of a 20 kV acceleration beam voltage and a working distance (WD) of 18.5 mm. Cathode images were acquired with a 20 kV acceleration beam voltage and a working distance (WD) of 16.0 mm. The Energy Disperse X-ray Analysis (EDX) spectra were collected at 20 kV on a 0.8 mm^2 area.

To analyse the cross-section and measure the thickness of electrodes, a small piece of sample was incorporated into a resin block that was successively polished and metalized using Ag.

4.9.3 Particle size distribution

Cathode electrodes (NMC811 based) were composed of particles of active material dispersed in a polyvinylidene fluoride (PVDF) based binder matrix. Since the distribution of the particles dimension is a useful parameter to monitor the aging, the progressive active material particles' disaggregation was checked and compared with the BOL (beginning of life) cell condition. This information can match with SEM analysis to confirm presence of particle cracking along the electrode structure.

An Antopaar 1090 PSA instrument was used to analyse NMC 811 cathode particle materials.

The analysis was performed using a particle size analyser based on the static light scattering principle. A laser beam was scattered by the dispersed particles sample and the intensity of light scattered was linked to the particles' diameter. The dispersion was performed in a liquid medium (water).

For cathodic materials, the analysis was performed in liquid dispersion to properly spread the particles. Before starting the test, it was necessary to remove the PVDF binder. NMC 811 electrode samples were treated at high temperature (350 °C for 1 h) and then the active material was detached from the Al current collector surface.

The analysis was performed without ultrasound dispersion to avoid further particles' disaggregation. The pump and the stirring were set at a high velocity (250 rpm), repeating the test five times, to assess the stability and the reproducibility of the measurement. The particle size distribution was estimated through the Fraunhofer diffraction equation, which predicts the angular location of the scatter maxima and minima as a function of an object's size.

4.9.4 ICP-OES

To quantify the amount of transition metal composing the cathode blend composition, an inductively coupled plasma (ICP) analysis was performed on calcined cathode powder (350 °C—1 h). A total of 0.25 g of powder was weighed on an analytical balance (accuracy 0.0001 g), transferred to a volumetric flask (250 mL), and digested with a hot aqua regia solution on a hot plate; nickel, manganese, cobalt, and lithium were quantified using a method with three calibrated points (0 ppm, 25 ppm, 50 ppm).

4.9.5 Raman spectroscopy[123–125]

During the present work two types of measurements were executed:

- Raman single point spectra;
- Raman mapping.

Raman single-point spectra are the result of the average of multiple single spectra, Raman mapping instead was performed by matching a multitude of Raman spectra, each one corresponding to a single pixel.

In order to collect data representative of a sufficient large zone of the electrode, a map of spectra was recorded by analysing areas with higher G bands and others with higher D bands.

To generate the Raman map/image, the following Raman spectral parameters were considered:

- Peak intensity, which yields images of material concentration and distribution.
- Peak position, which yields images of molecular structure and phase, and material strain/stress;
- Peak width, which yields images of crystallinity and phase.

Raman spectroscopy analysis on anode samples were conducted in collaboration with the Centre for Research and Technology Hellas (CERTH), in Thessaloniki.

Electrodes samples were first washed in order to remove the electrolyte residues and then analyzed by using a confocal ex situ raman spectroscopy.

The used excitation wavelength of the laser source was 785 nm.

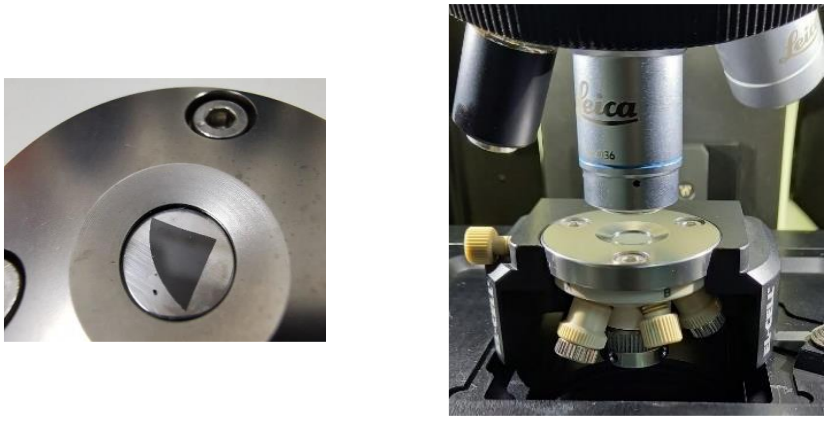

Figure 23 – Sample holder under the microscope lens.

Measurements were conducted by using a specific cell setup, provided by EL CELL®. A lens with a x50 magnification was selected, as visible in Figure 23. The sample was cut and positioned under a specific sapphire window, which gives contribution to the Raman spectra, to be excluded for the current analysis. Raman single-point spectra every 0.5 microns were collected (330), giving back an average spectrum which represented the sample conditions along the analysed surface. This method represents a valid approach to get a “big picture” from surface inhomogeneous samples. Si/C anode electrodes were analysed, to appreciate structure changes with aging. High attention was dedicated to the research of lithium plating. Metallic lithium can be detected using Raman spectroscopy by analysing the vibrational spectra of the

lithium-plated surface, which is distinct from the non-plated surface. The change in the vibrational modes due to the presence of lithium on the surface can be used to identify the lithium plating presence. This method can provide information on the thickness and distribution of the lithium plating on the surface, helping in the analysis of battery performance and aging.

This very dense chapter presented “methodologies”, with different meaning and purposes:

- Li plating detection methods;
- Fast charging methods;
- Experimental methods implemented in this thesis for designing the charging strategies;
- Characterization methods applied on the samples (non-destructive and destructive) as showed in Table 3.

All these methods will be used to set the initial conditions for the charging strategies first and to analyse samples after an impactive cycle aging campaign.

Table 3 - Summary of the used characterization methods

Characterization method	**Destructive/Non-destructive**	**Applicable to:**	**Useful for:**	**Applied in the thesis on:**
Charge/discharge cycling	Non-destructive (*destructive if working at material level)	Full cell	SoH% estimation	Full cell
EIS/ACIR and DCIR	Non-destructive (*destructive if working at material level)	Full cell	Internal resistance evaluation	Full cell
ICA	Non-destructive (*destructive if working at material level)	Full cell	General aging status/estimation of residual charge with respect to voltage	Full cell/Materials
SEM-EDS	Destructive	Electrodes	Morphology information	Anodes and Cathodes
PSD	Destructive	Electrodes	Dimension of particles	Cathodes
XRPD	Destructive	Electrodes	Mechanical particle degradation/chemical information	Cathodes
Raman spectroscopy	Destructive	Electrodes	Mechanical particle degradation/chemical information	Anodes
ICP-OES	Destructive	Electrodes	Stoichiometry information	Cathodes
GC-MS	Destructive	Electrolyte	Formulation information	Electrolyte
TGA/DSC	Destructive	Separator	Material composition	Separator

5 - Ante-mortem characterization

Chapter 5 contains the *ante-mortem* analysis performed on the sample, to collect important information to be used as a comparison for the following post-mortem analysis. Here non-destructive and destructive analysis are presented.
Cycle aging data performed on modules are reported and considered as preliminary analysis for the core of this project.

5.1 The electrical characterization

Before starting with the cycling aging campaign, it was decided to collect enough information about the cell, both from electrical and from material point of view, to better define the cycling constraints, operating in safety conditions.
The selected cell was a cylindrical 18650 cell, provided by a Chinese manufacturer.
First, looking at the manufacturer datasheet, the information in Table 4 were collected.

Table 4 - Li ion cell sample datasheet extract

Voltage limits (V)	2.5-4.2
Nominal voltage (V)	3.6
Max charge current	1C（25℃ not for cycle life）
Max discharge current	3C（25℃ not for cycle life）
Nominal Capacity (Ah)	2.9
Temperature range (°C)	0~45°C (for charge) −20~60°C (for discharge)
Cell characteristics	
Weight (g)	45.2
Length (mm)	648.0
Diameter (mm)	184.0

For the electrical test, one sample was selected and cycled.

After two low C-rate cycles (C/10) performed to “promote” the waking up of the cell after a long period of stock (SEI rupture after calendar aging), a quasi-stationary cycle (C/50) was performed, to gain information about the full useful capacity, which is confirmed to be around 2.9 Ah, as declared by the manufacturer. The coulombic efficiency of 99.5% confirmed the good status of the cell. Data are showed in Figure 24. The slow rate cycle performed permitted to also extrapolate information about the so-called ICA peaks (Figure 25), which are specific for the type of materials used, as well as giving information about the SoH of the cell tested. Further details will be given later in the next chapters, for now the test was performed to be used as future comparison rather than as a crosscheck for the material verification (last peak at 4.1V is peculiar for high nickel content NMC materials).

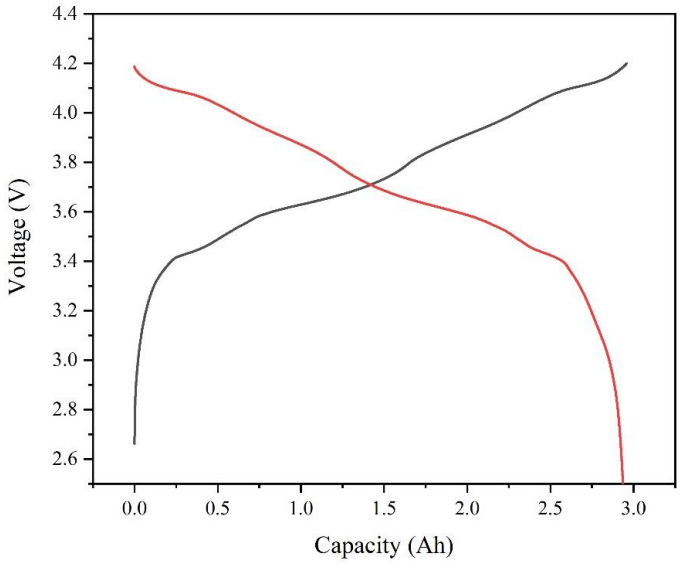

Figure 24 - Voltage vs capacity curve

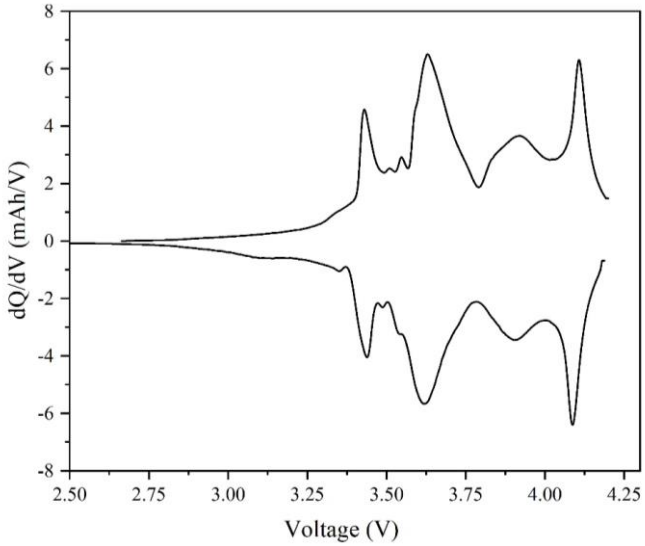

Figure 25 - ICA of the BOL sample

EIS measurements foreword

To evaluate the good reproducibility of the methodology some statistical analysis was performed before starting with the real measurements.

One 18650 cell (BOL conditions) was selected. The sample did not undergo cycling before EIS, that was performed at 3.62 V, 50 SoC%, at 25°C. a sinusoidal signal of 10 mV of was used, sampling from 10 kHz to 10 mHz. Five repetitions were executed, calculating the average, standard deviation and % error of both real and imaginary component for each selected frequency.

For an easier evaluation the full range of frequencies was divided into three main ranges, for each the percentage of error on the measurement was reported, as visible in Table 5.

Table 5 - Percentage error on EIS measurements

	Impedance (Re)	Impedance (Im)
High frequencies (10kHz – 1Hz)	0.4%	1.9%
Medium frequencies (1Hz –50 mHz)	1.5%	3.4%
Low frequencies (50 mHz – 10 mHz)	1.1%	1.8%

It is possible to notice that both Real and Imaginary components of the impedance present the highest error values at the medium frequencies.

Generally, the data obtained do not show high experimental errors on the measurements.

Moreover, since the middle range of frequencies highlights the phenomena correlated with SEI and charge transfer (CT), it is expected that some limited SEI rupture, formed after a prolonged period of calendar aging, is starting to occur among the repetitions, because of the AC input.

This electrochemical phenomenon could have an effect intensifying the error results.

From what it was observed, the hypothesis is that, once stabilized, the EIS measurement on one sample can provide good quality results, lowering the error.

Once performed the evaluation on the quality of the measurement, EIS tests were conducted on a BOL cell, after a specific number of cycles, to visualize the first significant changes (Figure 26).

As mentioned, the cell was first cycled with two C/10 cycles. To be concise, this procedure was called “priming” here in this work. It was seen how before the “priming” the cell charge transfer resistance (R_{ct}) was very high, with a fast decrease just after a few cycles, electrolyte resistance on the contrary (R_{el}) maintained a constant value, confirming the stability of the electrolyte within the applied conditions.

The stabilization of this value was observed between 50 and 100 cycles performed at C/2 between 3 and 4.2V.

The main hypothesis of this behaviour is linked to the rupture of a thick SEI formed during the so-called “calendar aging” occurred during the stock period.

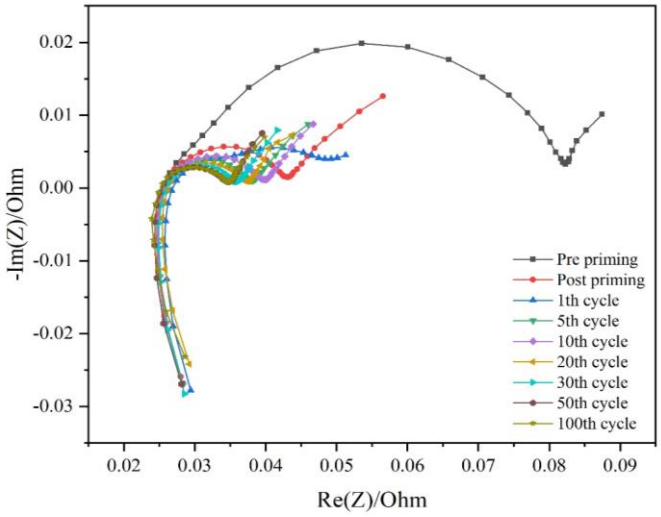

Figure 26 - EIS on cylindrical BOL samples

The inductive behaviour at high frequencies associated to the cables was neglected when the fitting was performed.

A very common equivalent circuit, already published in literature[126] (Figure 27), was used.

It is possible to evaluate the main resistance contributions trend, as reported in Figure 28.

It was observed a decreasing trend for R_{ohm}, after some punctual increment, hypothetically related to electrolyte degradation after the first cycles. R_{sei} also showed a decreasing trend, with stabilization after the first cycles. As mentioned, the main hypothesis is related to the disruption of a thick SEI layer formed during the stock of samples (calendar aging). After its disruption, during the first cycles, new SEI will be formed during the cycling campaign, causing an increase of this parameter with aging.

R_{ct} showed an important decrease after the first low current charge/discharge cycles, then a stabilization of this value confirmed the good health of the cell, at the beginning of life.

A comparison between BOL conditions and aged samples will be provided later.

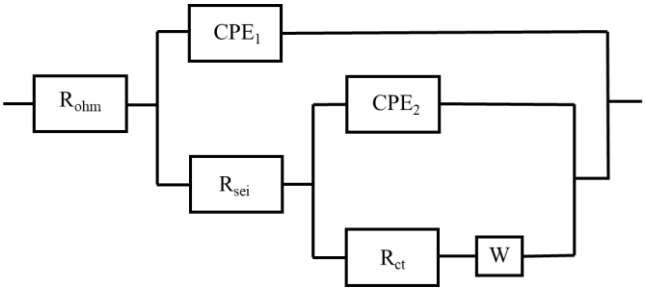

Figure 27 - Equivalent circuit for EIS fitting

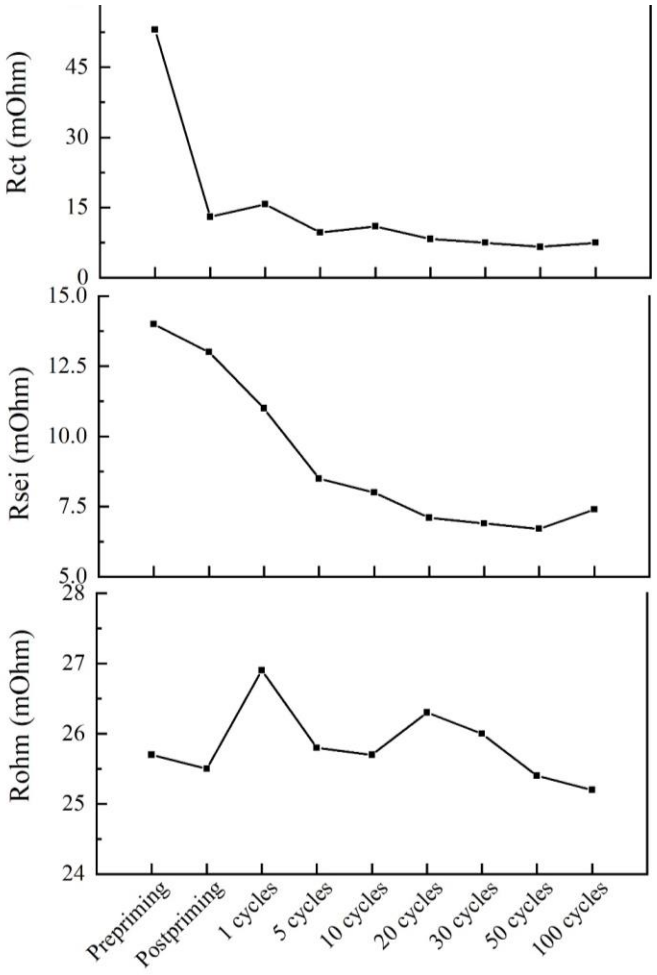

Figure 28 - Resistance trend after initial cycles

5.2 Physical-chemical characterization

To study the materials, a selected 18650 Li ion cell was disassembled.

The cylindrical cell, as in Figure 29, was opened and dismantled in a MBraun glove box, with a controlled argon atmosphere (H_20 < 0.1 ppm, O_2 < 0.1 ppm).

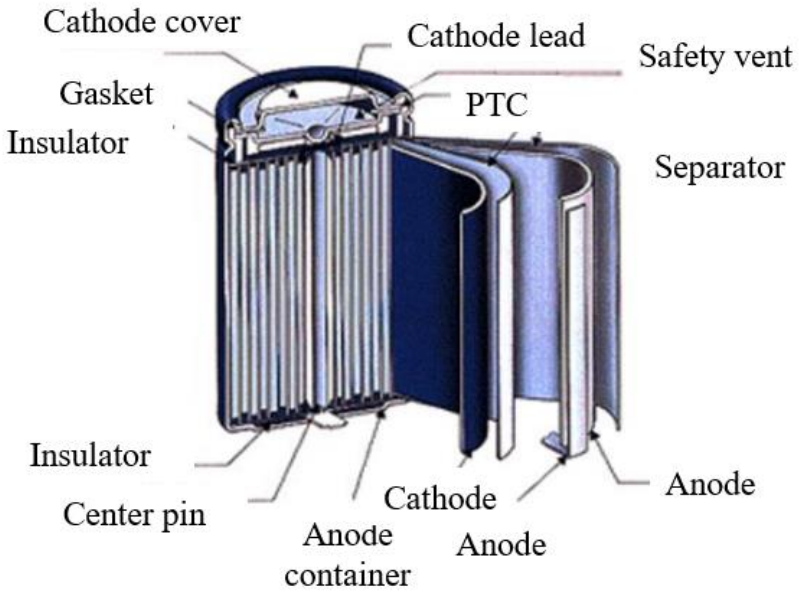

Figure 29 - 18650 cylindrical cell parts

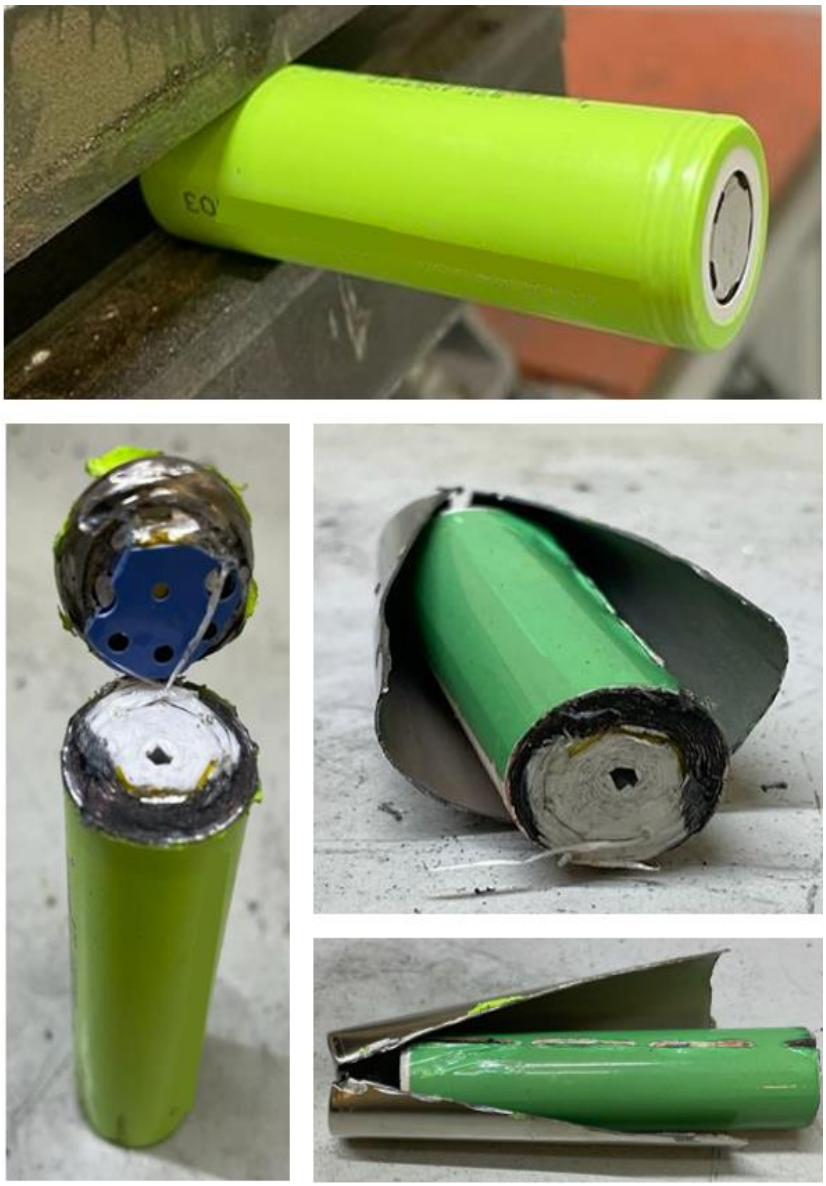

Figure 30 - 18650 cell used as sample for the activities

For the physical-chemical characterization, the cell teardown (Figure 30) was conducted after discharging it at 2.2 Volts, to limit anode degradation by arriving at 0 Volts. The aluminium can was first cut from the top, removing all the passive safety equipment present (PTC etc.), by using a Dremel® instrument, with a rotative blade. Once the external case was completely removed, the jellyroll (Figure 31).

was unwrapped, obtaining the anode and cathode foils, separated by the separator foil.

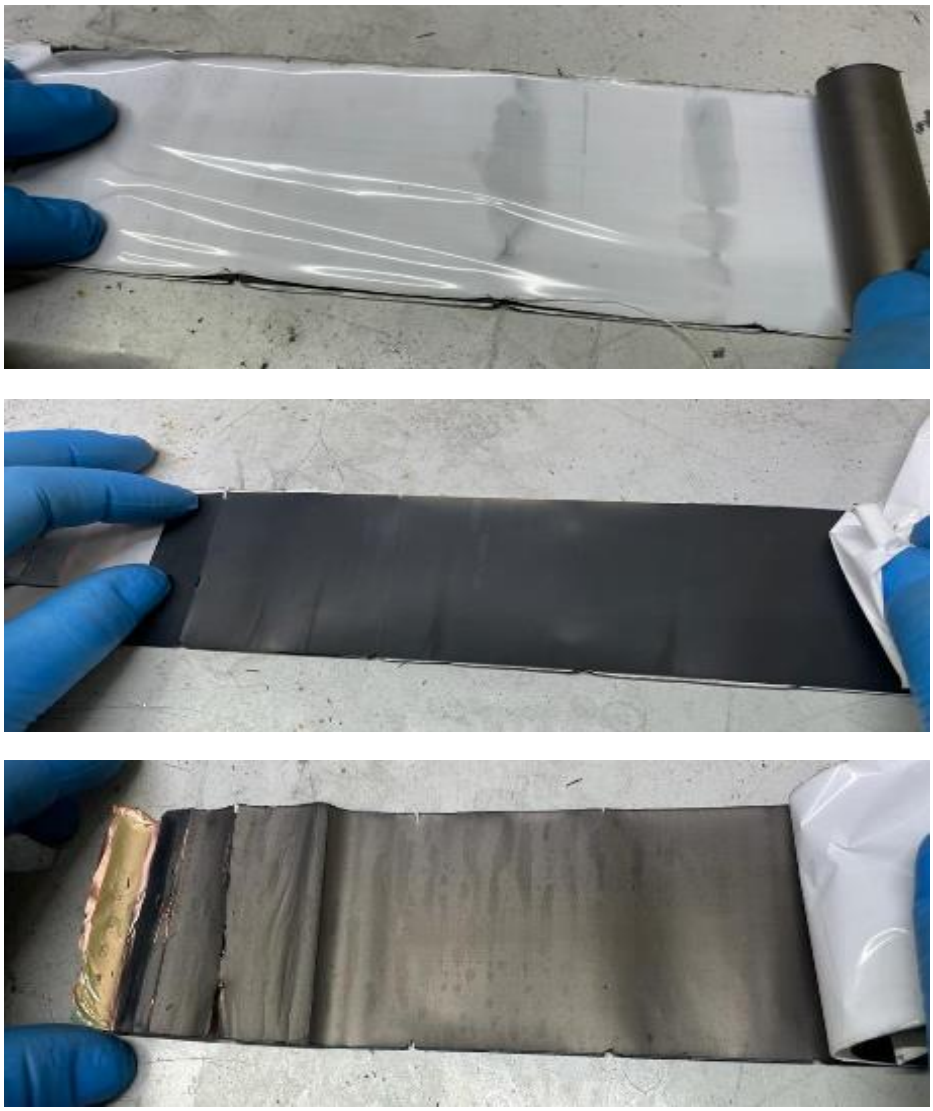

Figure 31 - Electrodes and separator foils

Table 6 - Electrodes and separator foils dimensions

Positive electrode Dimensions (mm^2)	633 x 58
Negative electrode Dimensions (mm^2)	633 x 59
Separator Dimensions (mm^2)	730 x 60

SEM-EDX analysis

Scanning electron microscopy performed on electrodes provided details about the general morphology of both cathodes and anodes, along with information about the thickness and, with the help of EDX, also qualitative compositional data.

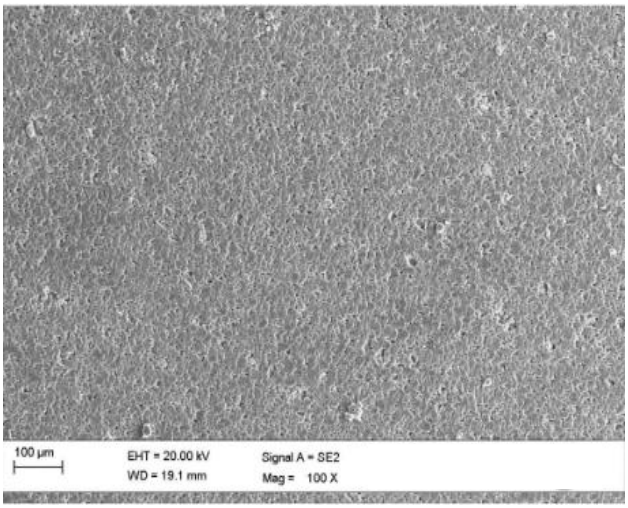

Figure 32 - SEM image of the Si/C anode sample

Figure 32 and Figure 33 show the anode morphology at different magnifications.

At 100x the surface seems to be well distributed, with a homogeneous particle size. At 1000x it is possible to appreciate the typical flake structure of the graphite.

From the EDX analysis, which is semiquantitative, it was possible to conclude that the anode active material was composed of a mixture of graphite with a small amount of silicon, which is present as localised agglomerates all over the electrode.

To better confirm this, the tests were conducted on different portions of the electrode, as visible in Figure 34 by the green spots on the images.

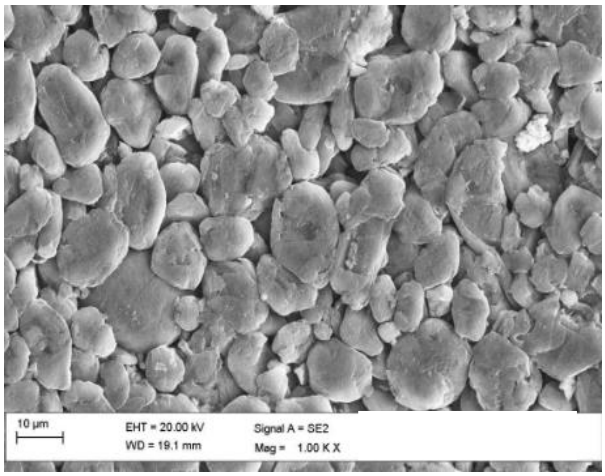

Figure 33 - SEM magnification at 1.00KX for Si/C anode

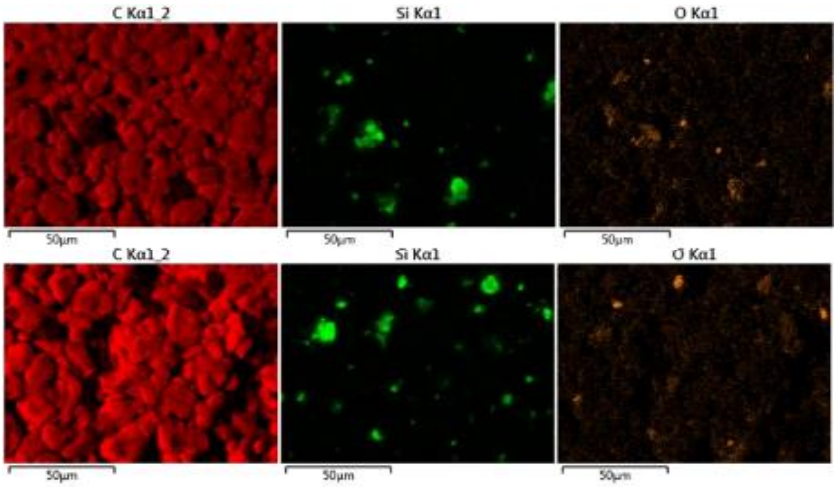

Figure 34 - EDX maps for anode sample

Measurements performed on the cross section of the sample (Figure 35) permitted to quantify the thickness of the active layer, which was around 80.7 µm.

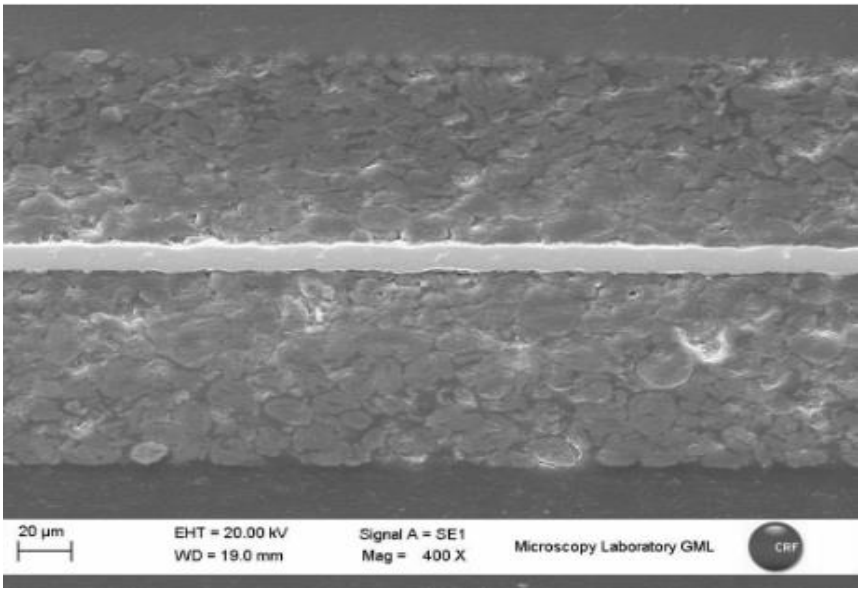

Figure 35 - Cross section image for anode sample

Regarding the cathode, SEM analysis was also performed to study the morphology. From the images (Figure 36 and Figure 37) at different magnifications, it was possible to appreciate the presence of spherical agglomerates (secondary particles), which belong to different families in terms of dimensional distribution.

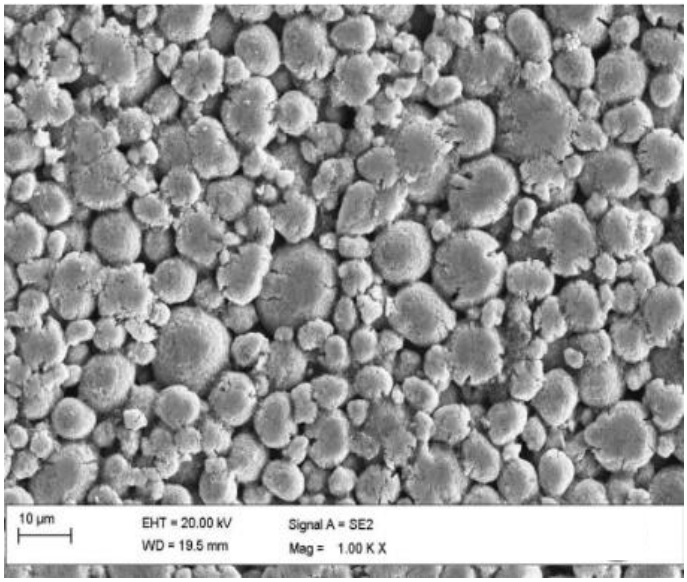

Figure 36 - SEM image of the NMC811 cathode sample

Particles appeared not damaged, except for some very limited cracks at the boundaries of the biggest particle agglomerates. Generally, these spherical clusters are composed by primary particles, also visible in Figure 37.

To collect information about the cathode active material thickness, cross sectional analysis was performed, as reported in Figure 38.

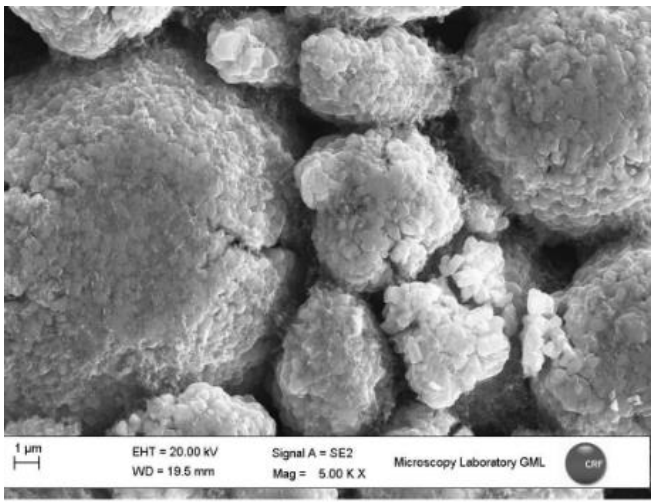

Figure 37 - SEM magnification at 5.00KX for cathode sample

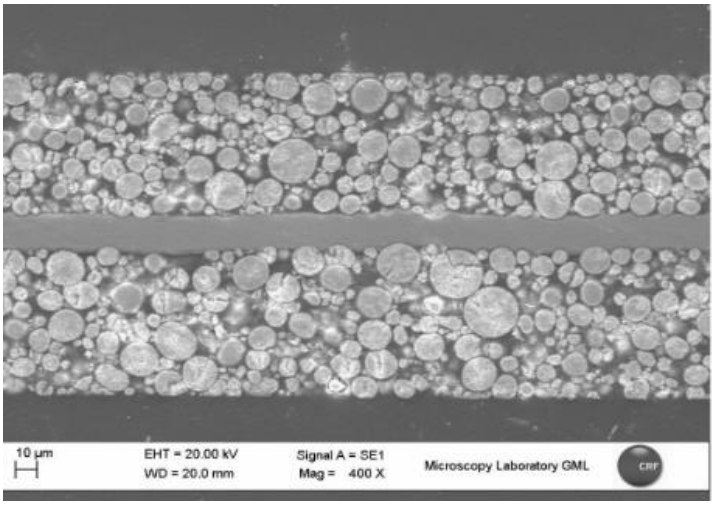

Figure 38 - Cross section for cathode sample

From the measurement an average cathode thickness of 70.6 µm was observed.

Particle size distribution

To complete the information about the morphology, particle size distribution analysis was performed on cathode particles. From the analysis, as visible in Figure 39, the average particle size distribution is 6 microns of radius.

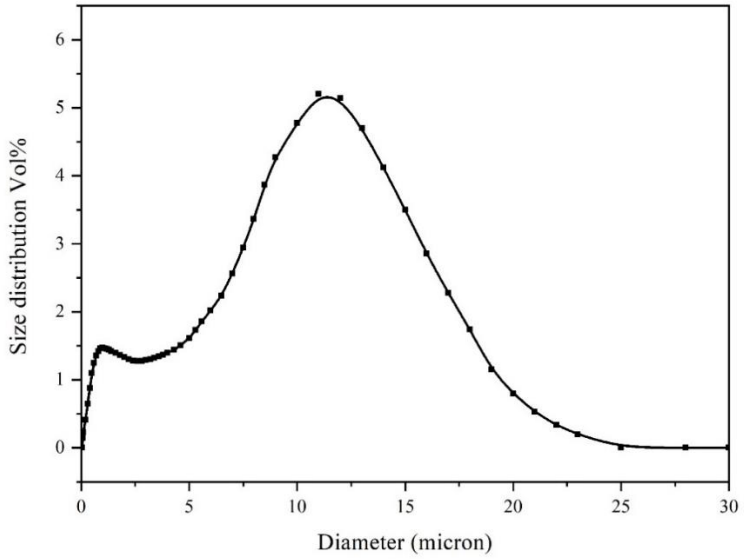

Figure 39 - Particle size distribution analysis

X-Ray Powder Diffraction (XRPD)

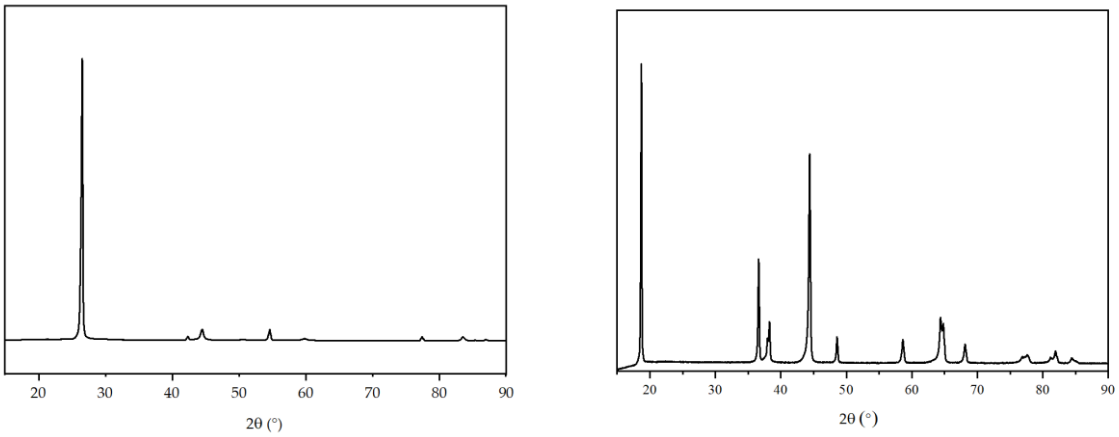

Figure 40 - XRPD on anode (left) and cathode (right) powders

Information coming from XRPD analysis on BOL sample (Figure 40) confirms the hypothesis of a graphite-based electrode (anode) and an NMC electrode (cathode). Given the qualitative nature of the measurement, further comparison and deepening (Rietveld refinement) will be performed later in the discussion.

Raman spectroscopy

Raman spectroscopy was performed on BOL anode samples (Figure 41, in order to collect information about the degradation status of the sample before cycling the cell. The ratio between D and G bands was calculated and used later in the discussion for the comparison with aged samples.

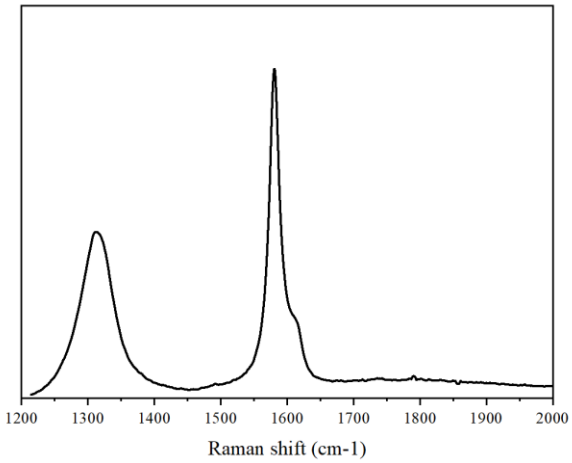

Figure 41 - Raman spectra for Si/C anode

Chemical composition

The information obtained from EDX analysis were compared with ICP measurements.

The analysis confirmed that the cathode chemistry belongs to a $LiNi_{0.8}Mn_{0.1}Co_{0.1}O_2$ (NMC811), as indicated by ICA measurement also.

Regarding the anode, the amount of silicon, detected also by EDX, was around the 2% wt., blended with graphite.

GC-MS and ionic chromatography were used to characterize the electrolyte mixture, confirming that EC/DMC (1:1) was used to disperse $LiPF_6$ salt. TGA/DSC analysing allowed determining that a PP-PE separator was used.

Half cell measurements

Anode specific capacity, measured on half cell (Si/C vs Li) was 4.3 mAh/cm^2, cathode specific capacity, measured on half cell (NMC811 vs Li) was 3.9 mAh/cm^2.

SoC% vs OCV curves, obtained by assembling half cells with the materials collected from the dismantling of the original sample, are reported in Figure 42 (Si/C vs Li) and Figure 43 (NMC811 vs Li).

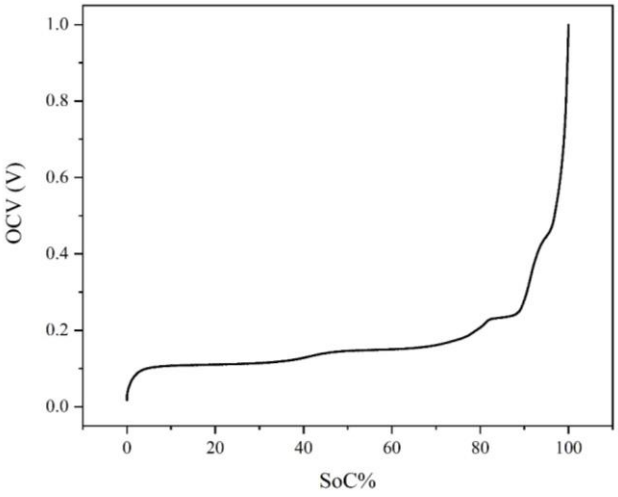

Figure 42 - SoC% vs OCV curve for Si/C

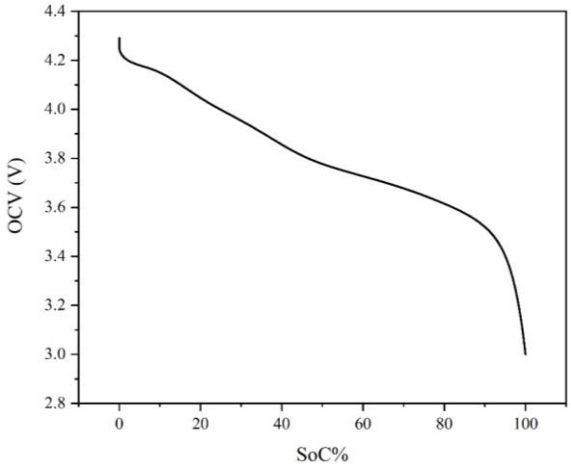

Figure 43 - SoC% vs OCV curve for NMC811

5.3 The cycle aging campaign

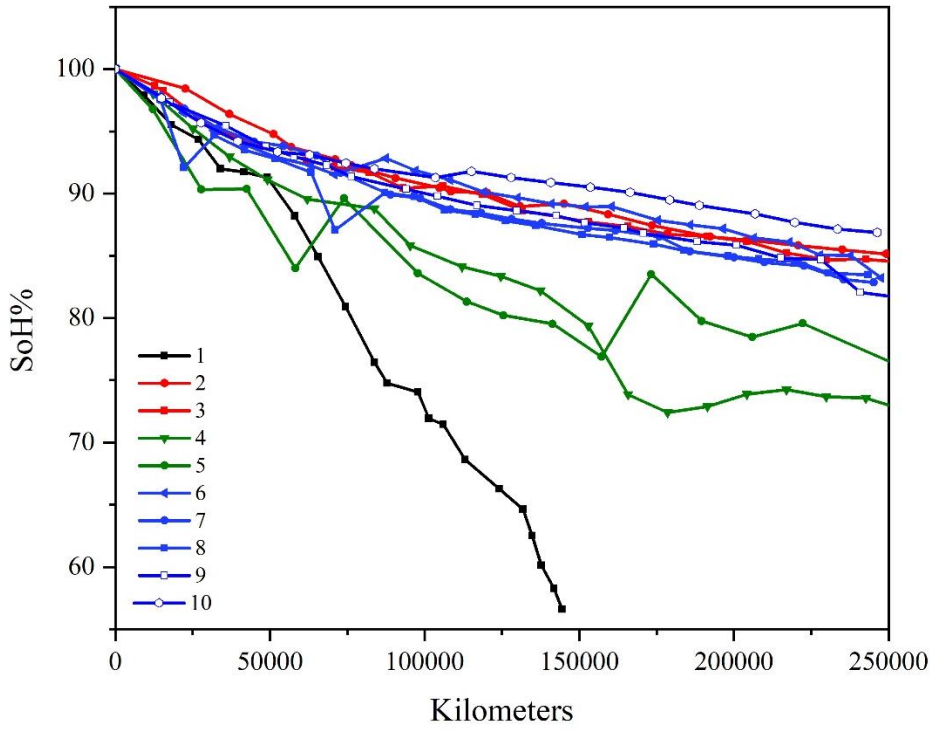

Figure 44 - Cycle aging on modules

Once defined and analysed the cell sample, two parallel activities were carried out.

Here the results obtained from an endurance cycle aging was showed.

The investigation was conducted with 5 cells connected in parallel, composing a module. The chosen setup was selected to work at a low voltage condition (below 5 volts), to respect the safety guidelines of the laboratory.

As a resume, the following parameters were taken into consideration:

- Cycling temperature;
- DoD%;
- Discharging profile;

Charging step was maintained constant and described later.

Table 7 summarizes the main working conditions adopted for the cycle aging, showed in Figure 44. To simulate real driving conditions, the sets of 5 cells were aged to reproduce the stress the battery pack will experience during its life. The experiments were performed by means of WTLC[127]-based power profiles and also by applying DCFCs, in order to trigger aging phenomena inside the Li-ion cell module. During the cycle life of the battery a total amount of 15-20% of Direct Current Fast Charge (DCFC) (1C up to 3.9V, C/2 up to 4.2V) were performed, in order to emulate real usage conditions with alternation of standard charges (typical night-long slow charge of the vehicle) and fast charges (if sudden need of charging in short time period occurs). Among two cycling aging steps, an "health condition test", usually called RPT (Reference Performance Test) was performed. It consists of charging the battery with a standard C/2 charge (up to 4.2V). Data collection for the cycling aging of the reported modules took around 3 years, revealing to be a time and energy consuming activity which must necessarily be slimmed down.

Table 7 - Cycle aging conditions for 14.5Ah modules composed by five 18650 cells.

Module	T (°C)	DoD%	Charging
1	25	4.2 – 2.75 V (WLTC)	C/2 (1C+C/2 once every five cycles)
2	25	4.2 – 3.2 V (WLTC based)	C/2
3	25	4.2 – 3.2 V (WLTC based)	C/2 (1C+C/2 once every five cycles)
4	40	4.2 – 3.2 V (WLTC based)	C/2 (1C+C/2 once every five cycles)
5	40	4.2 – 3.2 V (WLTC)	C/2 (1C+C/2 once every five cycles)
6	30	4.2-3.2 V (WLTC based)	C/2 (1C+C/2 once every fifteen cycles)
7	30		
8	30		
9	30	4.2 – 3.2 V (WLTC-based)	C/2 (1C+C/2 once every five cycles)
10	30	4.2 - 3.2 V (WLTC-based)	C/2 (1C+C/2 once every five cycles)

5.3.1 WLTP focus

Before being marketed, passenger cars and light commercial vehicles undergo a series of tests to ascertain their compliance with the regulations. The tests to evaluate consumption, CO_2 and pollutant emissions are carried out in the laboratory and are based on specific driving cycles. In this way the tests are reproducible and the results comparable. This is important as only a laboratory test, which follows a standardized and repeatable procedure, allows consumers to compare different car models.

On 1 September 2017, the new WLTP procedure came into force, replacing the NEDC protocol (New European Driving Cycle).

WLTP uses new Worldwide Harmonized Light-duty vehicles Test Cycles (WLTC) to measure fuel consumption, CO_2 emissions and pollutant emissions of passenger cars and light commercial vehicles. The new protocol aims to provide customers with more realistic data, better reflecting the daily use of the vehicle.The new WLTP procedure is characterized by a more dynamic driving profile and with more significant accelerations. The maximum speed increases from 120 to 131.3 km/h, the average speed is 46.5 km/h and the total cycle time is 30 minutes, 10 minutes more than the previous NEDC. The distance travelled doubles from 11 to 23.25 kilometres. The WLTP test consists of four parts according to the maximum speed: Low (up to 56.5 km/h), Medium (up to 76.6 km/h), High (up to 97, 4 km/h), Extra-high (up to 131.3 km/h). These parts of the cycle simulate urban and suburban driving and driving on country roads and highways. The procedure also considers all the optional contents which influence the aerodynamics, rolling resistance and mass of the vehicle, determining a CO_2 value which reflects the characteristics of the individual vehicle. Since this kind of protocol was first designed for Internal combustion engines (ICE) vehicles, to adapt it for e-mobility application, the power consumption of the electric motor is taken into consideration. Figure 45 shows an extract of the current demand of the e-motor of a typical segment-A car. As visible a certain amount of current is extracted by the battery pack, negative current peaks are predominant. It is also notable the presence of sporadic positive current peaks, which correspond to the regenerative breaking which provide back energy to the battery pack.

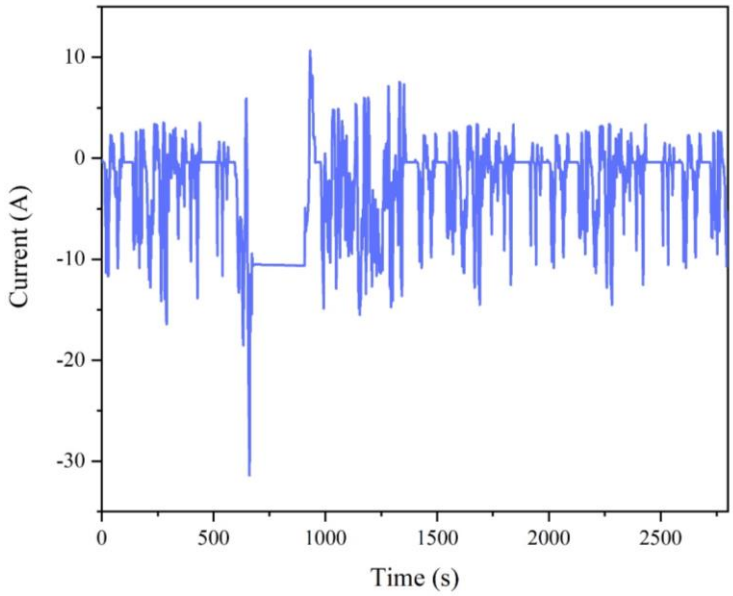

Figure 45 - WLTC driving cycle (Current input)

To summarise, for all the present work, a commercial high-energy-density (215 Wh/Kg) cell with Si/C|EC/DMC (1:1), 1M $LiPF_6$|NMC811 was selected. The choice was primarily guided by three main factors:

- The cylindrical 2.9 Ah cell format and dimension has permitted to work with medium-high levels of safety, compared to other common formats in the automotive field.
- The cell is today mounted on the battery pack of one vehicle of the Stellantis fleet.
- The cell has a chemistry belonging to the 3a generation, according to European standards guidelines[118].

This chapter provided data coming from electrical and physical-chemical analysis performed on the selected cylindrical cell sample, to collect useful information that will be used as a comparison for the future analysis, when the aging results will be showed. Information collected in this chapter are propaedeutics for the following of the work.

6 - DCFC profiles design: data collection

Chapter 6 presents the output obtained by the methodologies used for the charging profile design, experimentally presented in Chapter 4. The information obtained are used to build five charging profiles that are here reported and compared to a Reference charging protocol.

6.1 Method 1: Evaluation of electrode potential measured in a three-electrode cell against a Li/Li^+

Method 1 was adopted to design a tailor-made charging strategy, to define specific limitations to charge the cell with two main results:

- Limitation of charging time;
- Limitation of lithium plating deposition.

The results collected from the three-electrode cell measurements performed with the laboratory scale setup at different C-rates provided information about the relationship between C-rate and cut-off voltage.

The data depicted in Figure 46 were obtained from the cycling of several cells, up to 1.32C (cell capacity 9 mAh). It shows the Si/C vs NMC811 cell (full cell) voltage as a function of time, at different C-rates.

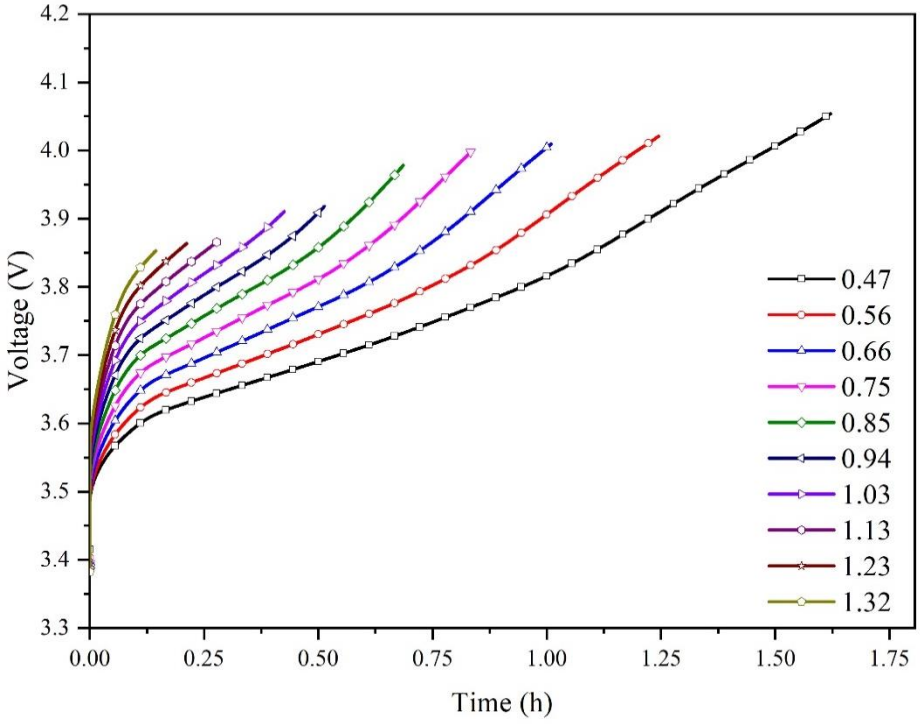

Figure 46 - Si/C vs NMC811 voltage response, at different C-rates

Figure 47 shows the Si/C vs lithium (half-cell) voltage as a function of time, at different C-rates. Looking at the anodic potential, we can extrapolate information about the cut-off voltage we have to select in full cell configuration. Taking as an example only one specific C-rate curve (i.e. 0.56C), on the Si/C vs Li curve (Figure 47), the point when the anodic voltage drops down to zero (vs Li/Li^+) corresponds to point we have to select as cut-off voltage in the Si/C vs NMC811 curve (Figure 46), defining the end of the n-th step in the definition of the multistage constant current profile.

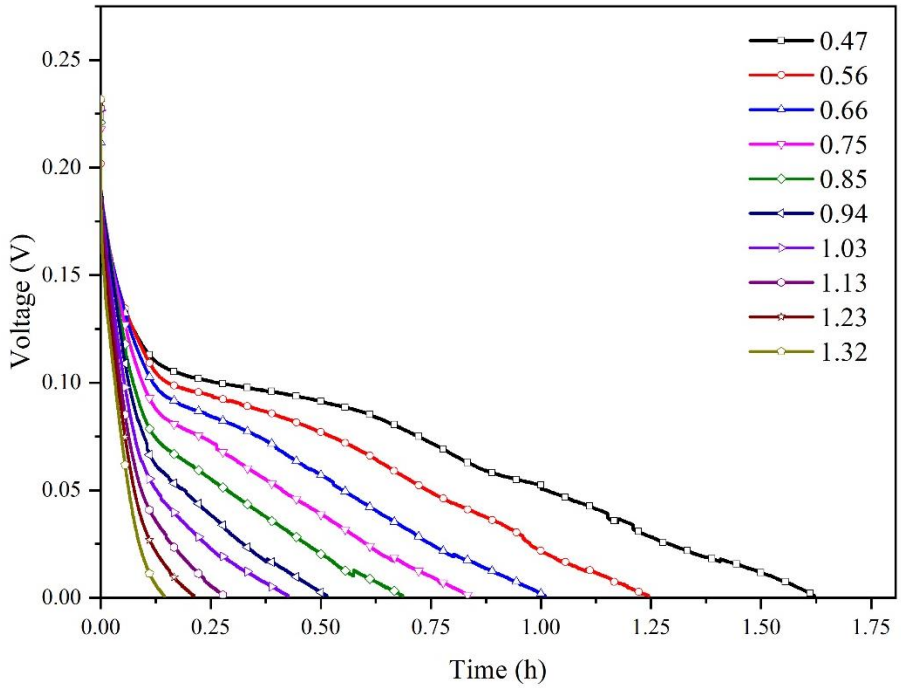

Figure 47 - Si/C vs Li voltage response at different C-rates

6.2 Method 2: Evaluation of the evolution of the DCIR as function of time, during charging process.

The methodology was used in comparison with the present method, to perform a double-check control on the original cell format trying to also find a faster methodology with no need of cell dismantling.

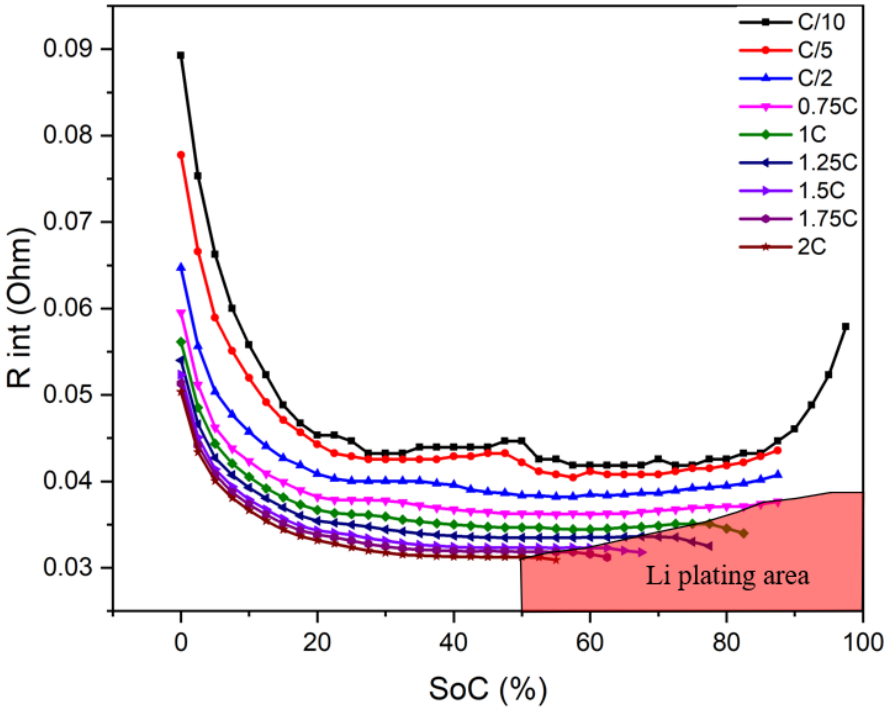

Figure 48 - internal resistance vs SoC%

As mentioned, Figure 48 reports the DC internal resistance of the cylindrical 18650 cell measured at different C-rates, during charge followed by a 3s rest step.

Analysing the internal resistance evolution as function of the SoC%, we can notice the typical "boat trend" of the DCIR, when Li plating is absent. Between 20 and 50% SoC, a general noise in the DCIR response was noticed, shifted at lower SoCs % increasing the current.

This can be attributed to the occurrence of higher overpotentials, because of the different kinetics of the diffusion processes, at the higher currents. Focusing on the right part of the graph, it is visible a decrease in the internal resistance at the highest SoCs%, starting from 1C charge rate, that can be attributed to the incipient lithium plating.

The representation of the internal resistance evolution in function of the SoC%, reported for all the tested C-rates, permits to locate a specific area on the plot, which takes the name of "Li

plating zone" and it is represented by a red limited polygon. This is a "virtual" limitation area which defines "permitted" and "forbidden" areas, when defining the charging steps.

6.3 DCFC profiles definition (MCC charging strategy)

The data and information collected from the methodologies previously described were analysed and used to define new MCC charging profiles, able to be compared to an already tested Reference profile. The data matrix collected permitted to design different charging profiles, respecting the limitations found with the conducted studies.

For the objective of this work, it was decided to design five new charging profiles, used in comparison with one double step standard profile (Figure 49). From now on, it will be called "Reference" profile. It is the charging profile today implemented in the BMS software for the fast charging of the battery pack where the 18650 cells are integrated.

The charging protocols were defined to have a well distributed panorama of profiles trying to propose two alternatives very close to the Reference, in terms of charging time and three profiles to be used when very high current charging is needed.

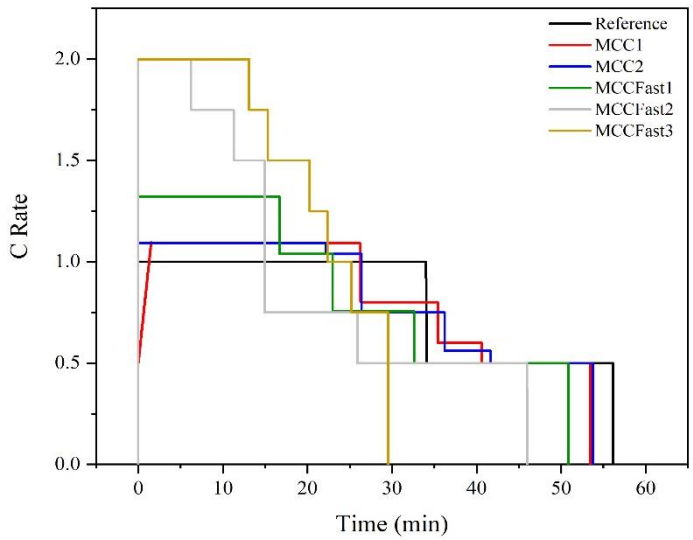

Figure 49 - C rate vs time charging profiles

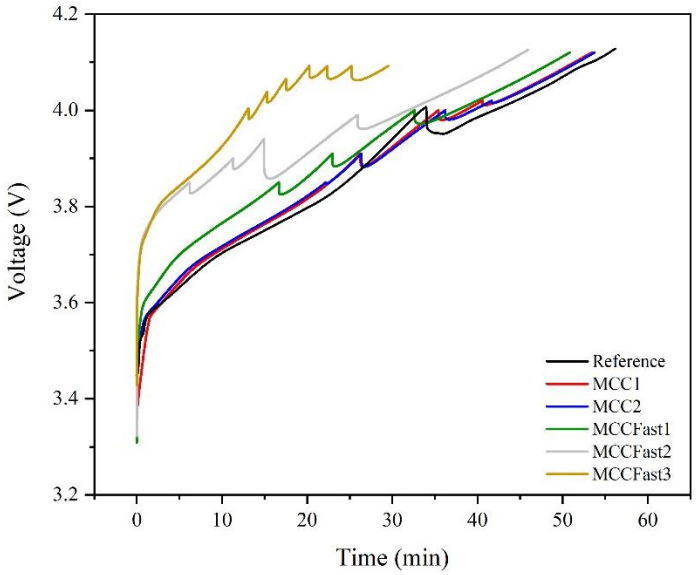

Figure 50 - Voltage response vs time charging profiles

As visible in Figure 50, the Reference profile is composed of a first step at 1C, until 3.9 V, then the end of the charging process is completed by decreasing the current at 0.5C up to 4.092V.

All the proposed charging profiles restore the same amount of energy inside the cell, with a difference in terms of time needed to complete the charge (Figure 51).

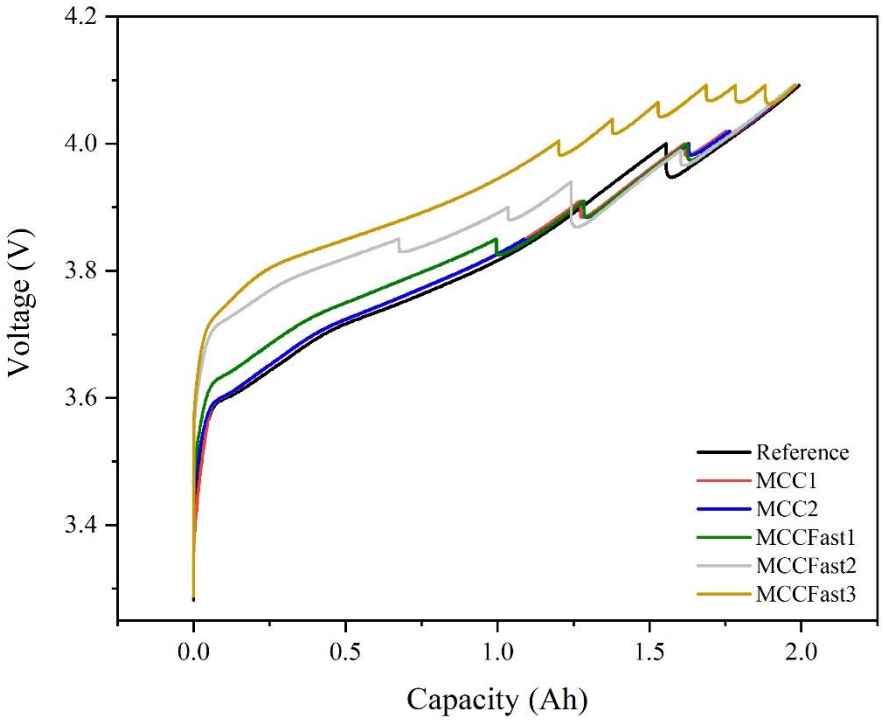

Figure 51 - Voltage vs Capacity

Since the lab scale cell was reproduced after a sequence of dismantling and reassembling operations and the setup used is not optimized as the commercial cell, we decided to consider the internal resistance of the reproduced NMC811 || Si/Graphite cell (EL-Cell setup) as a worst case.

MCC1

The first designed charging profile was obtained from the three-electrode cell (EL-Cell) tests. It was decided to start the charge with an initial current ramp, to guarantee smooth current and voltage increases in the first seconds of the process. The internal resistance test method was used as additional information to fix the cutoff voltages.

MCC2

For the second designed profile the results obtained from the three-electrode cell were used to determine cut-off voltages and current limits. With respect to MCC1, the initial current ramp

was omitted. The cut-off voltage of the first step was decreased to 3.850 V (against 3.910 V of MCC1), a second step was added, and the current in the third step was reduced from 0.600C (MCC1) to 0.560C. Internal resistance measurements were used for a redundancy check on cut-off voltages.

MCCFast1

This third profile was developed to primarily reduce the charging time, maintaining a comparable capacity retention during cycle aging, with respect to the reference profile. As for the previous cases, this profile was designed using data coming from the EL-Cell configuration, cross checking information from internal resistance tests. Here, an initial charge of 1.32C was used, maintaining the same cut-off voltage used for the first step in MCC2.

MCCFast2

To develop the MCCFast2 profile, it was decided to push the MCCFast1 concept up to its charge current limits.

The creation of this profile was performed using data collected from the internal resistance evolution measurements. Since this approach was performed directly on the commercial 18650 cylindrical cell, the degradation effects due to the dismantling of the cell followed by the assembly in the EL-Cell configuration operations caused by the assembling of the EL-Cell were absent, thus the collection of data have permitted the creation of a faster profile. Double check with the EL-Cell three electrode method was performed.

MCCFast3

For designing this profile, the R_{int} vs SoC% test was used, to charge with a very high current, at the beginning of the process.

It was decided to move at the boundary of the “Li plating zone”. The strategy provides a very fast charge profile, able to charge the cell in around 30 minutes.

6.3.1 – The implementation of a derating methodology[128,129]

A derating method consists of improving the battery pack life, by intentionally limiting or reducing the operating working parameters of the battery system, to extend its overall lifespan and enhance its reliability.

This is important in applications where the battery cell longevity is a critical factor, such as in electric vehicles (EVs), renewable energy storage systems, etc.

When a derating function is implemented, the aim is to permit the battery system to operate in less stressful conditions, with respect to the initial working conditions.

Generally, this approach can help mitigating factors that contribute to degradation and aging:

- High temperatures;
- High charging/discharging rates,
- Deep charge/discharge cycles.

By operating the battery cell within a "comfortable" range, degradation processes can be slowed down, leading to a longer lifespan.

Literature suggests some derating strategies, commonly employed to improve battery pack life:

- Temperature Control: Working within an optimal temperature range can significantly improve the lifespan.
- Charging and Discharging Rates: Limiting the charging/discharging rates can reduce stress on the electrodes and electrolyte, helping to preserve their integrity over time;
- State of Charge (SoC) limits: Working within a restricted state of charge window (avoiding full charges or complete discharges) help minimizing chemical side reactions, such as lithium plating and electrode material mechanical damaging.
- Voltage Limits: Setting the proper voltage limits can be helpful in avoiding overcharging or over discharging.

Usually, a derating function aim to find a correct balance between the maximization of the cell performances, ensuring a long-term reliability.

For the scope of this work, two approaches are tested, in order to start appreciating the implementation of a derating methodology on the applied charging protocols.
Specifically, the derating function is implemented only on MCCFast3 charging protocol, which is the most stressful attempt proposed.

- Derating based on both the reduction of the cell capacity and by the scaling of the cut-off voltages for each step of the charge protocol (every 150 cycles (Cell MCCFast3A);
- Derating limited to the reduction of the cell capacity every 150 cycles (Cell MCCFast3B).

Since MCCFast3 charging protocol was designed to extreme the limits imposed by the Li ion cell selected, the two derating attempts were included to study their effects in terms of degradation.
For comparison, a third cell (MCCFast3C) was aged with no derating function application.
Results will be showed later.

Table 8 - DCFC profiles

C-Rate	Cutoff Voltage [V]
Reference	
1.000	3.900
0.500	4.092
MCC1	
From 0.500 to 1.090	Slope = 6.6×10^{-3}
1.090	3.910
0.800	4.000
0.600	4.020
0.500	4.092
MCC2	
1.090	3.850
1.038	3.910
0.750	4.000
0.560	4.020
0.500	4.092
MCCFast1	
1.320	3.850
1.038	3.910
0.756	4.000
0.500	4.092
MCCFast2	
2.000	3.850
1.750	3.900
1.500	3.940
0.750	3.990
0.500	4.092
MCCFast3	
2.000	4.004
1.750	4.039
1.500	4.092
1.250	4.092
1.000	4.092
0.750	4.092

The designed DCFC profiles, summarized in Table 8, were tested by the implementation of an established aging protocol, performed on two batches of commercial cylindrical cells.

To start the aging program, a preliminary measurement of each cell capacity was performed, for all the following comparisons. The aging protocol was formed as follow:

- Charging: performed by applying for each cell, one of the profiles described above;
- Rest: each charging phase was followed by a resting time (30 min);
- Discharging: at the end of the resting time, the cell discharge started at 1 C up to a voltage value equal to 2.98 V;
- Rest: the discharging phase was followed by a resting time (30 min).

This sequence was repeated in a loop. During the aging (cycle life), a capacity check was performed, often known as reference performance test (RPT), to control the state of health (SoH). It was decided to perform a quite short verification for cell heath status control.

For the first batch it consisted on:

- Standard charge C/2 CCCV up to 4.2 V (CV step end condition at I < C/100);
- CC discharge at the expected 1C down to 2.5 V.

The 1C discharging rate used for the discharge does not represent a significant stress for this high-energy-density Li-ion cell, according to the datasheet of the product (3C is the maximum current accepted at 25°C, not for prolonged cycle life). Nevertheless, since the discharge procedure was commonly applied to all the samples' matrix, we can consider a comparable aging effect, with possibility to compare the test results reciprocally.

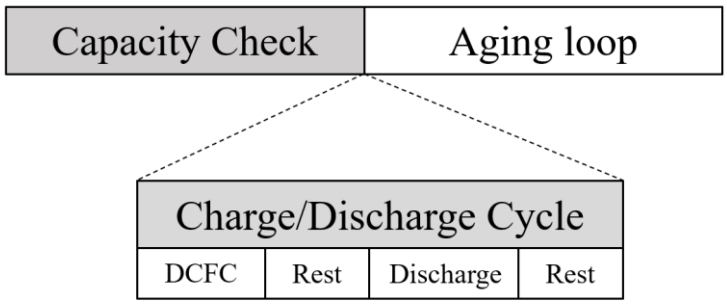

Figure 52 – Cycle aging loop

Figure 52 shows the loop implemented on the battery cycler station, to age the cells for a long period of time. The aging loop among capacity checks was described above. Every cycle charge-rest-discharge-rest sequence was repeated 75 times before the capacity check.
For the second and principal cycle aging campaign some changes were adopted, both in the cycling and during the capacity check.
It was decided to:

- Calculate the incremental capacity analysis at the beginning of life (BOL) and at the end of life (EOL);
- Cycling the cells for 50 cycles before going to the capacity check;
- Performing the capacity check at lower C-rates.

This chapter collected the information obtained by the application of the methodologies described in chapter 4. Inputs coming from both techniques were compared and integrated to design five fast charging profiles, proposed as alternatives to be confronted with a "Reference" charging protocol. Details about the charging steps used and information about the cycle aging structure were here reported.

7 - Cycle aging results and *post-mortem* analysis

Chapter 7 reports information about the cycle aging test performed after the implementation of the proposed charging strategies to the selected samples.
At the end of the cycle aging campaign an extensive post-mortem analysis is reported, both using non-destructive and destructive techniques. All the proposed methodologies are here described with a comparison to the BOL sample conditions, in order to better appreciate the entity of the aging, for each EOL sample analysed. Data are reported by collecting all the samples together, method by method, to ease the evaluation.

The first batch of cells was aged for 500 cycles, for the evaluation of the electric performances and for collecting repeatable data to ensure the methodology and the good manufacture. This aging campaign requested the implementation of three cells for each profile, cycled and tested every 75 cycles, to verify the stability of the samples and procedure. Since the results have a small standard deviation (0.075), this confirmed the good reproducibility of the manufacturing process for the selected cylindrical 18650 cell.
During this first aging campaign the attention was focused on the capacity loss, after 500 cycles. Some cells were dismantled to appreciate Li plating at the visual inspection.
Meanwhile a second batch of cells was aged for 1000 cycles (or up to 80% SoH), to enlarge the experimental matrix and to focus the attention on the *Post-mortem* analysis, at the end of the cycling campaign. During the second batch aging campaign, a further charging profile was added (MCCFast3), to have a comparison with a faster charging protocol (around 30 minutes vs almost 60 minutes for Reference charge).
Even if the first batch reached a limited number of cycles (500), not sufficient to age the cells arriving at the end of their life (EoL), it was useful to highlight the differences among the charging profiles selected for the present study.

7.1 Capacity fade trend

Figure 53 shows the results coming from the first aging campaign, performed up to 500 cycles.

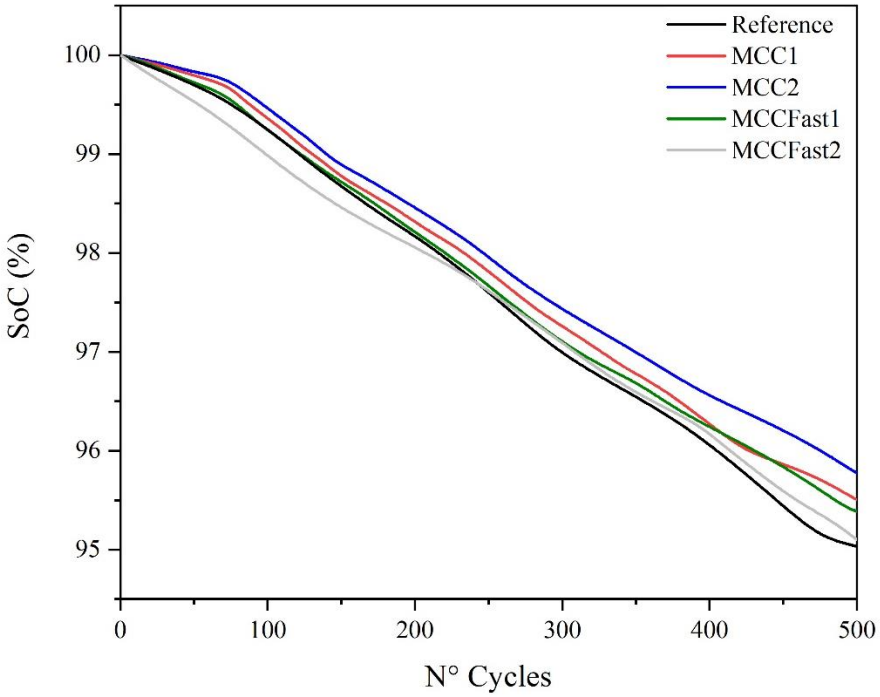

Figure 53 - first cycle aging campaign, up to 500 cycles

The SoH% value was calculated as follow:

$$SoH = \frac{(Measured\ capacity)_i}{(Measured\ capacity)_0}$$

Where the $(measured\ capacity)_i$ corresponds to the value expressed in Ampere per hour (Ah) measured at the n-th capacity check, then normalized by the $(measured\ capacity)_0$, which is the value measured at the beginning of the cell life (first capacity check value).

The first aging campaign showed how the MCC1 and MCC2 profiles presented the best results in terms of capacity retention, with a reduction in the charging time with respect to the Reference profile of 3 minutes.

MCC2 is the profile which preserved the highest capacity, after 500 cycles. MCCFast1 presented a capacity comparable to the Reference profile up to 250-300 cycles, saving 6 minutes

on the charging time. From 300 to 500 cycles the aging trend presented some differences, with MCCFast1 which better preserved the capacity during the cycling.

MCCFast2, after an initial pronounced capacity fade, hypothetically due to the highest C-rate (2C up to 3.850 V), arrived at 500 cycles with a retained capacity higher than the cells aged with the Reference profile.

Figure 54 shows a comparison in terms of capacity measured after each cycle (for charge and for discharge) between Reference and the two comparable charging profiles, from 0 to 75 cycles. MCC1 and MCC2 also presented a better charge-discharge capacity.

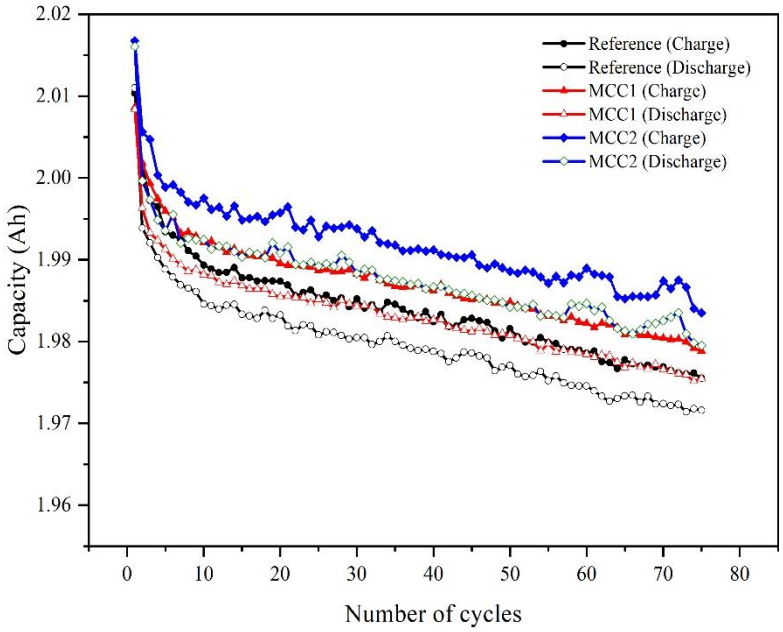

Figure 54 - Capacity throughput during one step of cycling

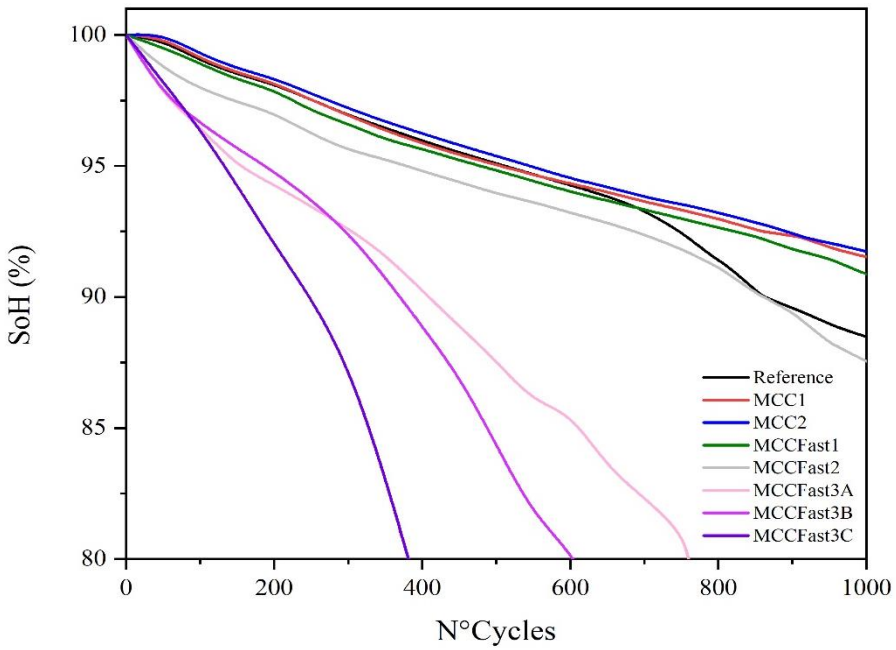

Figure 55 - second cycle aging campaign, up to 1000 cycles (or 80% SoH)

The second cycle aging campaign, implementing the DCFC profiles designed, showed the trend visible in Figure 55. It is possible to appreciate the presence of a linear trend aging up to 1000 cycles for MCC1, MCC2 and MCCFast1 samples. As expected MCCFast2 and Reference DCFC profiles significantly aged the cells, showing a severe slope change around cycle number 700. Generally, literature[68,75,76,79,130,131] reports the solid electrolyte interphase (SEI) formation as major responsible for a linear aging trend. The change in the aging trend, visible in the graph SoH% vs n° cycles by a slope increase, indicates the upcoming irreversible lithium plating phenomenon[79,132], with relative loss of cyclable lithium and thus capacity fade. MCCFast2 started with the worst capacity retention, because of the high applied C-rate (2C) at the beginning of the charge. The hypothesis for this fast capacity loss just after a few cycles could be attributed to the occurrence of concurrent phenomena, both at the cathode and at the anode side. From the cathode side, NMC secondary particles, during the first cycles, could tend to crack themselves, permitting the liquid electrolyte to permeate among the cracks, forming new SEI, which means loss of active lithium[133]. At the same time, even if the profile was designed

to avoid Li plating, the geometry could affect the cell behaviour. A plane geometry electrode will not be subjected to the same mechanical stress of a spiral shape electrode, as inside a cylindrical cell. Here, the hypothesis could be related to the presence of high deformation areas, in particular in the inner rolls of the electrode foils, where the pressure is higher and some local inhomogeneities could promote the formation of Li plates[134]. Even if MCCFast2 started with the worst capacity retention, Figure 55 shows how it arrived at 1000 cycles with a capacity loss like the Reference.

7.2 Incremental capacity analysis results

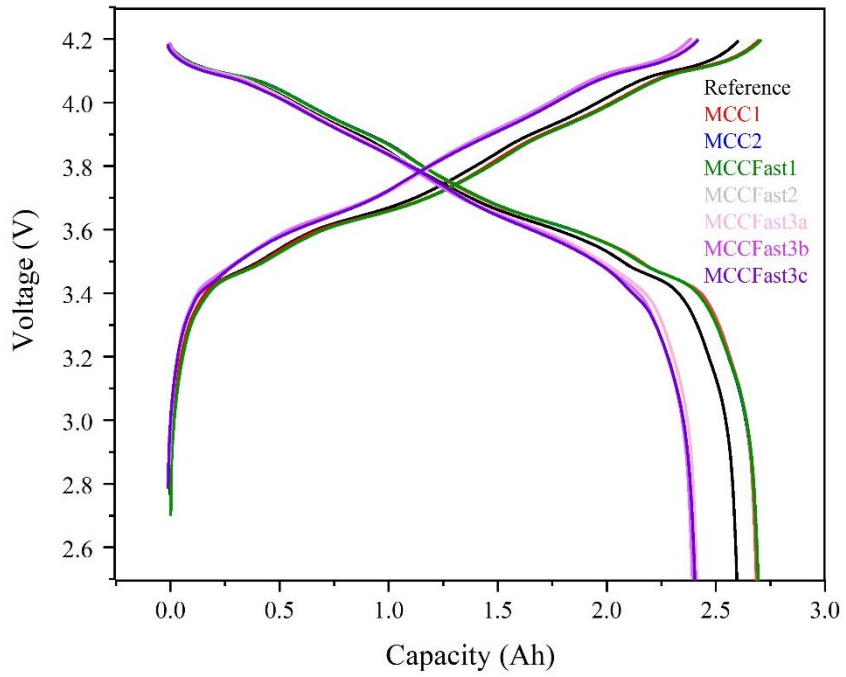

Figure 56 - voltage vs capacity curves

Figure 56 resumes the voltage vs capacity curves for Reference, MCC1, MCC2, MCCFast1, MCCFast2 and MCCFast3 profiles. It is evident how MCCFast3, which was implemented to

have a charging procedure able to restore the 100% of the energy within 30 minutes, aged significantly with respect to the others, reaching the 80% SoC before 1000 cycles.
MCC1, MCC2 and MCCFast1 arrived at 1000 cycles with a very comparable capacity. Reference and MCCFast2 demonstrated to have a very similar capacity retention.

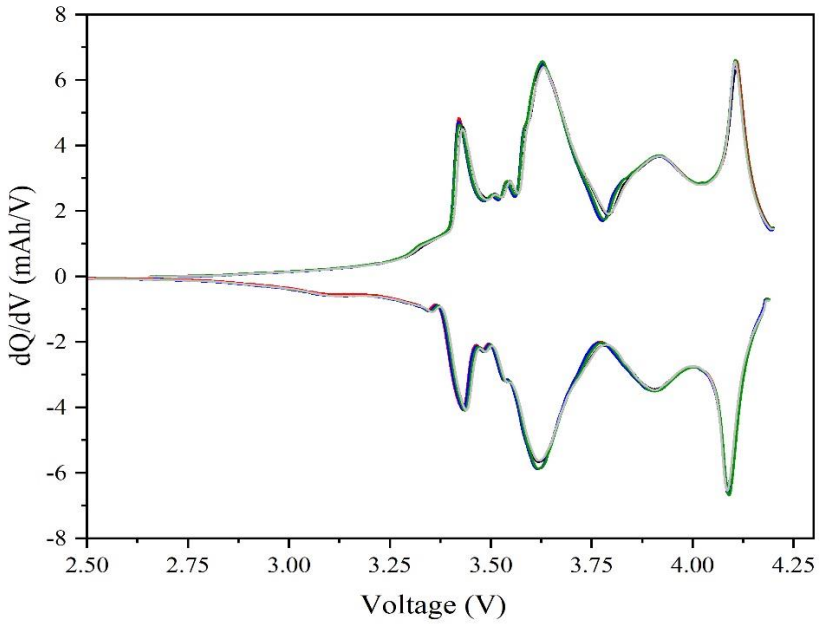

Figure 57 - incremental capacity analysis for BOL conditions cells

Before reporting the results linked to the End-of-Life (samples), the plot with the ICA trend for all the tested samples at their Beginning of Life (BOL) was here reported (Figure 57), in order to exclude misunderstandings in the interpretation of results at the end of the cycle aging campaign. The ICA response for BOL conditions sampled from all the tested cells shows a very good overlapping of the curves, indication of a very reproducible trend, symptom of good manufacturing.
To compare all the results coming from the testing charge protocols (EOL condition), in Figure 58 only one BOL curve was included, as comparison, visible with an orange line.

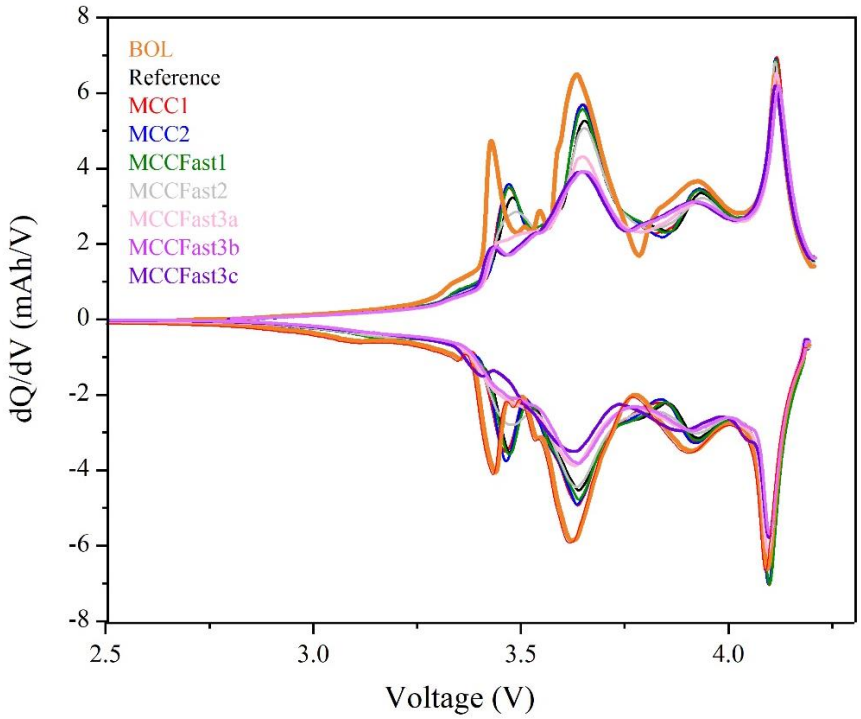

Figure 58- incremental capacity analysis for EOL conditions cells

All the tests highlighted in Figure 58 were performed on 18650 cells.

To better visualize data, ICA responses are plotted by groups here below.

Figure 59 shows ICA responses for MCC1, MCC2 and MCCFast1 cells, versus BOL conditions.

Given that these cells reached 1000 cycles respectively at 91.53, 91.74 and 90.88% SoC, with a very close retained capacity, they present a general peak shift to higher voltages, with respect to BOL.

The shifting trend can be indicative of an internal resistance increment inside the cell, because of the interdependency of multiple aging factors linked to the cycling. The prolonged aging, even if conducted with charging profiles designed and customized for the tested cells, induced a concurrent shift and area reduction of the peaks from I to III.

Generally, the area reduction is commonly linked to loss of active material phenomenon, inducing a decrease in the cell capacity.

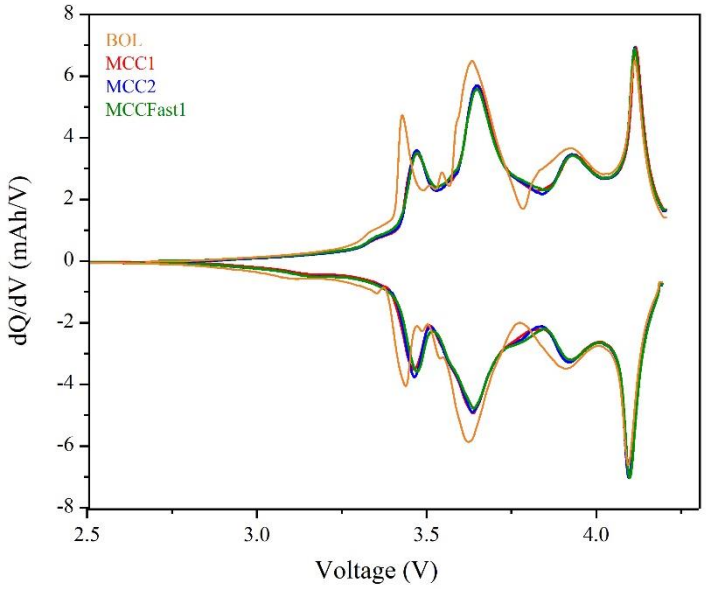

Figure 59 - ICA trend for MCC1, MCC2, MCCFast1 cells (vs BOL)

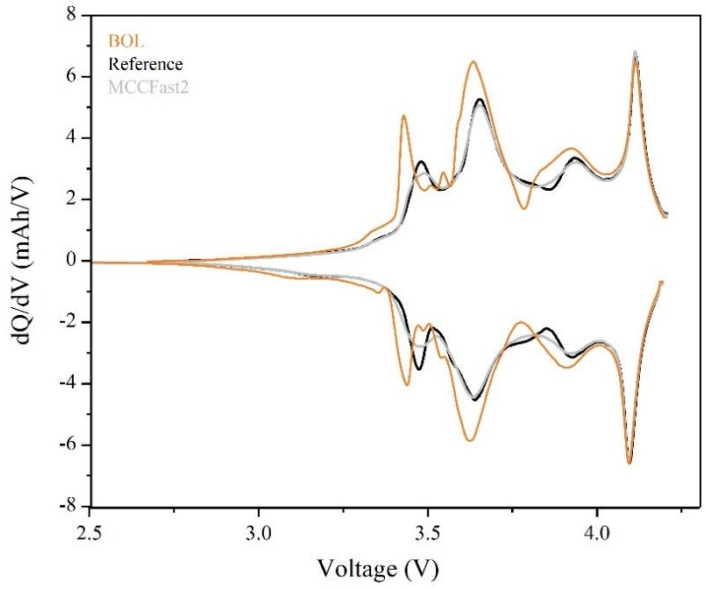

Figure 60 - ICA trend for Reference and MCCFast2 cells (vs BOL)

Figure 60 shows the output at the ICA test of Reference and MCCFast2 samples. They reached 1000 cycles respectively at 88.48 and 87.55% SoC.

With respect to the results showed in Figure 59, anode peak presents a little heavier depression, symptoms for a more severe aging condition on the graphite electrode. At the same time cathode peaks presented a reduced peak area.

This trend is much more visible in Figure 61, where MCCFast3 protocol (in the three testing conditions) is showed. As expected, given the severity of the applied protocol, the ICA response is in line with the health status of the samples (around 80% SoC%).

With respect to BOL conditions, graphite peak appear almost absent, index of a significant anode aging, with high possibility of Li plating presence.

NMC presented depressed peaks, symptoms of degradation.

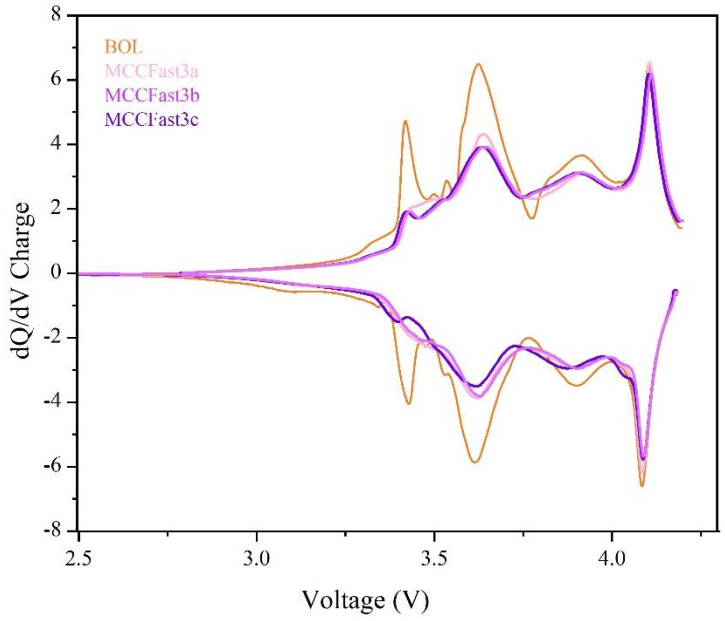

Figure 61 - ICA trend for MCCFast3 cells (vs BOL)

Generally, peak areas results reduced, in comparison to BOL sample, proportionally to the severity of the applied protocol.

The first peak (at 3.4V) highlighted the occurrence of Li plating, when present, confirmed also by the *post-mortem* analysis.

It was observed that the cells with no Li plating presented only peak shift (higher resistance) and area reduction, which can be linked to SEI formation during the cycle aging.

When Li plating is present, the peak shift effect was almost absent. The hypothesis for this can be linked to the limitation of intercalation reaction inside graphite (with decrease in internal resistance). At the same time an important peak area depression is visible, indication of a loss of active lithium.

An important decrease in the peak area indicates a loss in the Li intercalation ability, suggesting that a portion of the active lithium was lost in the plating reaction on the graphite surface.

On the contrary, the Peak IV, attributed to the H_2 -> H_3 phase transition, did not present a huge decrement, as for the other peaks, remaining almost equal to BOL conditions.

No significant detrimental lattice shrinkage along the c-direction occurred, as indicated in literature[135–137].

When working with high nickel content NMCs, the phase transition from H_2 to H_3 can lead to (003) peak shift to higher degrees, accompanied by Li reordering (Li diffusing into Ni^{4+}-rich sites) that can further convert H_3 to $H_{3\text{-}2}$. A fast shrinkage of the c-axis at potentials above 4.15 V is a clear indication of this phase transition.

Furthermore, the generated microregion of NiO_2 in the intralayer of the NMC811 lattice (because of the phase transition from H_2 to H_3) can lead to an irreversible transformation of the NMC811 structure.

This phase transition becomes severer as Ni portions further increase to extreme numbers as indicated by rising peaks of the differential capacity curve centred at 4.15 V. Here, the fading of this peak leads to capacity fade and is referred to as the “deleterious effect.”

Given that the charging protocols were designed to stop the charge step at 4.092 V, no severe damages occurred at the cathode structure.

7.3 Impedance spectroscopy (EIS) interpretation

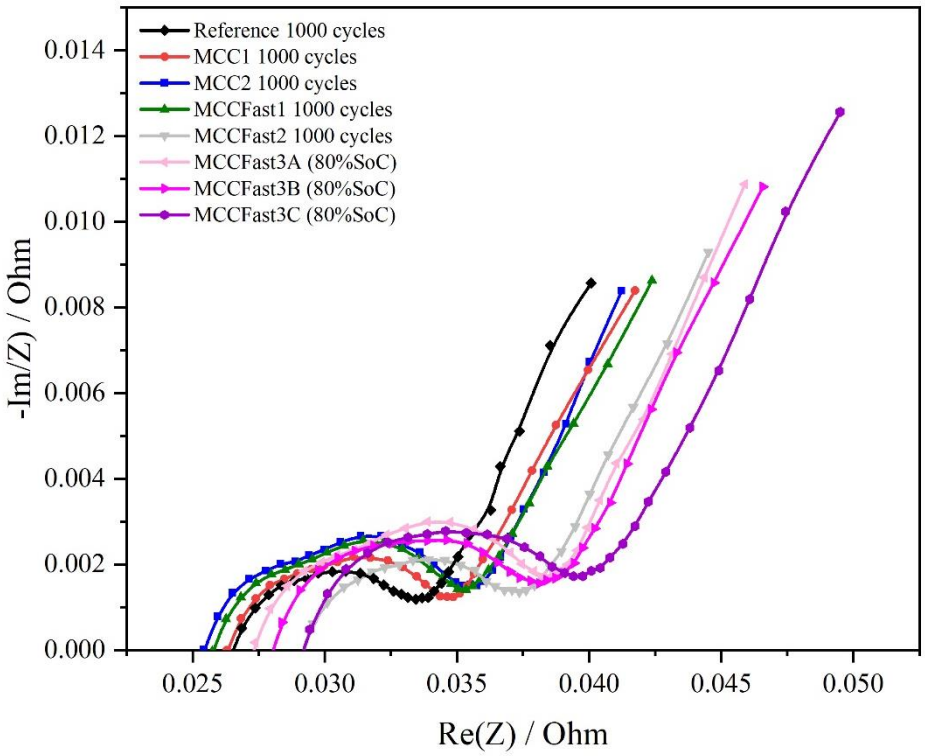

Figure 62 - EIS Nyquist plot response

Figure 62 shows the impedance spectroscopy performed on the cycled cells. After 1000 cycles (and 80% SoC for MCCFast3), the charging protocols caused different aging to the cells.

It is evident that the electrolyte resistance (R_{ohm}) varies in the range between 25 to 30 mOhm.

EIS data were fitted by using the equivalent circuit already described in Figure 27.

For what concern the electrolyte resistance, MCC2 seems to have maintained the best performances, with the lowest resistance, as visible by the fitting results displayed in Figure 63. This can be indicative of the proper design of the charging profile.

MCCFast1 and MCC1 cells presented an electrolyte resistance intermediate between MCC2 and Reference sample, confirming the SoH% trend observed after 1000 cycles.

As expected, the tailoring of the charging strategy influences positively the aging behaviour, enhancing and prolonging the cycle life.

MCCFast2 charging strategy, as expected, had a significant impact on the cell performances, with an electrolyte resistance around 29 mOhm, after 1000 cycles.

MCCFast3 protocol demonstrates a proportion aging behaviour, showing a pronounced electrolyte resistance for MCCFast3C protocol, where no derating functions were implemented. MCCFast3A, which aged by taking care of a derating function based both on cell reduction capacity and by reducing the cut-off voltage of each charging step, when needed, behave better (more cycles at the 80% SoC). MCCFast3B, which was derated only by reducing cell capacity along the cycle aging, presented an intermediate condition, as expected.

As a general comment, when an increase of ohmic resistance is observed, one of the hypothesis is that the loss of lithium to form side reactions (SEI, Li plating) could have caused a decrease in the conductivity of the electrolyte, as reported[138].

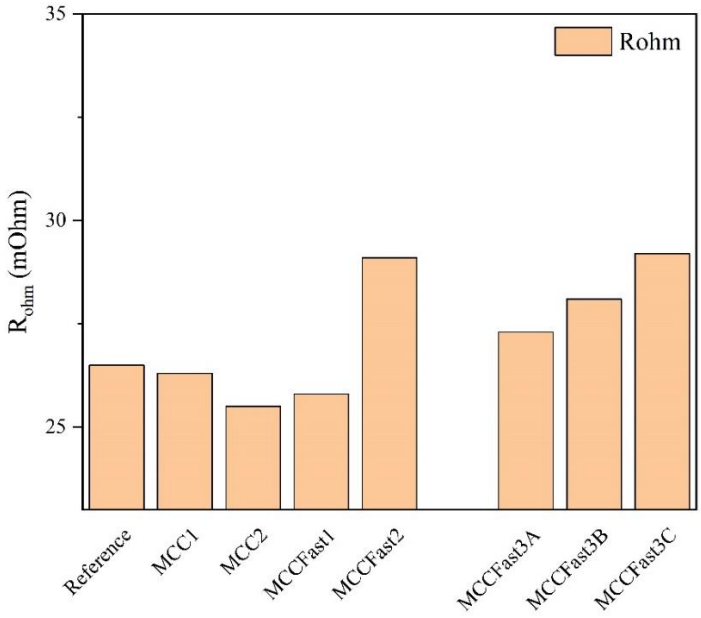

Figure 63 - Ohmic resistance from fitting of EIS measurements

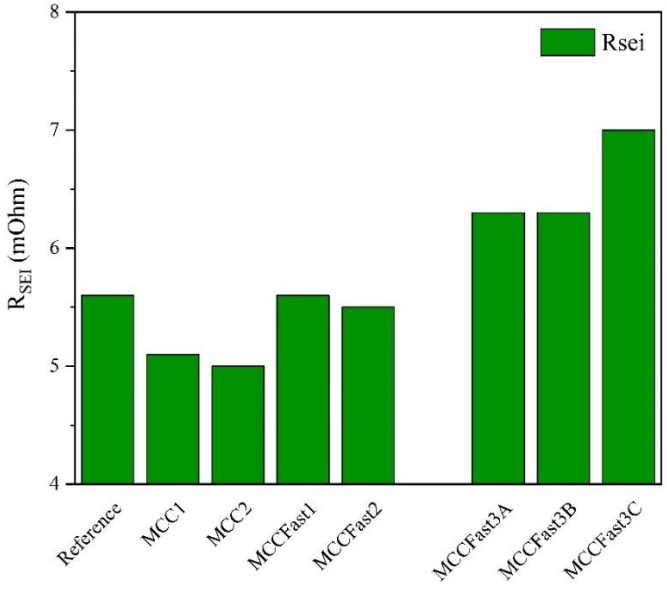

Figure 64 - SEI resistance from fitting of EIS measurements

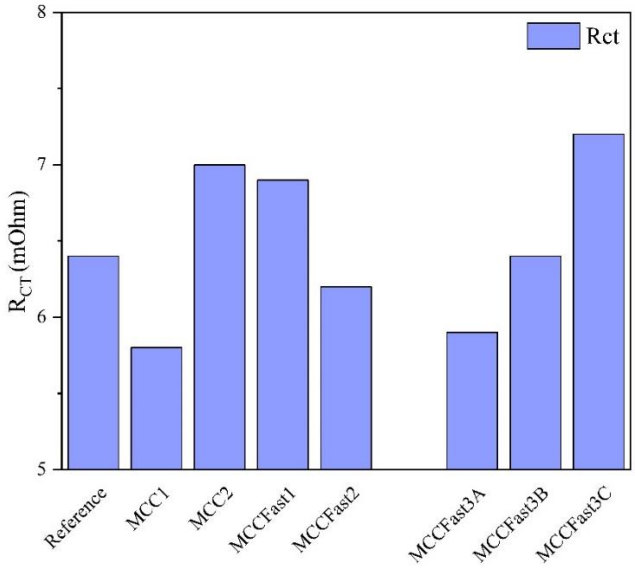

Figure 65 – Charge transfer resistance from fitting of EIS measurements

In the high and medium-frequency ranges, the two semicircles (overlapped in the analysis reported in Figure 62) represent the total interfacial resistance from the solid electrolyte interphase (Rsei) and the charge transfer resistance (Rct), respectively.

Figure 64 suggests that an increase in the SEI thickness for Reference, MCCFast1 and MCCFast2 occurred, in line with the applied protocols.

MCCFast3, that was designed to completely charge the cell in 30 minutes (high applied C-rates) presents the worst conditions in terms of SEI thickness. MCC1 and MCC2, designed to replace Reference protocol, present the best SEI conditions, confirming to be a valid alternative.

At medium frequencies the charge transfer resistance is visible. As reported[139], the R_{ct} behaviour can be linked to material loss. Structural/mechanical degradation, chemical dissolution/decomposition and lithium loss can be translated into an increase of R_{ct}, generating a worsening of the cell conductivity.

Generally, this can cause an increase of transport obstacle con ions and electrons, translating in partial inactivity of active material and contact loss.

Figure 65 shows that all charging protocols perform in a very similar manner, with values of R_{ct} between 5 and 7 mOhm, for the worst cases.

Surprisingly, MCC2 presents one of the worst values, suggesting some electrode degradation which will be further investigated by other analysis.

7.4 Internal resistance vs SoC% results

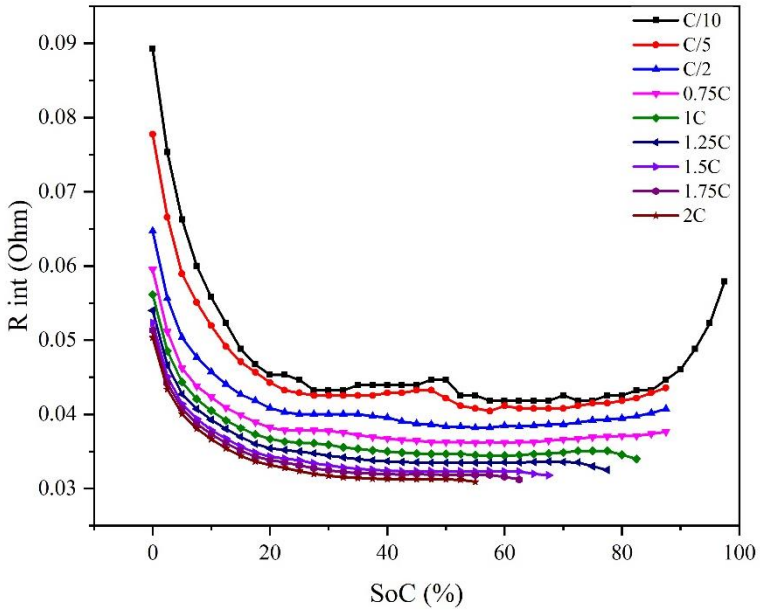

Figure 66 - Internal resistance Rint vs SoC(%)

The internal resistance vs SoC (%) method used to define the charging protocols was also implemented at the end of the cycling campaign, with a double objective:

- Aging evaluation test;
- Derating method.

Figure 66 shows the internal resistance trend as a function of SoC%, for different C-rates. It is visible the typical behaviour of the ohmic resistance, which tends to decrease passing from lower to higher SoCs, with a final increment when reaching the highest voltages. Generally, the internal resistance is affected by the state of charge and the relationship is not necessarily linear. At the lowest state of charge, when the anode is empty from Li ions and the cell is discharged, the internal resistance tends to be higher. This can be explained with a low amount of mobile lithium ions available for the electrochemical reactions driving the current flow. This limited

availability can result in an increased resistance to the movement of electrons and ions within the cell.

When reaching mid-state of charges, the internal resistance typically decreases. In this case, more lithium ions are available, allowing for better ion mobility and lower resistance to current flow.

When arriving to the highest state of charges, when Li ions populate the anode, the cell internal resistance may increase again.

This can be mainly attributed to the occurrence of side reactions occurring when charging (electrode degradation, formation of undesirable compounds, changes in the SEI layer), which can all contribute to higher internal resistance.

As mentioned, when Li plating occurs, an instant decrease in the ohmic resistance is observed, as reported in literature[140]. For the BOL cell, it was observed that at 1C charge, around the 80% SoC the cell starts to suffer from Li plating.

After 1000 cycles, the internal resistance vs SoC (%) test was repeated, in order to control the status of each single cell, focusing on how the charging methods influenced the samples.

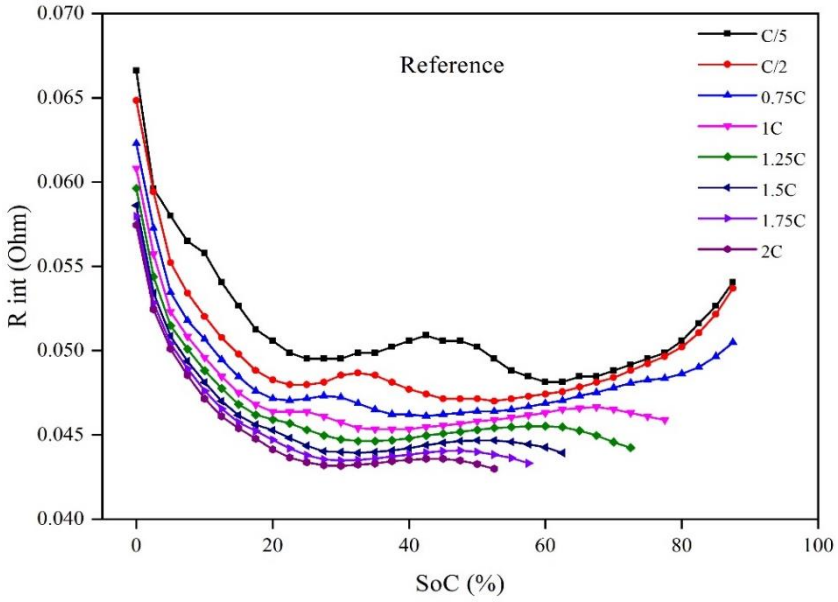

Figure 67 - Internal resistance vs SoC% for Reference sample

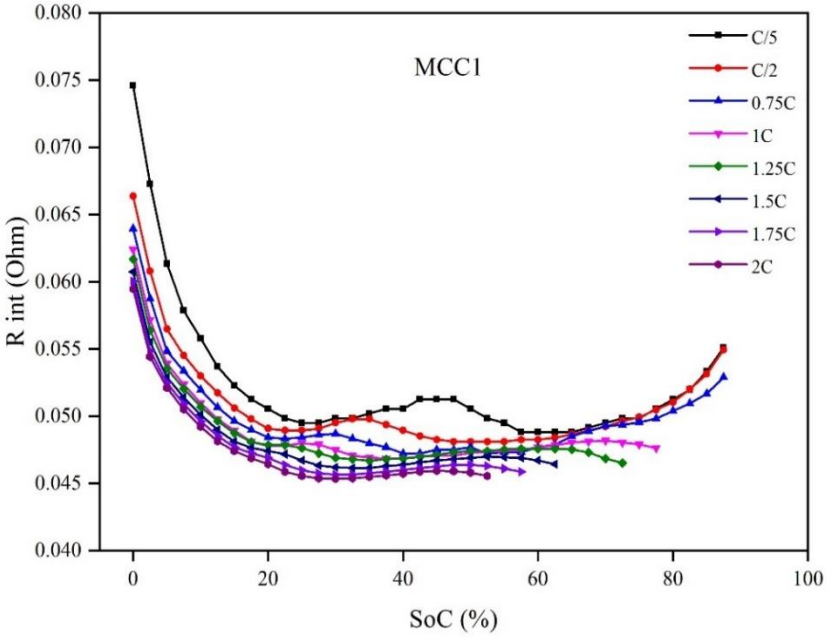

Figure 68 - Internal resistance vs SoC% for MCC1 sample

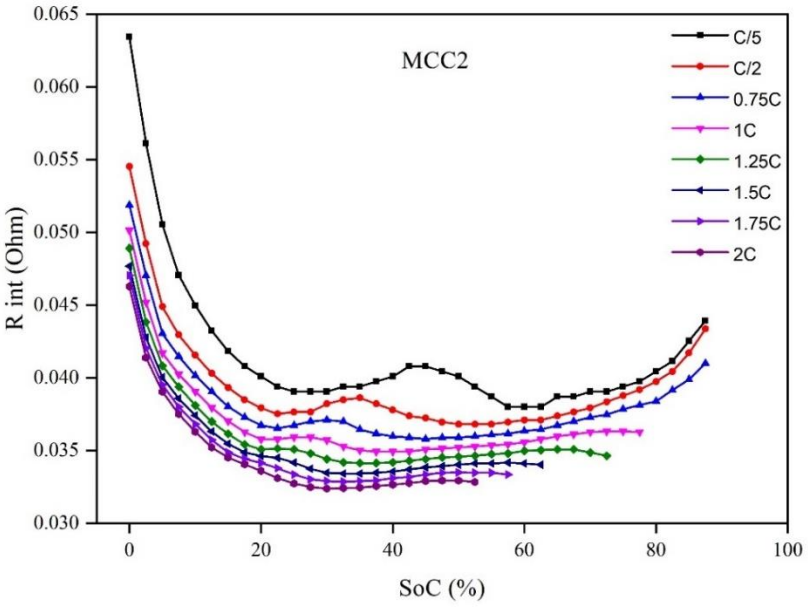

Figure 69 - Internal resistance vs SoC% for MCC2 sample

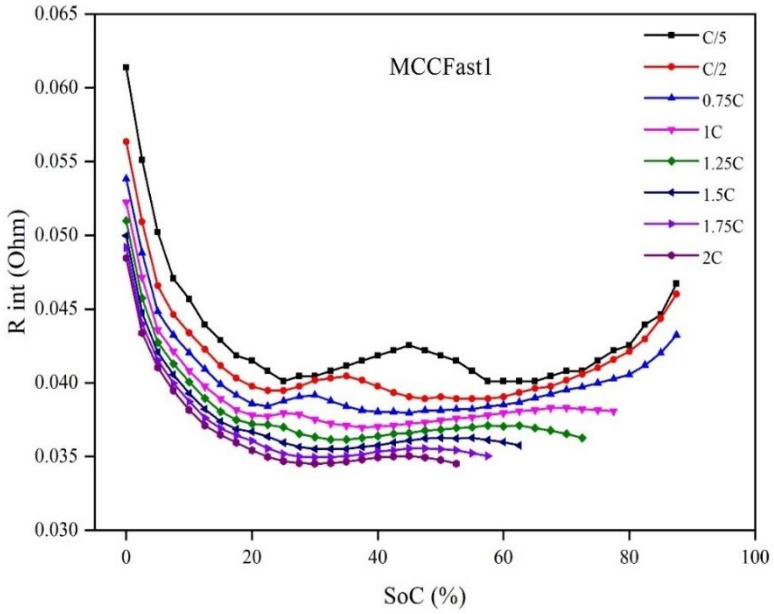

Figure 70 - Internal resistance vs SoC% for MCCFast1 sample

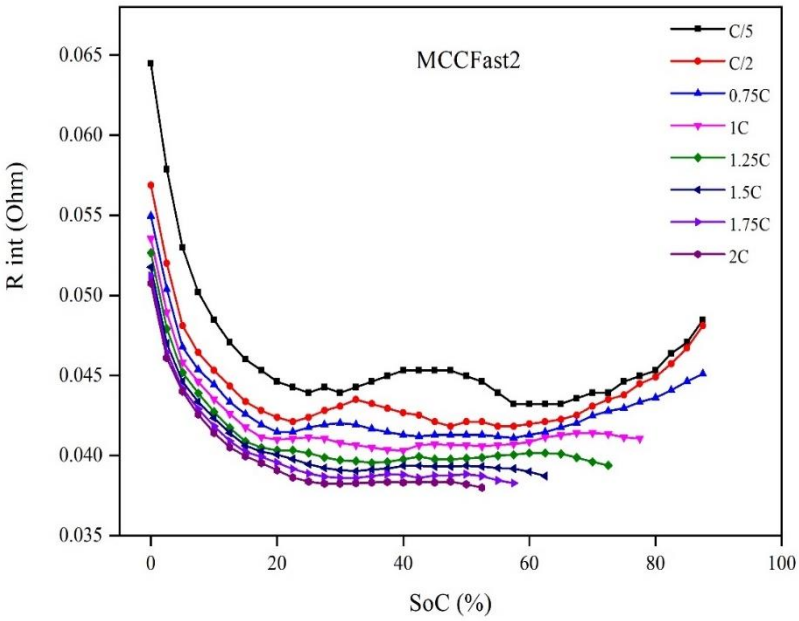

Figure 71 - Internal resistance vs SoC% for MCCFast2 sample

Looking at the internal resistance vs SoC(%) curves after the end of the cycling campaign, the data collected from the cycled cells present some significant differences, with respect to the BOL sample (Figure 66).

From Figure 67 to Figure 71 the internal resistance vs SoC% trend for the aged cells are reported.

Considering for instance the 1C curve for all the samples it was possible to compare the onset of Li plating (visible when a plateau in the internal resistance vs SoC% plot is reached), in Table 9.

Table 9 - Onset Li plating SoC% for the EOL samples

Cell condition/Charging protocol applied	C-Rate	Onset Li plating SoC%
BOL	1C	75-78
EOL - Reference	1C	65
EOL - MCC1	1C	70-72
EOL - MCC2	1C	75-78
EOL- MCCFast1	1C	70-72
EOL- MCCFast2	1C	70

It was found that Li plating occurred sooner for Reference and MCCFast2 cells, data in accordance with the aging trend observed. This can be an indication of the main driver for sudden loss of capacity.

If compared to the other samples, Reference suffered from this phenomenon between 5 and 10% SoC before, with respect to the others (MCC1, MCC2, MCCFast1).

MCC2 exhibited the best performances, retaining a very similar behaviour, comparable to the BOL conditions.

Even if the data collected were obtained by scaling (derating) the current based on the measured retained capacity after 1000 cycles, the inversion in the slope of the internal resistance trend at the highest C-rates (above 1C) takes place at lower SoCs, if compared to the BOL conditions.

As expected, a simple reduction of the current based on the measured capacity (Ah) is not sufficient to develop a proper derating function. To prevent irreversible lithium plating formation, a change in the cut-off voltage (or alternatively a more pronounced current reduction) is needed to protect the cells over their lifetime.

7.5 Visual inspection

After non-destructive tests, the cells were dismantled for the post-mortem analysis of materials. Each single cell was torn down by removing the external aluminium can, opened with a cutting tool from the superior cap, to have the entire jellyroll. Figure 72 reports the anode foils conditions, for all the cells. It is notable the presence of lithium plating (red arrow) for Reference and MCCFast2 DCFC cycling conditions.

These samples presented a significant amount of lithium deposition on both electrode sides (10 x 3 cm^2). MCCFast1 showed a very limited initial lithium plating zone. MCC1 and MCC2 (except for a very narrow line in case of MCC2 sample) does not present absence of lithium deposition.

Cathode foils present loss of active material adhesion, which tend to remain adherent to the separator foil.

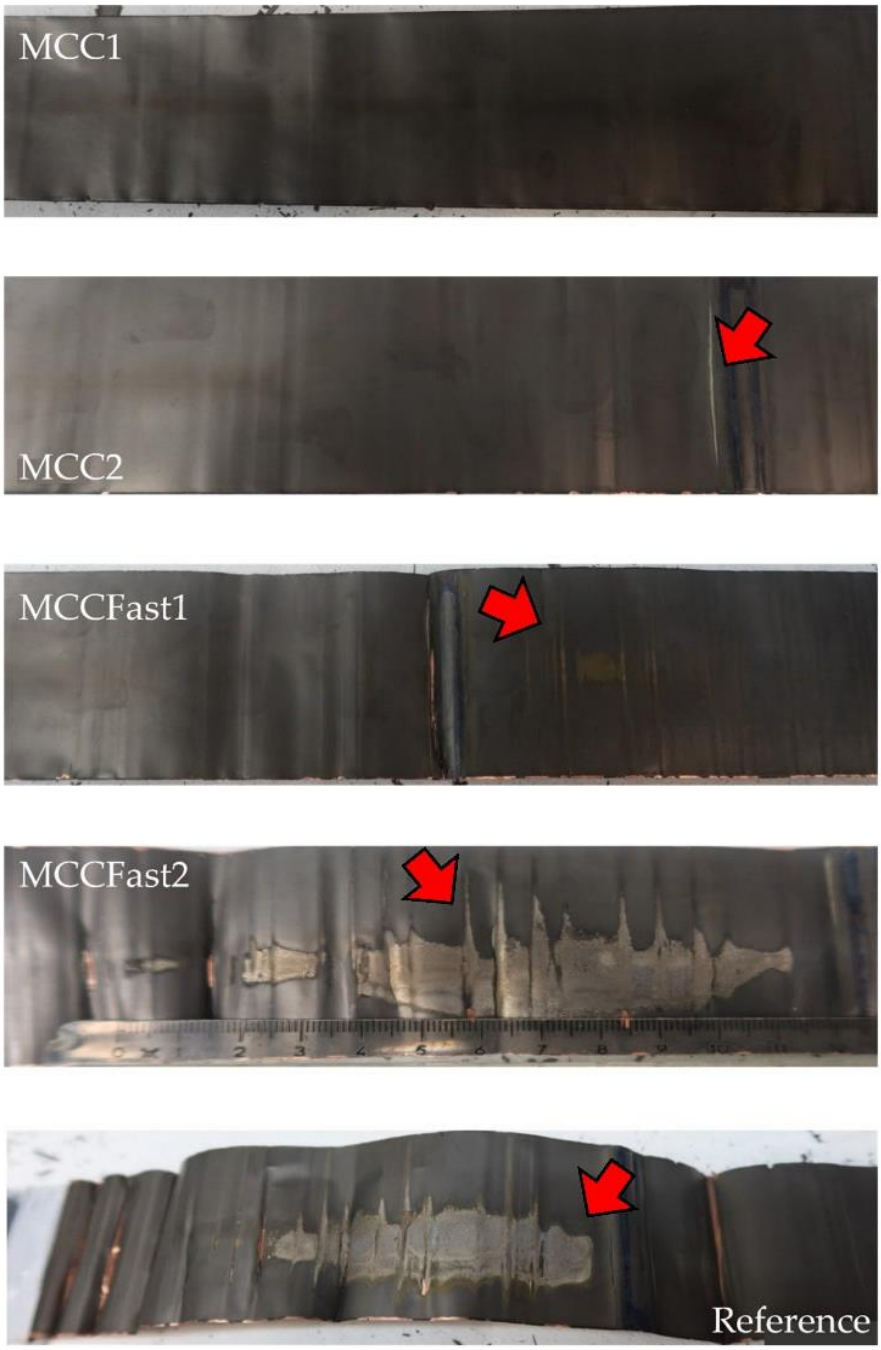

Figure 72 - Si/C anodes electrodes, visual inspection

The following images (from Figure 73 to Figure 77) show in more detail the electrode conditions after dismantling, for each cell aged with its specific DCFC profile. The dismantling process results partially disruptive, with electrolyte loss (mainly via evaporation) and lithium salt deposition on the electrode surface, bringing to corrosion damages over time.

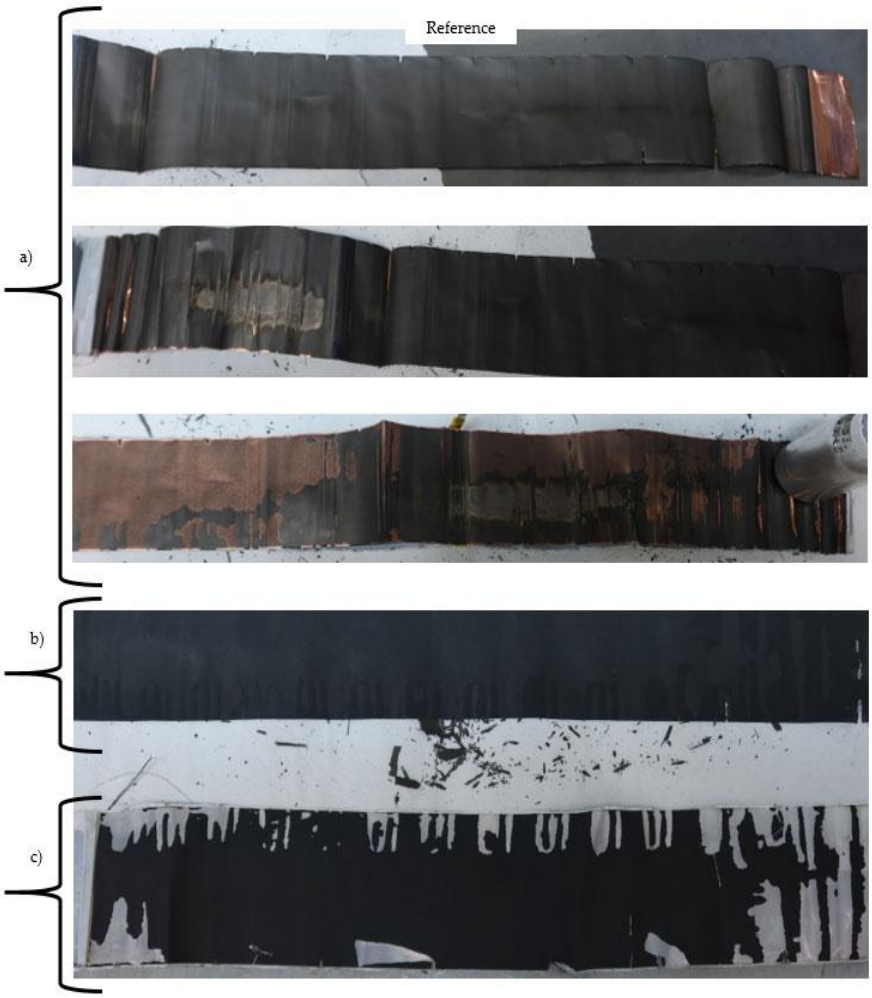

Figure 73 - Reference sample conditions

After dismantling, Reference sample (Figure 73) showed a localised Li plating area present in both coated sides, on the anode surface. The lack of a homogeneous Li plating, which would appear on the whole anode surface, suggested a strong influence of the cell geometry, which

affected the general health of the cell, together with the charging applied conditions. Cathode electrode presented high tendency to be detached, with most of the cathode active material (CAM) remaining adherent to the separator. This phenomenon can be linked to the severity of the charging protocol, which forced Li ions to enter in the NMC structure, causing detrimental effects such as cracking of the secondary particles and tendence to disaggregation, because of the volume changes during cycling.

Figure 74 - MCC1 sample conditions

MCC1 sample showed an anode completely free from evident Li plating (Figure 74), with only a partial tendency to anode detachment in some parts of the electrode foil.
The cathode foil resulted more compact than the Reference, with more active material adherent to the electrode foil during the dismantling process.

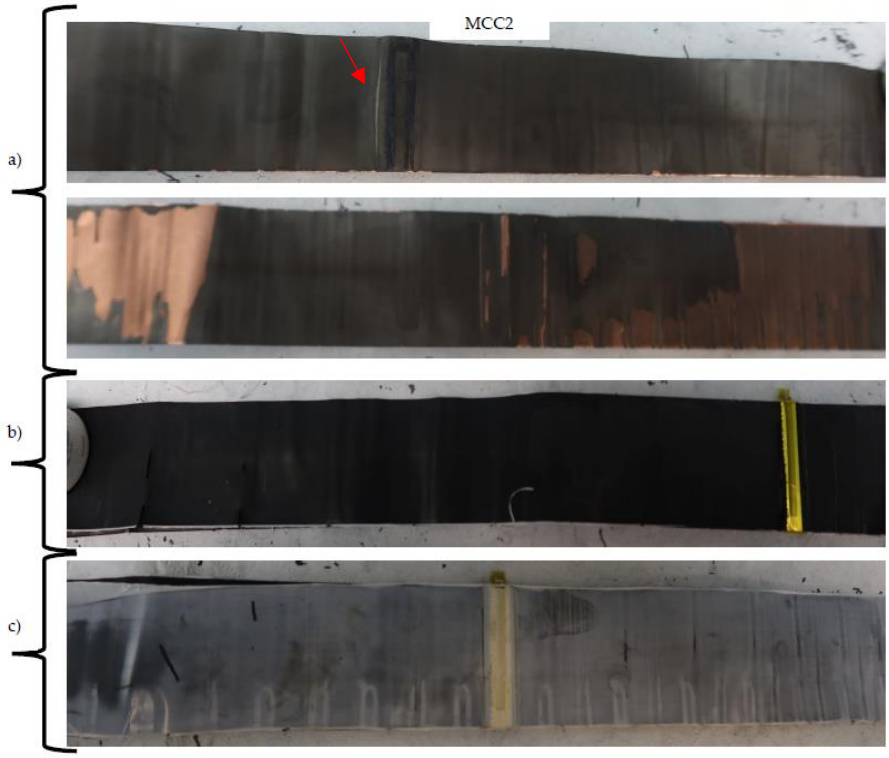

Figure 75 - MCC2 sample conditions

MCC2 sample, which concluded the aging campaign at 1000 cycles with the best retained capacity among the tested samples, do not present Li plating on the anode surface (Figure 75), except for a very limited area in close to the mandrel, where the cell is rounded during the manufacturing process (indicated by a red arrow). Thus, even using the mildest aging protocol, we observed Li plating in a very narrow region of the electrode characterized by the bending of the current collector.

Cathode foils presented no significant detaching, with limited amount of material adherent to the separator during dismantling.

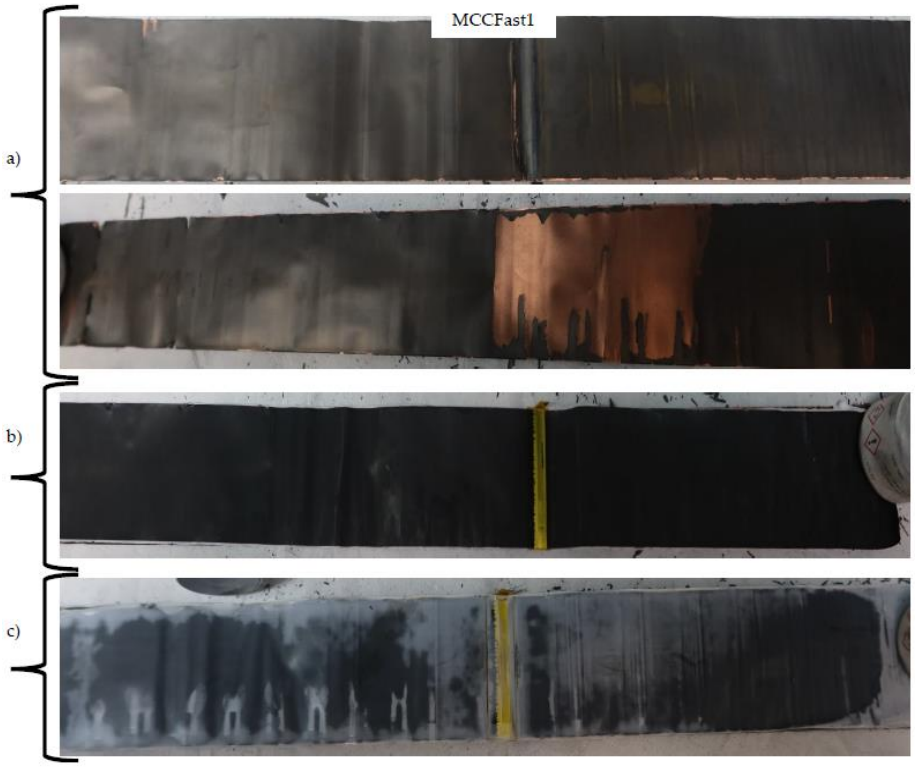

Figure 76 – MCCFast1 sample conditions

MCCFast1 anode sample presented a very limited area where Li plating started to occur. With respect to Reference sample, the entity of the deposits was limited both in terms of area and thickness, qualitatively appreciable also at a first look because of the colour (Figure 76).
Cathode foils presented no severe damage after dismantling, at the visual inspection.

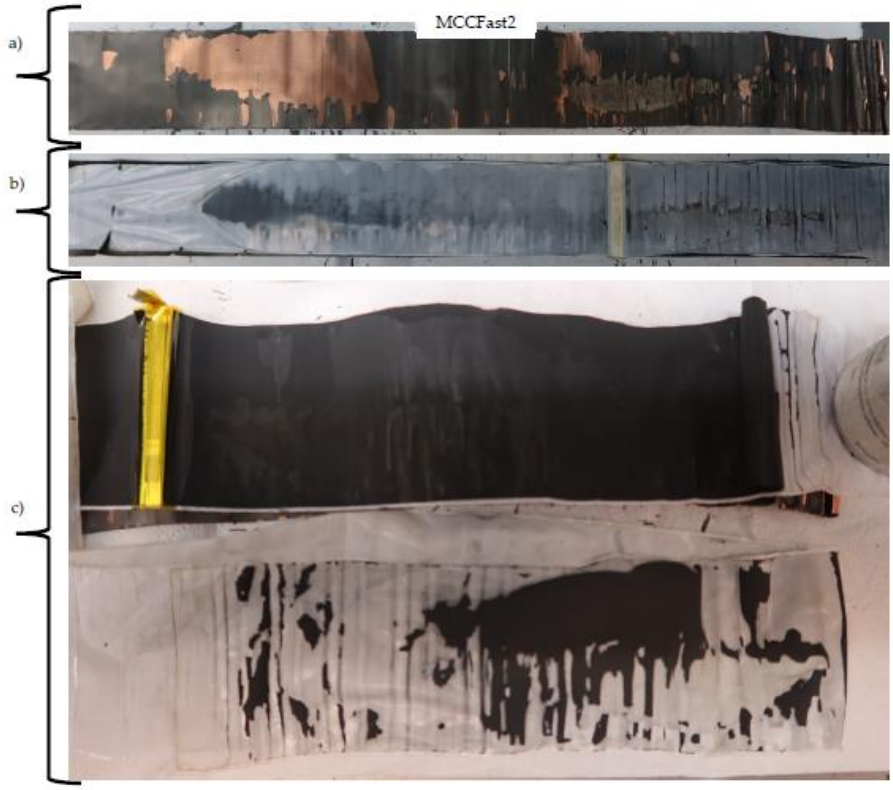

Figure 77 - MCCFast2 sample conditions

MCCFast2 sample showed a general deterioration at the anode side. From both sides there was an area affected by Li plating, again in proximity of the tab welding. The rest of the anode presented high tendency to exfoliation, with parts of the coating completely absent after the dismantling (Figure 77).

Cathode presented a moderate tendency to exfoliation, with a significant amount of material which remained adherent to the separator foil.

Figure 78 - MCCFast3B electrodes

From the dismantling of cell cycled with MCCFast3B protocol (Figure 78), it is easy to observe the presence of Li plating at the anode side.

The main difference with the other samples stays in the amount of lithium deposits, which is widespread also in middle areas of the electrode. Anyway, some portions of the anode resulted free from lithium deposition.

The cathode appeared exfoliated, as for the other cases.

Since MCCFast3A and MCCFast3C were not disassembled, because of other non-destructive analysis expected on these samples, some assumptions can be made.

MCCFast3B should be representative of an intermediate condition between no derating application (MCCFast3A) and complete derating application (MCCFast3C).

The collected images are in good agreement with the electrical results, summarized in Table 10.

Table 10 - SoH% after 1000 cycles (or 80%)

	Reference	MCC1	MCC2	MCC Fast1	MCC Fast2	MCC Fast3
SoH %						
No derating	88.48	91.53	91.74	90.88	87.55	(C) 79.80 (780 cycles)
Capacity derating	-	-	-	-	-	(B) 77.80 (650 cycles)
R int vs SoC% + capacity derating	-	-	-	-	-	(A) 78.10 (400 cycles)

Generally, at the visual inspection, anode foils presented the most severe damages in the inner parts of the cell, with the predominance of the effect of the electrode curvature[141–143], coupled with the effect of the high current applied could have a direct effect on the aging of the materials. During the normal aging process, the inhomogeneous current distribution becomes a crucial effect for the capacity loss acceleration.

The applied pressure on the electrode foils increases passing from the external to the internal layers. The inner rolls are geometrically influenced by the presence of a thick element, the tab, used to link, wrap and electrically connect the two parts of the electrode foil[144]. This electrode portion, in the case where the current applied is more intense, is affected by localized lithium plating.

The observed phenomenon[145] can be linked to the effect of the electric field on the most sharply curved surface. This effect describes the formation of a more intense electric field in areas where the surface of the conductor has a smaller radius of curvature, as for the case of the electrodes in the inner parts of the jellyroll.

As a general comment, when lots of material has a strong tendency to exfoliate from the current collector during the unwinding process, the main hypothesis can be related to the drying-out of the electrolyte that makes electrodes to flake off.

Looking at Figure 79 we can see how all the tested charging profiles restore the same amount of energy inside the cell (2 Ah), with differences in terms of time. If from one side we noticed how MCCFast2 aged faster than the other strategies, with a capacity retention comparable to the Reference strategy, from the other it is important to underline that MCCFast2 restores the highest amount of energy in the first 15 minutes, with a 20% charging capacity more than the Reference (Table 11).

MCCFast3, which can restore almost 70% of the charging capacity in the first 15 minutes, was specifically designed as “ultra charge” application (always remembering the kind of cell chemistry we are working with) to be used only in special situation, when high rapidity would be needed.

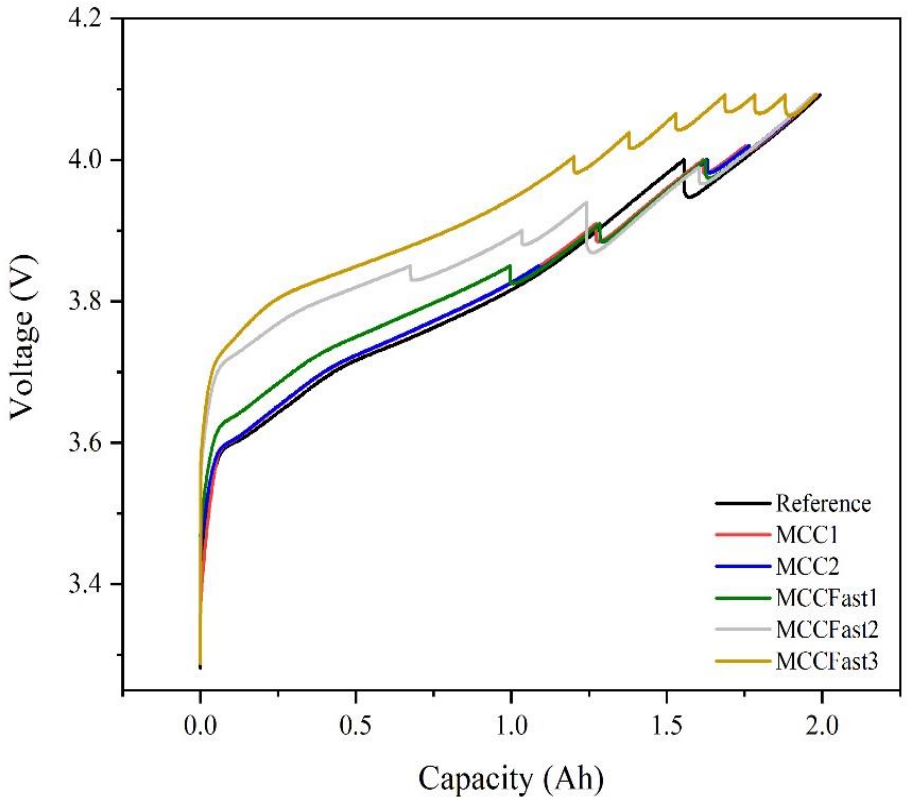

Figure 79 - voltage vs capacity

Table 11 - Time for charge for DCFC profiles

Time for charge (minutes)		**5**	**10**	**15**	**20**	**25**	**30**
SoC%	Reference	16	25	33	41	50	58
	MCC1	16	25	35	44	53	60
	MCC2	17	26	35	44	53	60
	MCCFast1	19	30	41	50	58	64
	MCCFast2	25	40	53	59	65	70
	MCCFast3	23	47	69	85	95	100

If MCCFast3 seems to have a very specific destination, MCCFast2 results resulted very promising.

This profile can be in fact used to fast charge (70% under 30 minutes) the battery when necessary, guaranteeing a very high energy throughput in the lowest time, among the selected profiles.

From the other hand, the Reference profile aged the cells more significantly with respect to the other profiles, restoring the lowest energy throughput, with no advantages in the use.

From the results we can conclude that occasional fast charging strategies can be performed with MCCFast2 approach, while normal charging should be applied with MCC1 or MCC2 profiles, which can be valid alternatives to the Reference profile.

7.6 Electrochemical testing

After the visual inspection the electrodes were washed in DMC (Dimethyl carbonate) to remove the lithium salt excess. Samples were collected to perform a variety of analysis, using electrochemical (Lab scale) and morphological techniques.

Electrode samples from 1000 cycles aged cells were cut using a puncher (18 mm diameter).

To avoid the use of preferential samples, once excluded the very limited area with Li plating, ten electrode disks were selected all over the electrode foil obtained from the original 18650 cell.

Areas affected by Li plating resulted very fragile and difficult to be handled without damaging the electrodes.

Once prepared, the choice of the electrode samples to build the lab scale cells was conducted randomly, by selecting electrode disks from specific boxes.

To be sure to guarantee a proper electric contact, the double side coated electrode disks were scratched from one side, to expose the current collector to the metallic plunger of the lab scale cell (EL-Cell ®).

To deeply understand the aging conditions, it was decided to assemble a three-electrode cell, using a lithium pseudo-reference electrode.

It was possible to monitor the anodic (Si/C vs Li) and the full cell (Si/C vs NMC811) potential. Cathodic potential (NMC811 vs Li) was measured by difference. An amount of 100 µL of 1M $LiPF_6$ in EC:DMC (1:1 vol.%) was used as electrolyte. Cells were assembled and activated with two C/10 formation cycles, estimated by rough evaluation of the cathodic material theoretical capacity. After formation the real capacity was calculated and used to set a C/50 charge-discharge cycle (2.5-4.2 V).

Here, the goal was to obtain the incremental capacity analysis (ICA) in a quasi-stationary state.

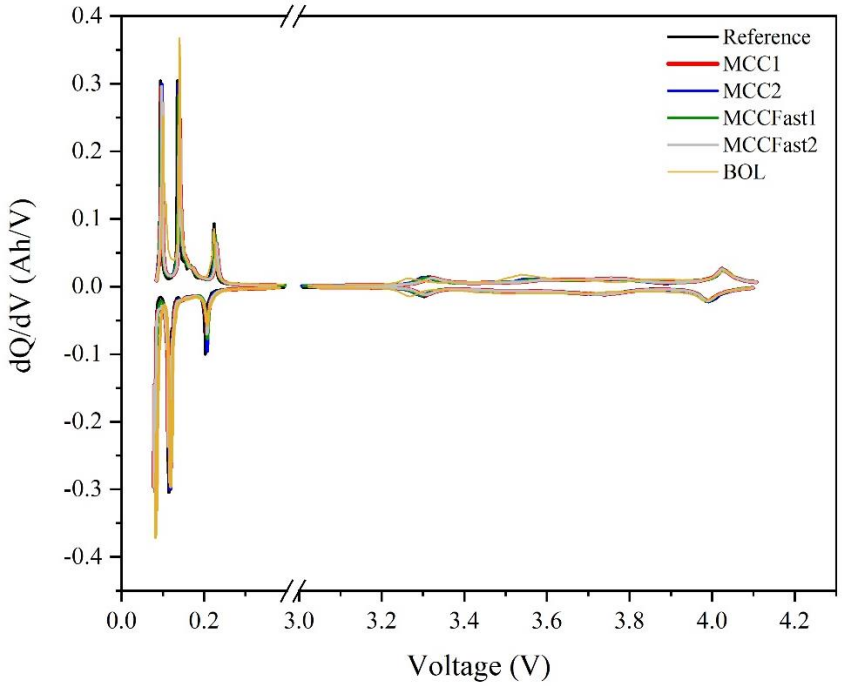

Figure 80 - Three electrode cell incremental capacity analysis

Figure 80 shows the results obtained.

The general good health of the samples is confirmed, with no severe damages inside the cells, except for the limited zones with lithium deposition, excluded by the ICA analysis.

Having a look at each single peak in both anode (left) and cathode (right) half-cell voltage response, a good match is present between samples, with correspondence between all the aged samples and the fresh condition (BOL) cell.

In order to better appreciate the ICA trends Si/C vs Li (Figure 81) and NMC811 vs Li (Figure 82) curves are reported. Generally, no significant aging was observed at the anode side, where no peak shift is observed, indicative of no severe resistance growth inside the cells.

A very limited peak area decrease, mainly attributed to the normal aging (i.e. SEI formation) with respect to the BOL conditions, is observed. This trend could be indicative of the Li plating as major driving phenomenon for the drop of capacity for Reference and MCCFast2 samples.

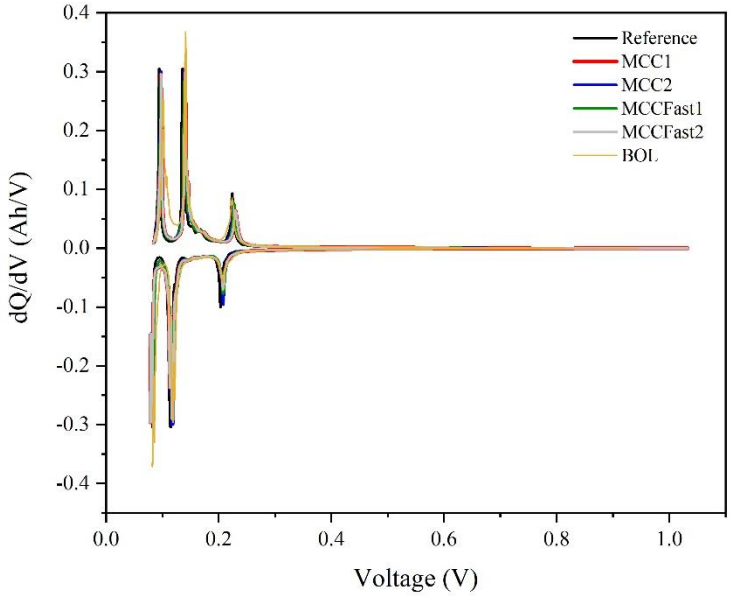

Figure 81 - Si/C vs Li ICA

Regarding the cathode, if zooming, a light peak shift was observed, if comparing the BOL conditions with the aged samples. As for the anode, this can be indicative of an increase in the internal resistance, as expected, caused by the prolonged aging.

High currents could in fact cause the collapse of the NMC secondary particles, with creations of microcracks and voids and consequent worsening of Li ion diffusion[21,146–148].

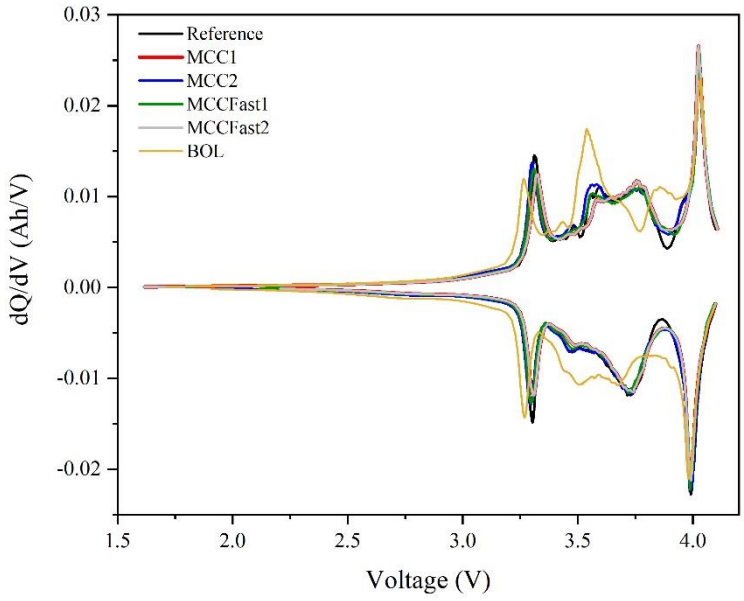

Figure 82 - NMC811 vs Li ICA

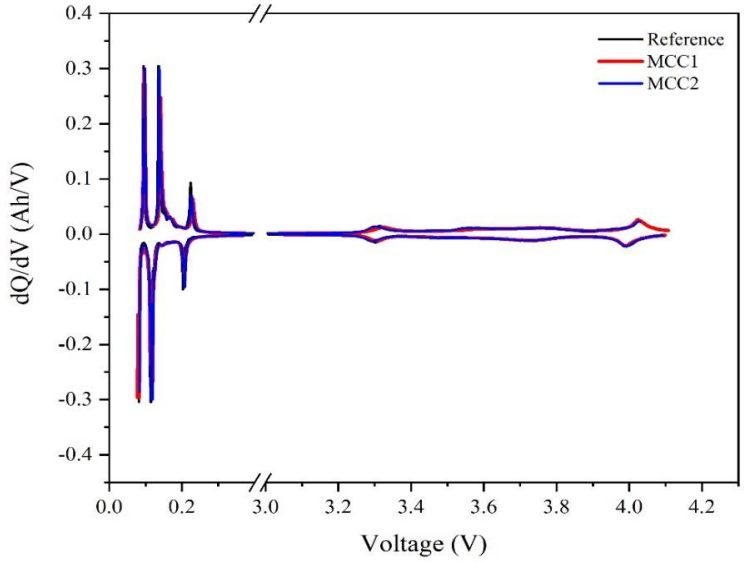

Figure 83 - Si/C vs NMC811 ICA for Reference MCC1 and MCC2 after 1000 cycles

To better analyse the results, it was decided to focus the attention on three specific samples (Figure 83).

1) “Reference” profile aged cell.
2) “MCC1” profile aged cell
3) “MCC2” profile aged cell.

Incremental capacity analysis on the three-electrode cells do not present significant differences in terms of peak position and area.

A little peak shift is visible for NMC response for MCC1 (right part of the graph), nevertheless no significant signs for active material loss or changes in electrochemical behaviour are visible in the samples.

As reported in the literature[149], if a significant loss of lithium content occurs, an indirect evidence is also observable with a shift to lower lithiation in the NMC, with more positive cutoff potential.

The tested samples present only a slight peaks depression, both for charge and discharge, with respect to the BOL sample, indication for lack of severe loss of lithium.

Regarding Si/C anode signals, the peaks above 0.15 V present limited depression, symptom of very limited active material loss. Peak at 0.10 V, which corresponds to the higher lithiation stage, is present, further confirmation of good conditions of the materials in the tested areas.

Bach et al.[149] reported their observation related to samples where visible Li plating was absent. In that case the materials suffered from normal aging. with regions affected by the loss of some active material and lithium plating. On the other hand, they reported that where portions of material suffered from heavy degradation, peak heights presented a smaller area than in the pristine cell, clear sign for active material loss.

In the worst-case scenario vanishing of peaks is also expected. Often, this is more common for the peaks which corresponds to the higher lithiation states, possibly attributable to lithium plating.

Coming back to this work, the tests demonstrated the good health of the aged samples, confirming the validity of the proposed charging strategies. Reference, MCC1 and MCC2 curves were closely overlapped, conversely to the overall incremental capacity response performed on the 18650 cells, as showed in Figure 58.

This can be a suggestion to confirm that the localized lithium plating occurred mainly for Reference and MCCFast2 cells, revealed to be the game changer for the aging campaign, accelerating the decade of the sample.

7.7 X-ray diffraction analysis

Samples from all the testing conditions were analysed by using a Rigaku Miniflex.

Patterns were recorded with a Bragg-Brentano flat geometry, using the Cu-K radiation (= 1.5406 Å; 40 kV, 15 mA) in the range $5° < 2\theta < 90°$ at step size of 0.02° interval using a scanning velocity of 1/min.

The sample matrix consisted in testing anode and cathode materials from the following samples:

- Reference;
- MCC1;
- MCC2;
- MCCFast1;
- MCCFast2.

All the samples were tested in dual forms:

- Powder electrodes after scratching from the current collector and ball milling, visible in Figure 84 and Figure 85 (up).
- Calendered electrodes form, visible in Figure 84 and Figure 85 (down), were tested by using an Ar atmosphere sample holder with a Kapton window, prepared in glovebox.

Calendered electrodes were tested with no further sample preparation, to test the samples “as is”, when working inside the cell. Since this setup could not guarantee the presence of preferential orientations, powders were tested.

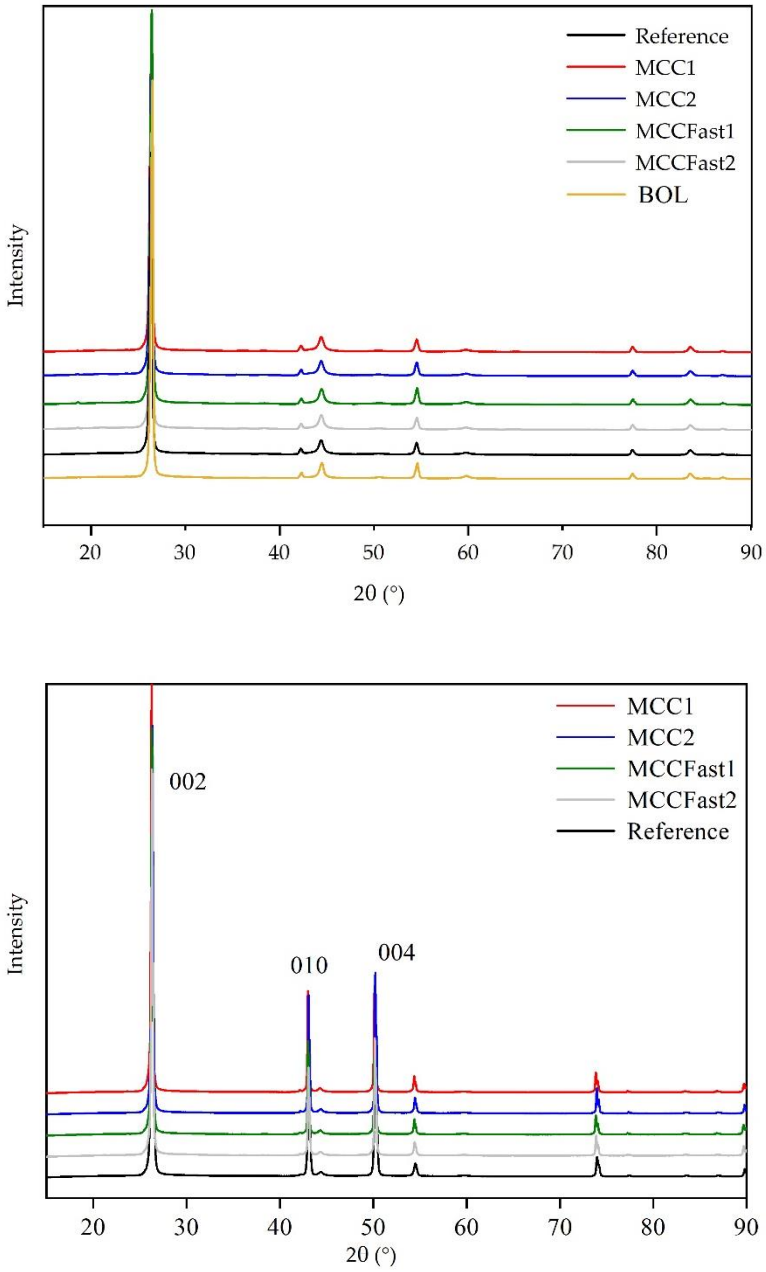

Figure 84 - XRPD on Si/C anode powders (up) and electrodes (down)

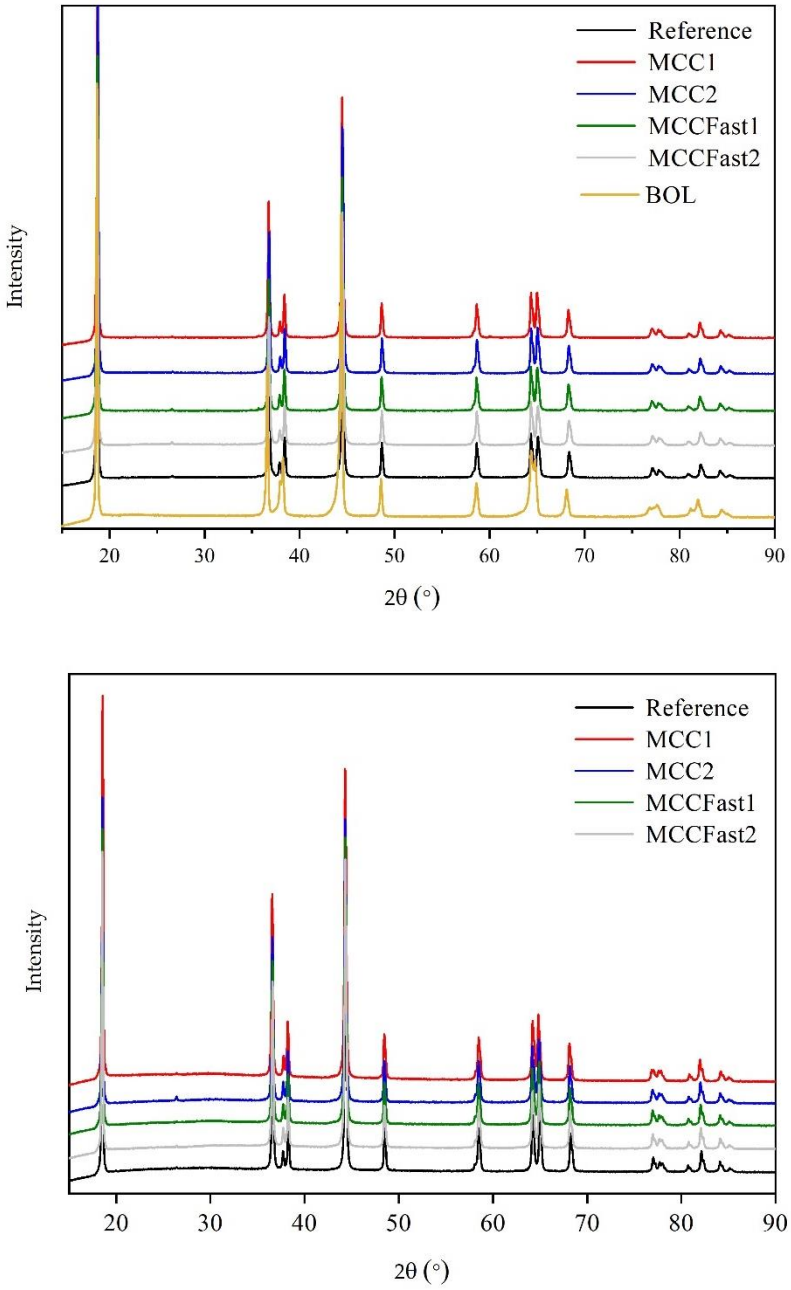

Figure 85 - XRPD on NMC811 cathode powders (up) and electrodes (down)

A Rietveld refinement (Figure 86) was performed on XRD patterns using the Rigaku ® PDF software in the 15° < 2θ < 90° range, considering a system composed by NMC 811, together with a small fraction of carbon, associated with the conductive agent present in the electrode formulation. A trigonal structure (e.g.: R-3m, 166) was assumed for the NMC 811 phase as a model for the refinement.

From the results obtained by the Rietveld refinement performed on NMC 811 cathode powders samples, in the tested DCFC conditions, it is visible that NMC 811 cathode material retained its initial hexagonal crystal structure (R-3m space group) in all samples.

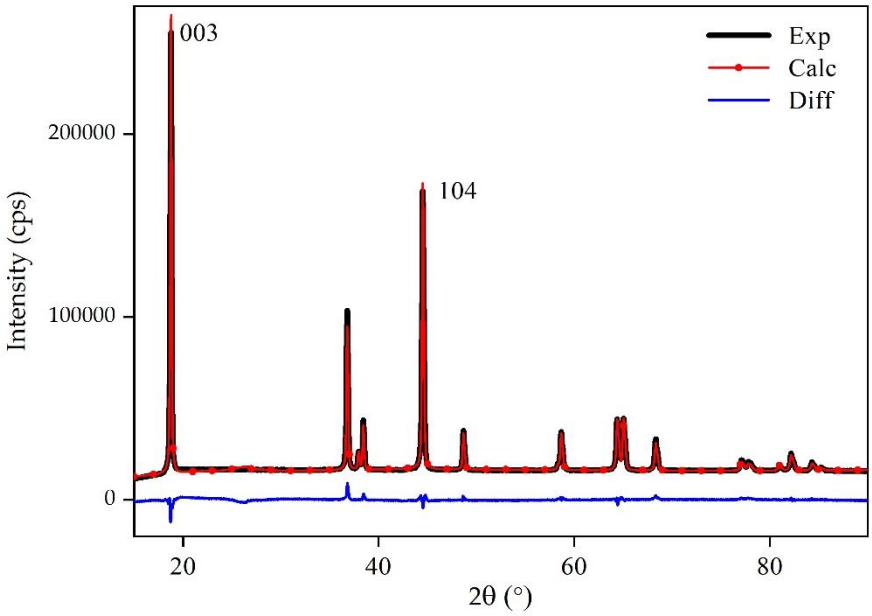

Figure 86 - Rietveld refinement for NMC811

Rietveld refinement, performed on cathode powders, revealed the evolution of the crystal lattice parameters a and c.

- Low a (Å) lattice parameter values for the most aged cells (Reference and MCCFast2).
- High c (Å) lattice parameter values for the most aged cells (Reference and MCCFast2).
- Absence of Li/Ni mixing.

As reported[150], the aging mechanisms generally cause a shrinkage of the lattice along a-axis and a stretching along c-axis.

Literature suggests that the origin of the lattice distortion is hypothesized to be linked to:

- Increment of repulsion forces increment between slabs, because of the decrease of the lithium content in the EOL electrode materials [110,151];
- Increment of the average oxidation state for nickel, manganese, and cobalt ions[152].

Since no major differences are evident from XRD data, we can suppose that the driving force that guides the aging is strongly represented by mechanical disintegration of secondary particles. From a crystallographic point of view, the changes in the primary particles lattice volume during the cycling (lithiation and delithiation) cause mechanical damages at the grain boundaries, with consequent material cracking.

Cation mixing hints

An important point to check for evaluating the aging entity at the cathode side is the presence of cation mixing[153].

Cation mixing occurs when cations in a crystalline material occupy sites previously occupied by other cations. In other words, cation mixing takes place when the cations in a crystal structure "swap places" with another, leading to a mixed occupancy of cation sites.

This can cause a plenty of effects on the material properties point of view, altering electronic, magnetic, or optical properties, or affecting thermal or mechanical behaviour. Rarely it can also promote the formation of new materials with unique properties.

Cation mixing phenomenon is usually observed in complex oxides, such as perovskites, spinels, and layered oxides, as well as chalcogenides, intermetallics, and zeolites. It can be controlled or manipulated through various synthetic methods, including high-temperature solid-state reactions, solution-based synthesis, and hydrothermal methods.

The specific case of the present work focused the attention of the cation mixing presence, to evaluate the aging entity inside the oxide cathodic structure.

To perform this evaluation, cathode peak intensity ratio performed on 003 and 104 peaks was measured.

It is known from the literature[154,155] how the relative ratio of the intensities I_{003}/I_{104} is associated to the presence of this phenomenon, presented in Table 12.

The degree of cation mixing decreases as ratio increases, values below 1.2 are indicative of significant aging.

Table 12 - Rietveld analysis lattice parameters

Lattice parameters from the Rietveld refinement for EOL 1000 cycles cells					
	Reference	MCC1	MCC2	MCCFast1	MCCFast2
a (Å)	2.867	2.871	2.870	2.870	2.868
c (Å)	14.258	14.252	14.249	14.252	14.257
I_{003}/I_{104}	1.49	1.54	1.59	1.54	1.53

The change in intensity ratio is a result of altered atomic arrangements and changes in the scattering factors associated with the different cations.

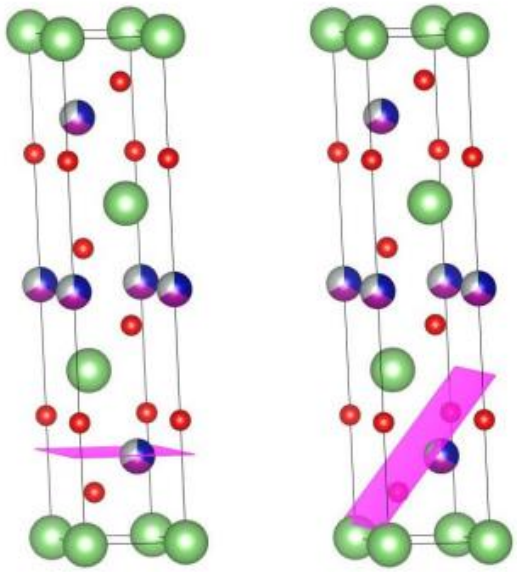

Figure 87 – NMC 811 structure representation (VESTA Software)

In Figure 87 the plane of (003) and (104) are showed using VESTA software.

TMs can migrate, being substituted by Li ions, the cation mixing phenomenon take place.

The reason for the change of (003) and (104) peaks intensity is attributed to the structure factor, which is determined by adding the contributions of scattered waves from individual atoms or molecules within the crystal.

Formally, the structure factor is indicated as F(hkl), where h, k, and l are the Miller indexes. These are representative of the crystallographic planes in the lattice.

The absolute value |F(hkl)|, gives insights into the strength of the scattering occurring at the specific Miller indices, providing information about the intensity of scattering from the crystal lattice.

Figure 87 shows the plane of (003) and (104). They are crossing each other in the position of TMs, and that is why when the Ni^{2+} ion moves to the location of Li^{+}, it leads to have a change in the intensity ratio.

From the data collected for the present work, all the values are above 1.49, indicative of the lack of cation mixing. Lattice parameter evolution and cation mixing absence are a clear sign of the general good health of the tested materials, confirming the good design of the charging strategy.

7.8 - Raman analysis

An average of all spectra recorded is considered in the following. Figure 88 shows an example of the methodology used to collect information from each sample, with the Raman microscope. For each “charging strategy” sample, white areas (higher D bands) and black areas (higher G bands) are analysed.

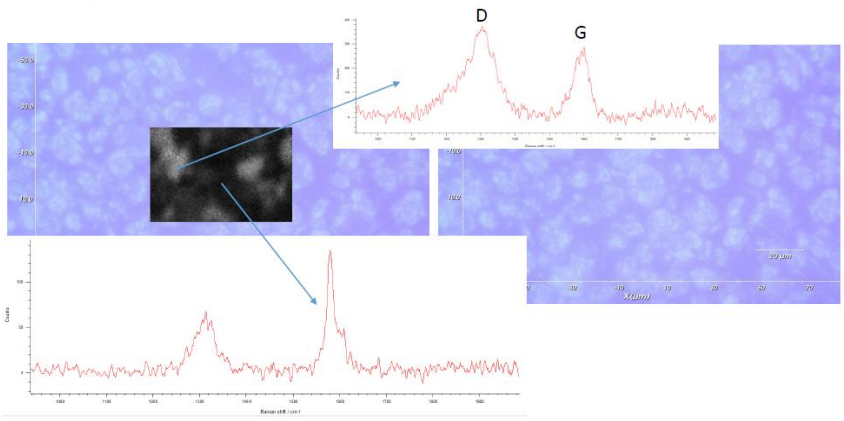

Figure 88 - Raman mapping

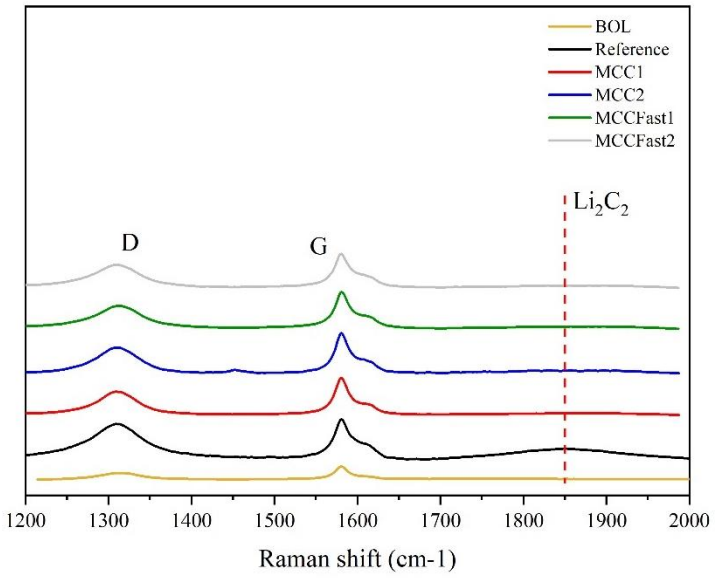

Figure 89 - Raman spectra for anode samples

Raman spectroscopy analysis was performed to detect Li plating where invisible at the visual inspection (areas where Li plating was observed were excluded by the analysis), together with other aspects linked to the aging degradation.

Figure 89 shows the Raman spectra obtained on the samples. For samples associated to the alternative charging protocols proposed in this work (as comparison with the Reference protocol) no peaks related to Li_2C_2 were observed, symptoms of no Li plating.

A band at ~1847 cm^{-1} is attributed to acetylide groups (−C≡C−), occurring in metallic lithium (both in the bulk and at the surface) and in electrochemically plated lithium, forming Li_2C_2, that can be used as a marker for Li plating evidence[139,156–158].

Only Reference sample presented a very broad and low intensity peak, that can be related to some irreversible Li plating presence. Nevertheless, given the lack of very narrow peak this affirmation needs to be further investigated with other measurements.

Other two notable features when performing a Raman analysis on graphite are the D and G bands of graphitic carbon.

The D band is related to the phonon scattering at the grain boundaries and/or structural defects (corresponds to A_{1g} - breathing mode).

The G band is a signal associated to the sp^2 carbons corresponding to the E_{2g} (plane C-C stretching).

The entity of the degradation, expressed as the number of defects in the graphite, was measured by calculating the ratio between the peaks I_D, at 1350 cm^{-1}, and I_G, at 1580 cm^{-1}. The larger is the ratio between I_D/I_G, the higher will be the degradation (graphite defects) of the sample[139,159].

From Table 13 it is evident how the Reference anode sample presents the highest degradation level, in terms of loss of crystalline structure.

Table 13 - Ratio between I_D/I_G for anode degradation evaluation

Sample	$\mathbf{I_D/I_G}$
BOL	0.19
Reference	0.87
MCC1	0.61
MCC2	0.64
MCCFast1	0.62
MCCFast2	0.68

7.9 – ICP-OES, SEM analysis and PSD

Table 14 - ICP-OES on NMC811 cathodes

MCC1					
Element	ICP [% m/m]	ICP [mg/l]	mg	mmol	Ratio
Ni	44.90	364.588	91.147	1.55	0.80
Mn	5.00	40.6	10.2	0.18	0.10
Co	5.70	46.284	11.6	0.20	0.10
Li	5.30	43.036	10.8	1.55	0.80
MCC2					
Element	ICP [% m/m]	ICP [mg/l]	mg	mmol	Ratio
Ni	48.00	389.76	97.44	1.66	0.80
Mn	5.50	44.66	11.2	0.20	0.10
Co	6.10	49.532	12.4	0.21	0.10
Li	5.70	46.284	11.6	1.67	0.80
MCCFast1					
Element	ICP [% m/m]	ICP [mg/l]	mg	mmol	Ratio
Ni	46.30	375.956	93.989	1.60	0.80
Mn	5.30	43.036	10.8	0.20	0.10
Co	6.00	48.72	12.2	0.21	0.10
Li	5.50	44.66	11.2	1.61	0.80
MCCFast2					
Element	ICP [% m/m]	ICP [mg/l]	mg	mmol	Ratio
Ni	46.10	374.332	93.583	1.59	0.80
Mn	5.30	43.036	10.8	0.20	0.10
Co	6.10	49.532	12.4	0.21	0.10
Li	5.40	43.848	11.0	1.58	0.79
Reference					
Element	ICP [% m/m]	ICP [mg/l]	mg	mmol	Ratio
Ni	46.90	380.828	95.207	1.62	0.79
Mn	5.80	47.096	11.8	0.21	0.10
Co	6.10	49.532	12.4	0.21	0.10
Li	5.40	43.848	11.0	1.58	0.77

BOL					
Element	ICP [% m/m]	ICP [mg/l]	mg	mmol	Ratio
Ni	52.50	426.3	106.575	1.82	0.79
Mn	6.40	51.968	13.0	0.24	0.10
Co	6.80	55.216	13.8	0.23	0.10
Li	6.60	53.592	13.4	1.93	0.84

ICP-OES analysis, visible in Table 14, reported that the ratio (8:1:1) among transition metals was retained, after 1000 cycles.

From this evidence, the migration of species at the anode side, coming from the cathode, was excluded.

To visualize the aging entity on the EOL cells, scanning electron microscopy (SEM) was performed on dismantled samples.

As expected, all specimens denote moderate signs of aging in both electrodes, indicating concurrent effects as responsible for the degradation of the cell's performances. Generally, NMC secondary particles presented the most pronounced mechanical degradation, with cracking widespread all over the surface. Regarding the graphite, where no Li plating was observed, the typical flake's structure seems to have a good retention, with no evident mechanical damages at the magnifications selected for the analysis.

In most cases, the samples were washed with DMC before SEM microscopy, to focus the attention on the active material structure. The washing operations were conducted to remove the passivation layer which otherwise would have covered the active material.

Only where Li plating was localized, no washing operations were adopted, to avoid external stress.

Samples were compared with BOL conditions to ease the comparison.

BOL SEM Analysis

As visible in Figure 90, BOL cell presents an NMC structure with particles of different dimensions, where generally a very limited starting cracking is visible along the surface. Since this sample do not underwent cycle aging, the main hypothesis for the presence of these cracks can be linked to the manufacturing processes (lamination) and/or to the first formation cycles. Graphite flakes seems very well distributed, with no evident damages (Figure 91).

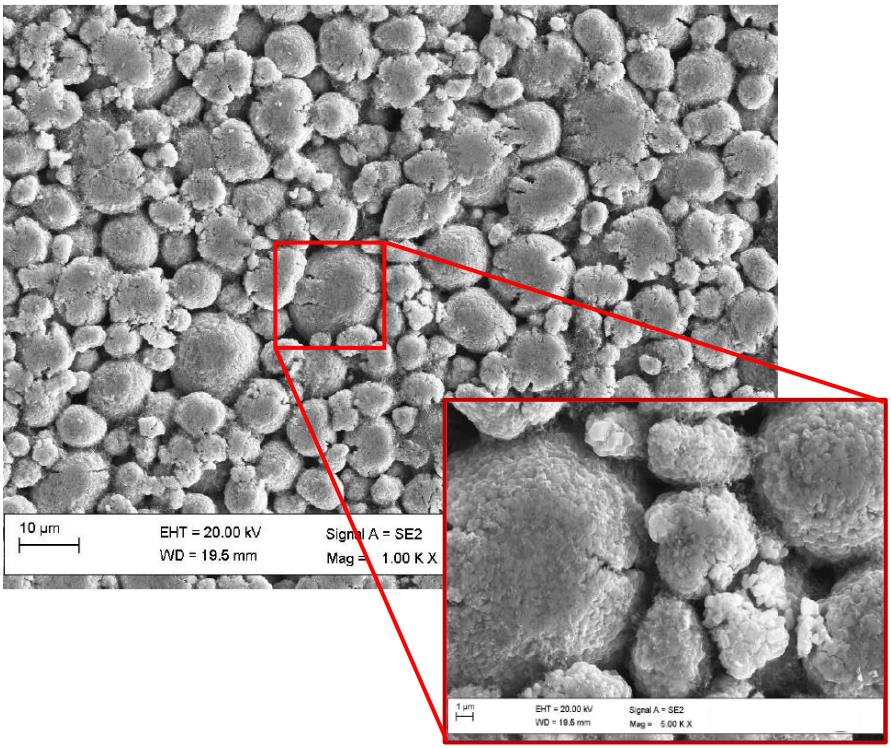

Figure 90 - SEM microscopy (NMC811 - BOL conditions)

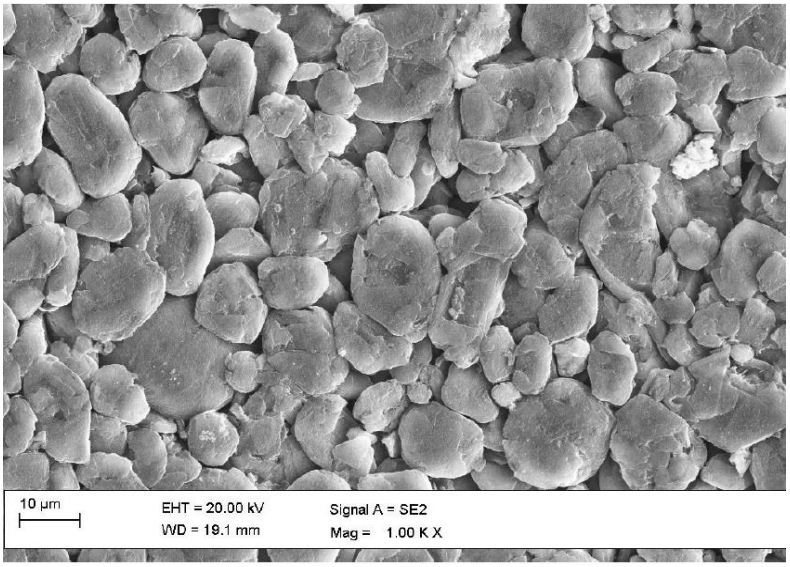

Figure 91 - SEM microscopy (Si/C- BOL conditions)

Reference SEM Analysis

Reference sample presented a limited area with lithium plating deposits, as described in 7.5 Visual inspection retaining a good shape graphite structure (as visible in Figure 92), in the areas not affected from Li depositions.

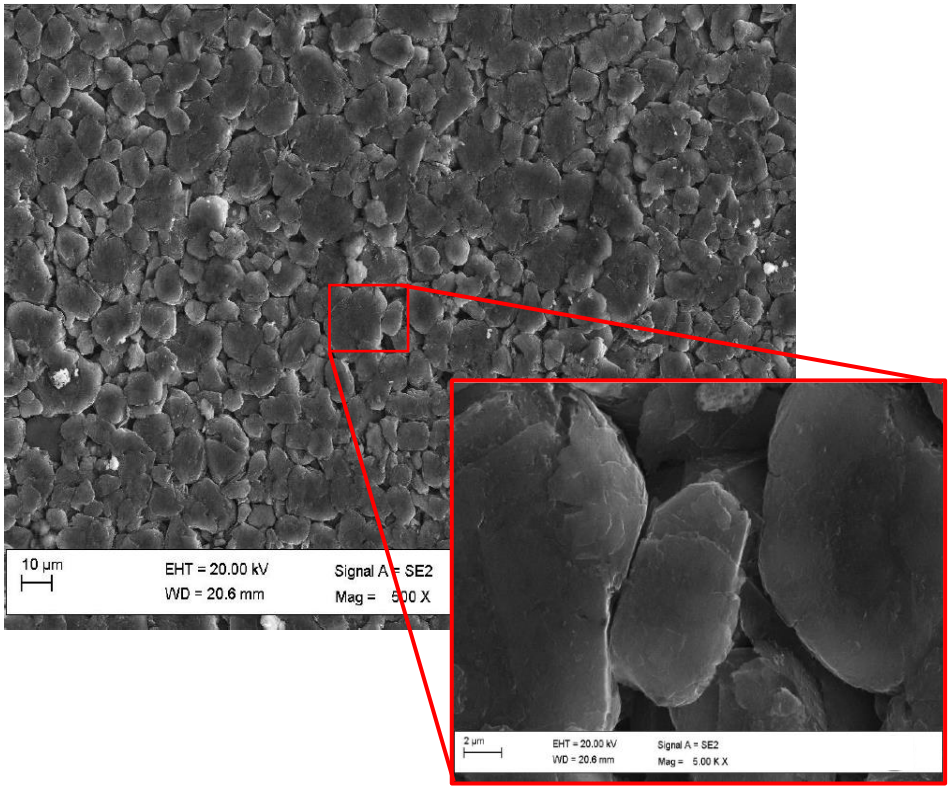

Figure 92 - SEM microscopy (Si/C - Reference conditions)

Where Li plating took place, in the inner parts of the jelly roll, lithium deposits were analysed at the SEM microscopy, presenting a homogeneous area which covered all the underlying graphite. Some fractures along the deposits are observed (Figure 93).

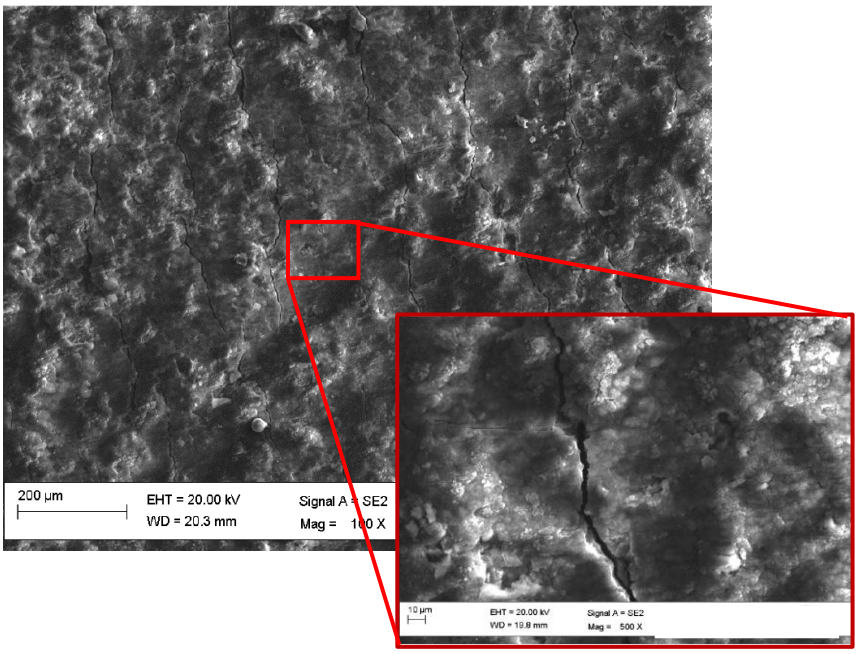

Figure 93 - Localized Li plating deposits

Reference sample also presented areas where Li plating is partially present on the anode surface. In Figure 94, lithium deposits are visible, with alternation of areas where graphite is present, even if the flakes' structure is not appreciable because of the low magnification, completely free from lithium.

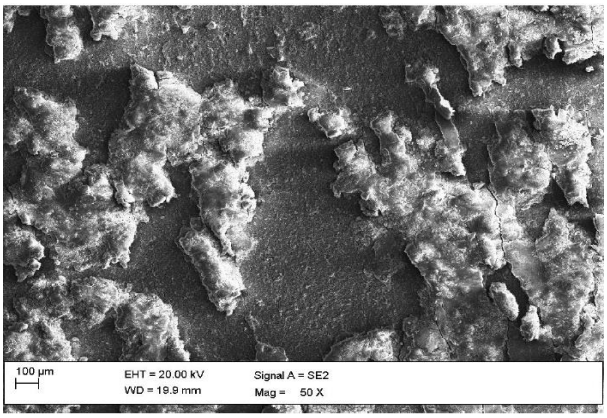

Figure 94 - Areas partially covered by Li plates

Regarding the cathode, NMC secondary particles appears partially damaged, with an increase of smaller agglomerates, at a first look, together with a multitude of particles completely cracked, pointed in Figure 95 with red arrows.

It was also observed, from the cross-section analysis, that most of the desegregation occurred at the interface between the cathode and the separator, with a plenty of small dimension particles along the surface.

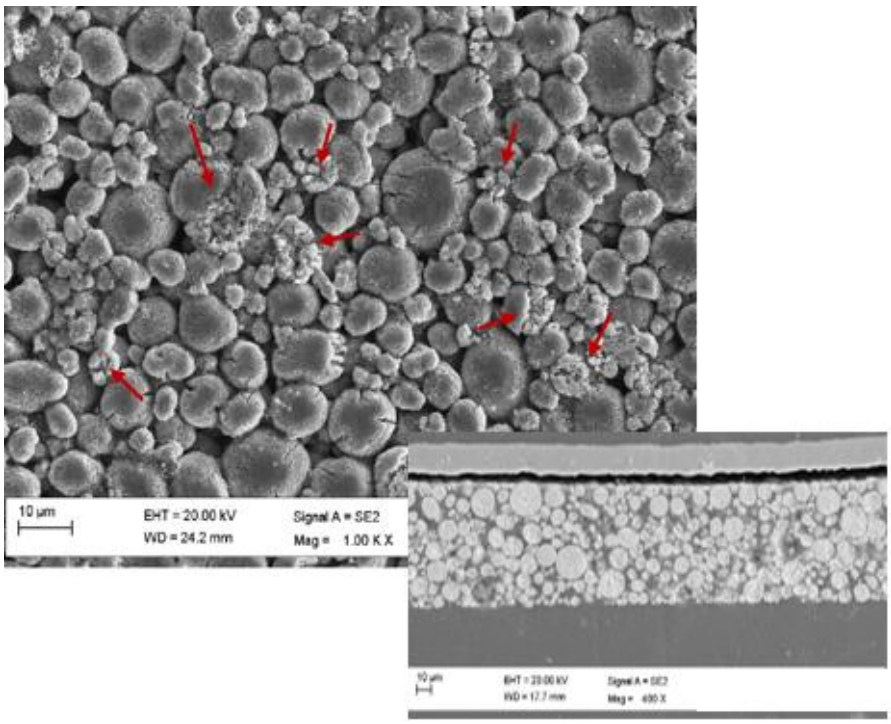

Figure 95 - NMC811 particles (microscopy and cross section image)

MCC1 SEM Analysis

As for Reference sample, graphite structure on MCC1 sample remained unchanged, at the SEM analysis, with a flake structure clearly visible at 1.00 KX magnification (Figure 96). Some round particles attributable to NMC are present, maybe due to some contamination during the cell dismantling.

Since from ICP analysis on NCM electrode the ratio among metal was retained (8:1:1), the migration of species from cathode to anode because of the degradation was not considered.

No Li plating areas were observed on this sample after 1000 cycles.

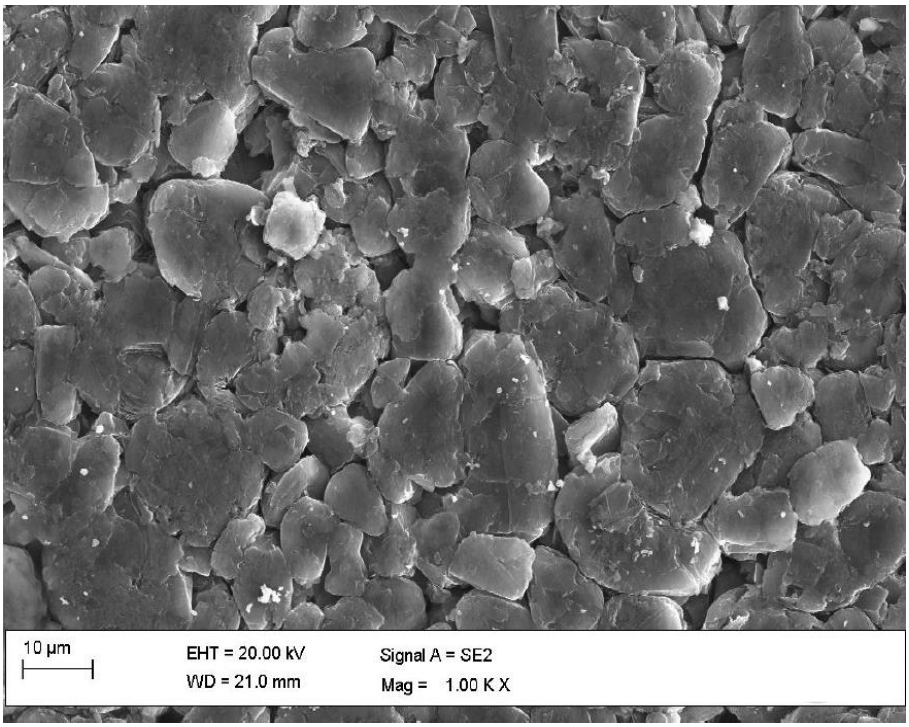

Figure 96 - SEM microscopy (Si/C - MCC1 conditions)

Cathode surface, visible in Figure 97, presents cracking all over the surface, with the smaller agglomerates that show the worst mechanical conditions (red arrows).

The biggest particles in fact statistically seem to retain better the initial conditions, with limited cracking at the boundaries, very similar to the BOL sample.

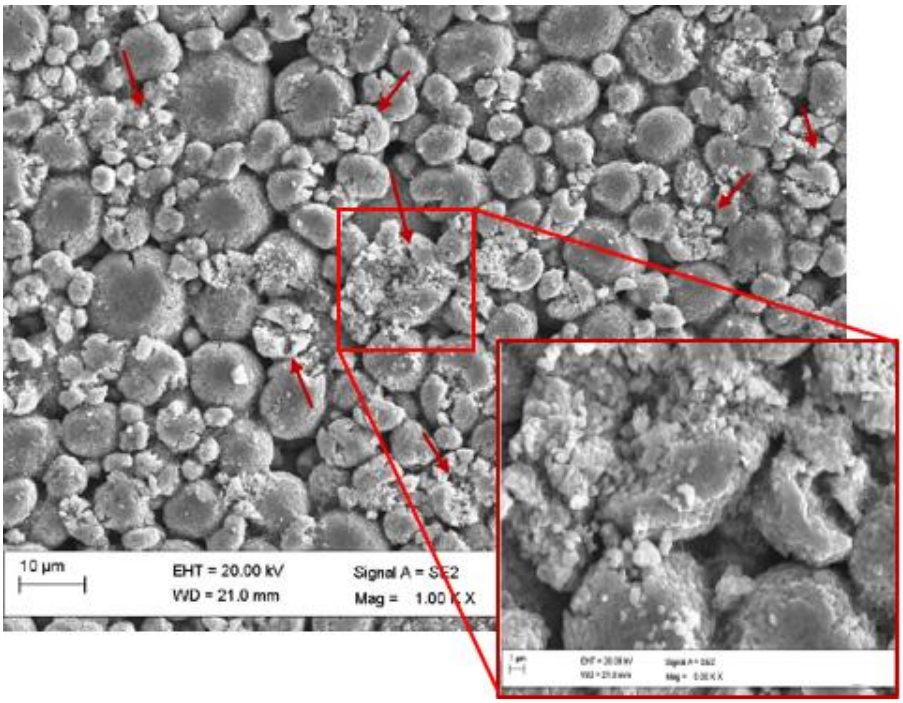

Figure 97 - SEM microscopy (NMC811 - MCC1 conditions)

MCC2 SEM Analysis

As for Reference and MCC1 samples, graphite structure on MCC2 sample retained the flake structure (1.00 KX magnification in Figure 98).

No Li plating areas were observed on this sample after 1000 cycles.

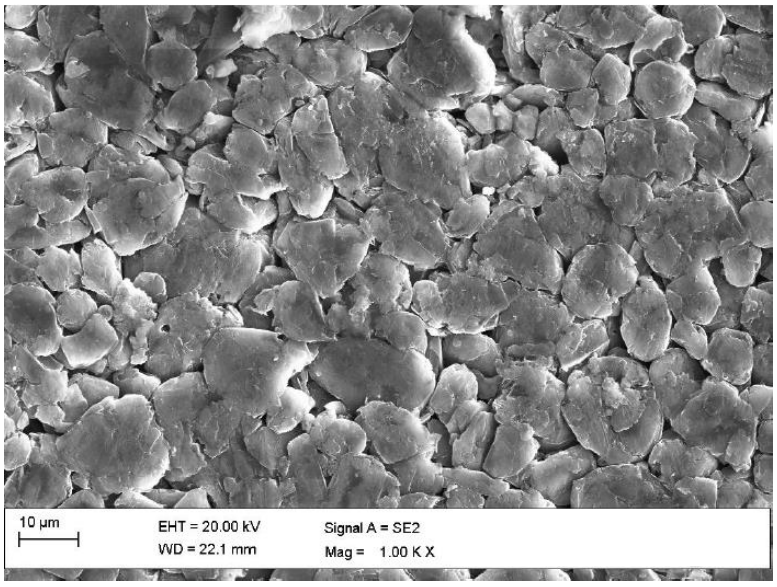

Figure 98 - SEM microscopy (Si/C- MCC2 conditions)

Cathode surface (Figure 99) presents limited cracking with the smaller agglomerates showing some complete opening of particles (red arrows).

Generally, SEM analysis demonstrate a MCC2 cathode better conditions with respect to MCC1 and Reference sample.

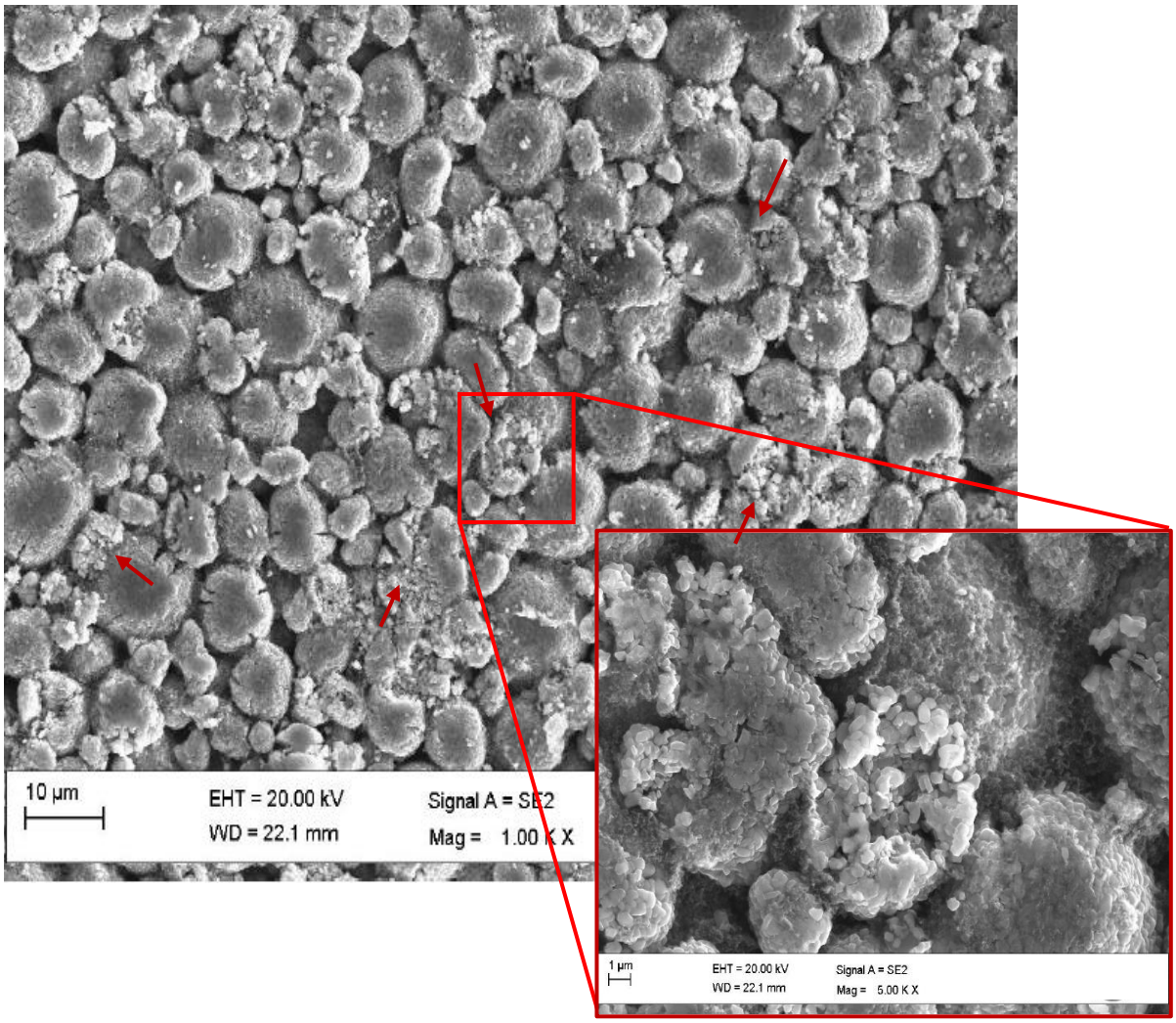

Figure 99 - SEM microscopy (NMC811 - MCC2 conditions)

MCCFast1 SEM Analysis

Graphite structure on MCCFast1 anode foil is visible, with flakes particles that appears partially covered by a film (Figure 100). The main hypothesis is related to the washing time and conditions. The washing with DMC, to remove the SEI layer, was not sufficient to remove all the passivation layer. Phosphorus and fluorine-based compounds were in fact observed via EDX analysis. Some localized Li plating, even if very limited, was found on the samples, at the teardown. Figure 101 shows an area covered by lithium-based products.

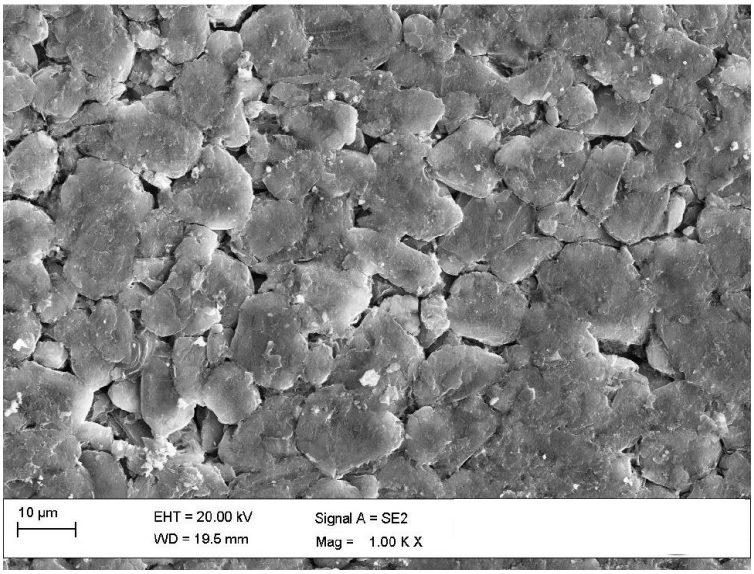

Figure 100 - SEM microscopy (Si/C - MCCFast1 conditions)

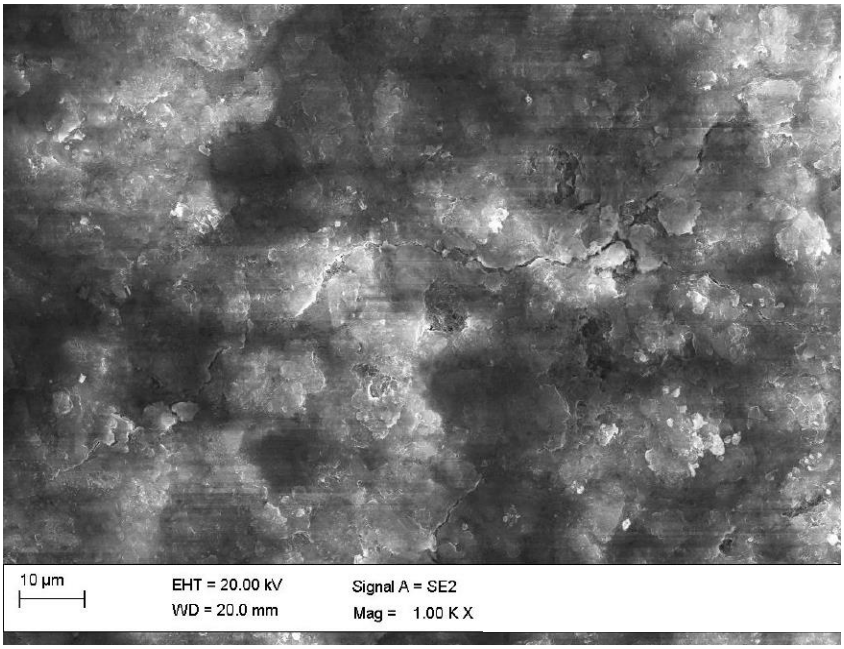

Figure 101 - SEM microscopy (Si/C - MCCFast1 conditions: Li plating deposit)

Cathode surface (Figure 102), as for the other case studies, presents widespread cracking of some particles (red arrows).

Generally, SEM analysis presents a comparable degradation with the other samples.

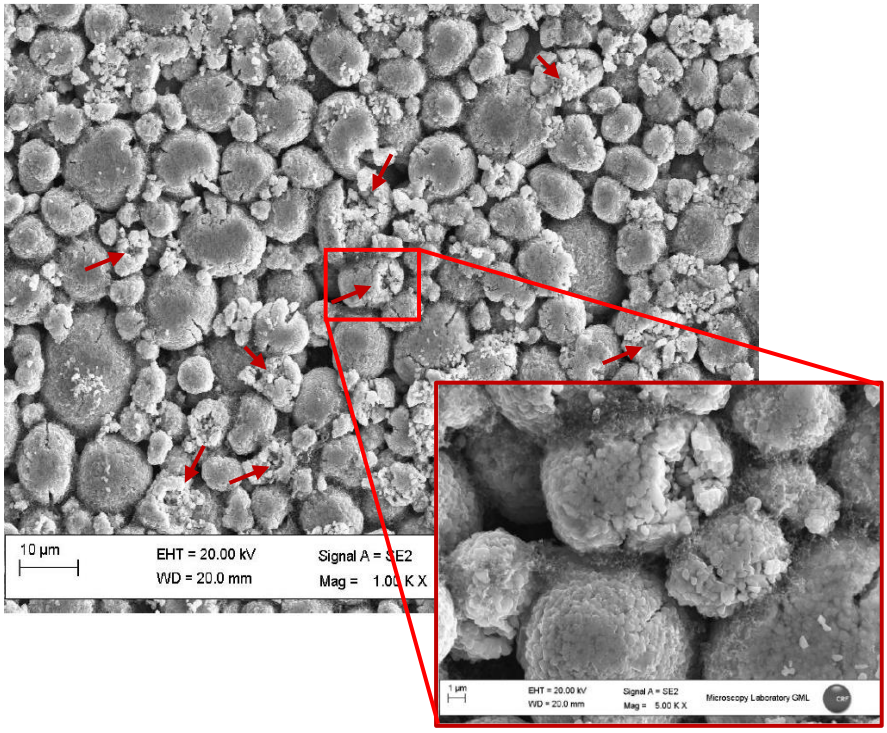

Figure 102 - SEM microscopy (NMC811 – MCCFast1 conditions)

MCCFast2 SEM Analysis

Graphite structure remained also in this case unchanged (Figure 103) with respect to the BOL conditions, presenting similarities with all the other samples analysed.

Since MCCFast2 sample presented some limited Li plating deposits, Figure 104 showed an area all covered by lithium, with a morphology completely different from graphite.

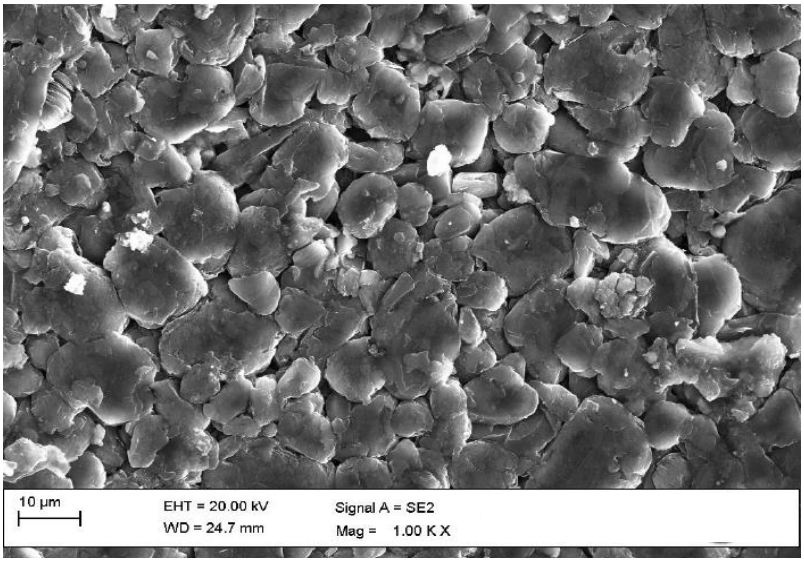

Figure 103 - SEM microscopy (Si/C - MCCFast2 conditions)

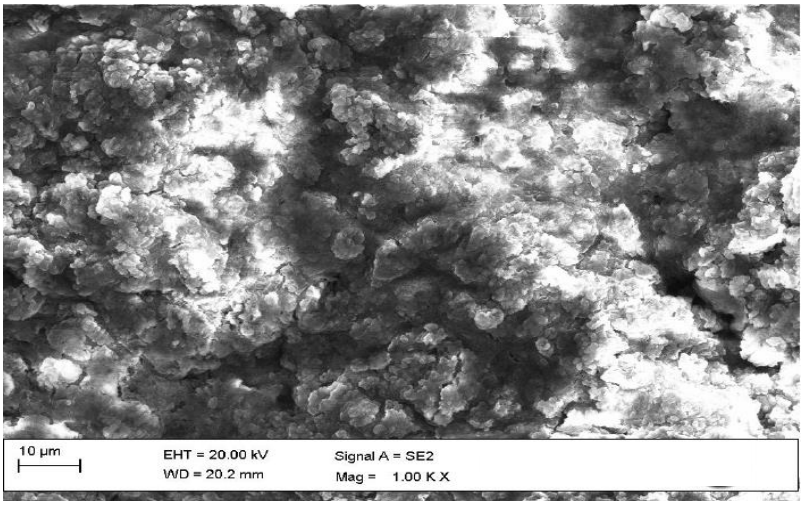

Figure 104 - SEM microscopy (Si/C - MCCFast2 conditions - Li deposits)

NMC particles present a very good shape conditions (Figure 105), demonstrating to retain one of the best morphologies after 1000 cycles, especially considering the high currents applied for the charging (2C as initial step, versus 1C for Reference profile).

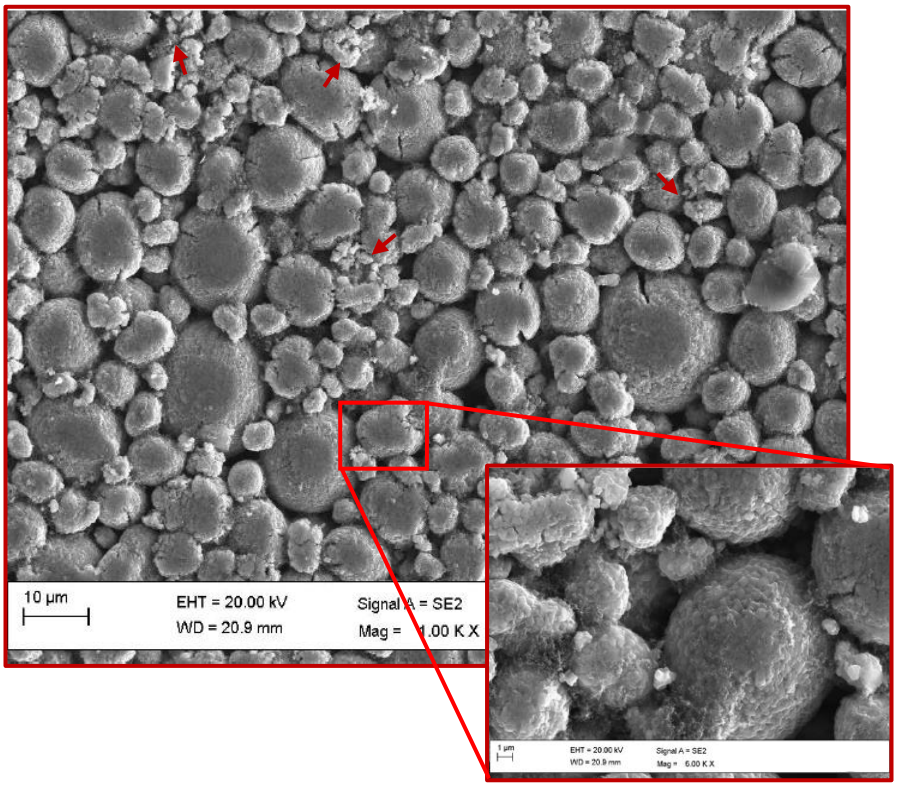

Figure 105 - SEM microscopy (NMC811 – MCCFast2 conditions)

To summarize, SEM analysis showed and confirmed what was already noticed from the other characterization analysis.

The main route cause for sudden loss of performances inside the tested cells was the occurrence of Li plating, which unleashes a non-linear loss of cyclable lithium. When absent, anodic structure properly supported the testing conditions, even if some with degradation from a crystallographic perspective. This was not observed with SEM analysis, but it was highlighted with Raman spectroscopy.

NMC 811 structure was generally damaged, with evident cracking and disaggregation of particles all over the structure, as also reported with simulations methods[160].

Surprisingly, the MCCFast2 cathode presented very good conditions.

Reference and MCCFast1 presented the worst NMC mechanical conditions. MCC1 and MCC2 retained a very similar cathode condition.

Particle size distribution analysis

Given the mechanical degradation noticed thanks to the SEM measurements, particle size distribution on cathode particles was performed, to better understand the particles behaviour when a specific current profile was applied for several cycles. Cathode powders were collected from the dismantled cells and pre-treated, as previously described.

Data show an interesting trend, where Reference sample confirmed the important mechanical degradation, showing a lower particle size distribution (D50), with respect to the BOL sample. It was observed an important decrease of the main peak around 10 µm, with the growth of a smaller family of particles around 1 µm, as visible in Figure 106.

On the contrary, MCC1, MCC2, MCCFast1 and MCCFast2 retained a particle size very close to the BOL conditions.

The results obtained for MCCFast2, given the severe cycling conditions, were of interest for future investigation. Even if it retained a capacity very similar to Reference sample after 1000 cycles, NMC particles in MCCFast2 cell preserved better conditions, with less mechanical degradation. The obtained results support the hypothesis that the selected currents and voltage steps permitted a better Li ion diffusion inside the cathode particles, limiting cracking and diffused particle disruption[161,162].

The obtained results confirm that the customisation of the charging step, tailored on the specific cell, could bring advantages from the life cycle point of view.

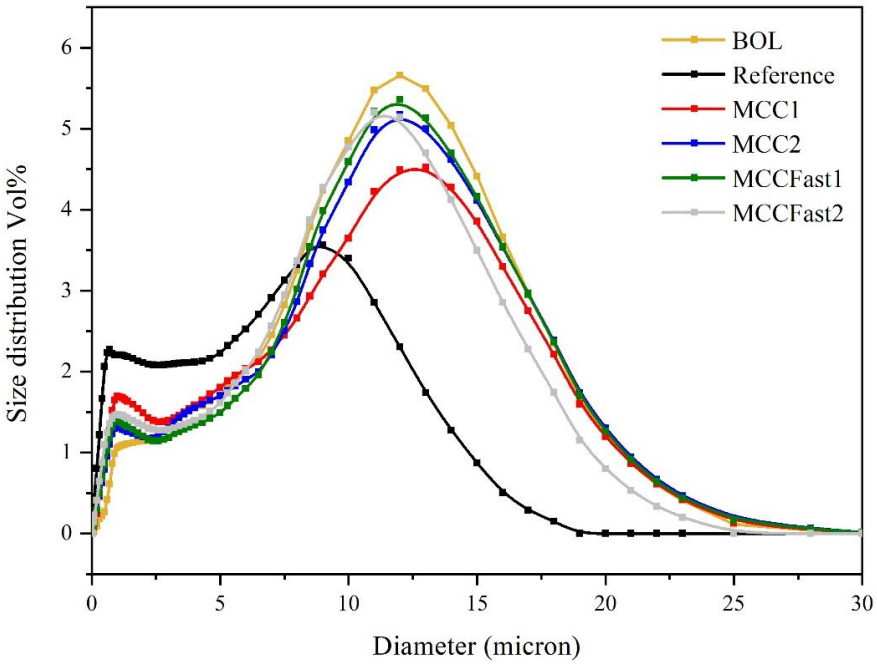

Figure 106 - Particle size distribution for NMC811 particles

Chapter 7 described the results obtained after the cycle aging campaign. Non destructive methods (ICA, EIS, DCIR) were first used to collect information without dismantling the samples, demonstrating to be powerful tools to discriminate about the aging condition of the cells after 1000 cycles (or 80% SoH). Non-destructive methods were then implemented, to go deep with the study of the materials inside. Generally, the observations were aligned to the hypothesis done with the non-destructive methods, open an interesting strategy for future on-board check on health of the cells. From the charging strategy perspective, good results were collected, demonstrating the tailoring as a winning approach for preserving cycling life.

Conclusions and Outlook

The present work arises thank to a collaboration between Università degli Studi di Torino and Centro Ricerche Fiat S.c.P.A, where the experimental activity was carried out, inside the Battery Laboratory, part of Material Engineering, Methods and Tools department (MEMT).

Given that the PhD project was designed and developed within the automotive field, the main goal was to answer to an applied research question, related to the always more predominant e-mobility sector.

Specifically, once the Stellantis Cell Engineering department selected the Li ion cell of interest, the question that gave birth to this project was to work on the cell, trying to find the trade-off among performances, lifespan, and risk limitation, to enhance the vehicle life cycle.

To answer to these automotive requirements, a three-years long project was carried out, among prolonged cycle aging campaign, physical-chemical characterization, and fast-charging protocols optimization. In particular, the contribution of this thesis to the project was related to the optimization of the charging step, working on the materials composing the cell inside the battery pack, to develop customized fast charging profiles, specifically designed on the product.

An intense characterization was included in the final phase of the project, thanks to the support of CRF laboratories and to the collaboration with CERTH, for the Raman analysis.

Starting from several preliminary tests, described in Chapter 4, the information was used as a starting point for this work, electrical and physical-chemical characterization provided the guidelines to go on with the activities.

Two different methodologies to determine the operating limits in terms of current and voltage have been proposed, to be respected for avoiding the deposition of metallic lithium at the anode surface.

The first methodology was selected to have a direct control on each electrode inside the cell. The evaluation of the electrode potential as a function of time, measured in a three-electrode cell against a Li/Li^+ pseudo-reference electrode, was used as confirmation. This methodology was considered as consolidated, based on well-known electrochemical principles able to

guarantee a precise check on electrode potential (i.e., anode vs. Li). On the other hand, it needs a complex preparative procedure, specific facilities (i.e., Glove box with argon flux) and has the risk to degrade the electrodes during the dismantling of the original cell.

Meanwhile, an evaluation of the evolution as a function of time of the DCIR during the charge process was used as alternative methodology. With respect to the previous technique, this method has no complex preparative procedure and no need of specific facilities. There is also no risk of degradation for the electrodes, since no dismantling operation is necessary, enlarging the panorama of possible users. It permits a fast check on Li plating evolution, resulting also easy to be applied to a high number of samples. On the other hand, further investigation is still required, scaling up the methodology on cells with higher capacities, different formats, and different anode chemistry. Both strategies were used to develop five alternative charging profiles, that were tested on 18650 cells and compared to a Reference double-step charging protocol.

The guidelines followed for designing the alternative charging protocols were led by the reduction of charging time, the improvement of capacity retention and as an indirect consequence, the safety.

If from one side the Li plating limitation was used as key feature to set the charging strategy, from the other several degradation mechanisms were taken into consideration thanks to a deepen cell characterization, performed after the cycle aging. From the combination between electrical non-destructive analysis and *post-mortem* characterization on the materials, an important number of information was collected.

From a charging time point of view, the alternatives to Reference permit to restore the same amount of energy, saving time. Specifically, MCC1 and MCC2 can be both proposed as direct replacement of the Reference protocol. They are competitive in term of charging time (3 minutes less than Reference for the complete charge) but preserving the material degradation. From the cycle aging campaign both cells cycled for 1000 cycles with a linear aging trend, suggesting no Li plating formation. ICA responses confirmed the expectations, reproducing the most similar trend with respect to BOL conditions. Internal resistance vs SoC% test, used as

“EOL” check, reported very comfortable results, permitting to charge the cells (i.e., at 1C) between the 5% and 10% SoC more than Reference protocol, without experiencing Li plating, even after 1000 cycles.

No Li plating was found on both cells, aged with MCC1 and MCC2 charging protocols, neither at the visual inspection or SEM microscopy, nor at the Raman spectroscopy, which highlighted that graphite retained among the “best in class” results in terms of crystallinity, with limited particle cracking. EIS spectroscopy then revealed an interesting ohmic resistance for both samples, with values closer to BOL conditions (25 mOhm). SEI resistance also reported very good values, demonstrating a very limited aging. Regarding NMC electrode, no chemical degradation was found, ICP reported that the ratio among metals were maintained, after the cycling campaign. XRPD analyses do not present cation mixing on cathodes, confirming that the degradation has mainly mechanical nature, because of the cracking of the particles caused by continuous volume changes during the cycling.

MCCFast1 charging protocol, that permits to complete the full charge 6 minutes before Reference, presented very good results also, in relation to the applied C-rates. After 1000 cycles it retained a cell capacity very close to MCC1 and MCC2, with a good response in terms of ICA peak position and area, meaning that the materials inside the cell are still working properly. EIS measurement reported a good ohmic resistance behaviour, indication for a good state of the health of the electrolyte also. Regarding the anode, the visual inspection reported only a very limited area where a start of Li plating was found. Nevertheless, Raman analysis demonstrated the good shape of graphite. As for MCC1 and MCC2, NCM particles do not present chemical degradation but only limited mechanical decay.

MCCFast2 and MCCFast3 deserve a specific mention. From one side, MCCFast2 protocol was designed to propose a faster charging profile, able to restore the full cell capacity in 45 minutes, against 56 minutes needed for the Reference protocol. From the other MCCFast3 protocol came up with the idea of pushing the cell to its limit. After 1000 cycles, MCCFast2 presented a capacity loss comparable to Reference sample. ICA also response showed a very similar result, with a peak depression comparable to Reference. From EIS measurements MCCFast2

presented a higher ohmic resistance, suggesting a worsening in the electrolyte conductivity, hypothetically linked to the formation of a thicker SEI. Regarding the anode, some Li plating was found in the inner layers of the jellyroll, in quantities comparable to the cell cycled with Reference protocol. Even if Raman did not show Li plating evidence, the crystallinity of the graphite got worse, nevertheless Reference protocol caused a more pronounced degradation with an increase of amorphous areas/grain boundaries. NMC, as in the other cases, maintained the stoichiometry, no cation mixing was observed, and particle size analysis did not show worsening of the agglomerates. Concerning MCCFast3, this protocol demonstrated lower performances in terms of cycle aging ability, reaching the 80% SoC, after less than 400 cycles, if no derating functions would be included. From the other side, this protocol can restore the full cell capacity within 30 minutes, versus 56 minutes of the Reference. Even if the post-mortem characterization was not performed on samples aged with MCCFast3 protocol, the visual inspection suggested the presence of Li plating along of the anode surface, which probably guided the aging of the cell. This hypothesis was further confirmed by ICA test, that indicates a significant depression of the graphite peak, indicative of an important loss of cyclable lithium. EIS confirmed the health status, presenting higher internal resistances, comparable to the cell aged with MCCFast2 protocol, but arriving at 1000 cycles.

To conclude, this project provided some advances in terms of fast charging definitions by using the so-called “Multi-stage Constant Current” (MCC) approach. The results obtained suggested that Reference charging protocol can be substituted with other charging protocols, able to prolong the cycle life. Specifically, our suggestion would be to implement in the BMS both MCC1, MCC2 or MCCFast1 instructions, for the daily-use charging. These strategies could be easily bettering the performances of the Reference protocol, both in charging time and in capacity retention. For faster charging MCCFast2 could be a very good option and MCCFast3 can be considered for very sporadic episodes, with the implementation of a proper derating function.

Concerning the methodologies, internal resistance test (R_{int} vs. SoC%) can be considered as a valid tool to set the initial boundaries of the cycling protocol, but also to control the limits on the cell, during the aging cycle.

It was observed how the implementation of a derating function, based only on the reduction of cell capacity over a lifetime, was not exhaustive for avoiding a lithium plating phenomenon. This technique seems to be promising to tune the charging steps continuously, by performing a periodic check on the battery system. Since it does not require complex instrumentation, it presents a concrete possibility to be implemented as an "on board" application on BMS.

As outlooks, object of future activities, the following open points need to be studied:

- Characterization of MCCFast3, to discriminate the effect of a derating function on the performances.
- Enlarging the cycle aging by implementing automotive protocols (WLTC) for the discharging step.
- Scaling up of the experiment at the module or pack level.
- Application of the methodology to bigger/different cell formats.

In fact, given the results observed on the selected 18650 samples, with some Li plating occurred where the electrode curvature was higher, another interesting point for the future will be the application of the internal resistance vs SoC% methodology to pouch or prismatic cells' format. Furthermore, since this work focused the attention on two main methods for the detection of Li plating, it would be interesting to investigate further by using other techniques, prioritizing the "on-board" methods, given the high interest coming from the main automotive players. Among them we can cite pressure sensors transducers (thickness increase measurement) and impedance sensors, for the early detection of Li plating.

List of abbreviations

Ah: Ampere Per Hour

AIBS: Aluminium-Ion Batteries

BEPA: Batteries European Partnership Association

BEV: Battery Electric Vehicle

BMS: Battery Management System

BOL: Beginning of Life

C: Capacitance

CAM: Cathode Active Material

CCCV: Constant Current – Constant Voltage

CEI: Cathode Electrolyte Interphase

CERTH: Centre for Research and Technology Hellas

CPE: Constant Phase Element

CT-CV: Constant Temperature - Constant Voltage

DCFC: Direct Current Fast Charge

DCIR: Cell Internal Resistance

DCIR: Direct Current Internal Resistance

DEC: Diethyl Carbonate

DMC: Dimethyl Carbonate

DoD: Depth of Discharge

DVA: Differential Voltage Analysis

EBA: European Battery Alliance

EC: Ethylene Carbonate

EDX: Energy Disperse X-Ray Analysis

EDX: X-Ray Spectroscopy

EERA: European Energy Research Alliance

EOL: End of Life

FEC: Fluoroethylene Carbonate

GC-MS: Gas Chromatography Coupled with Mass Spectroscopy

GEIS: Galvanostatic EIS

HE: High-Energy

HOMO: Highest Occupied Molecular Orbital

HP: High-Power

HPIC: High Pressure Ionic Chromatography

ICA: Incremental Capacity Analysis

ICA: Incremental Capacity Analysis

ICE: Internal Combustion Engine

ICP-OES: Inductively Coupled Plasma Optical Emission Spectroscopy

IL: Ionic Liquid

LAM: Loss of Active Material

LCO: $LiCoO_2$

LFP: $LiFePO_4$

Li-S: Lithium-Sulphur

LIBS: Lithium-Ion Batteries

$LiMO_x$: Lithium Transition Metal Oxides

LLI: Loss of Lithium Inventory

LLZO: $Li_7La_3Zr_2O_{12}$

LRLO: $Li_{1+Y}M_{1-Y}O_2$

LUMO: Lowest Unoccupied Molecular Orbital

MCC: Multistage Constant Current

MIBs: Magnesium-Ion Batteries

NCA: $LiNi_{0.8}Co_{0.15}Al_{0.05}O_2$

NEDC: New European Driving Cycle

NMC: $LiNi_xMn_yCo_zO_2$

OCV: Open Circuit Voltage

ORI: Ohmic Resistance Increase

PC: Propylene Carbonate

PEIS: Potentiostatic EIS

PEO: Polyethylene Oxide

PPO: Polypropylene Oxide

PVDF: Polyvinylidene Fluoride

R: Resistance

RPT: Reference Performance Test

RT: Room Temperature

SEI: Solid Electrolyte Interphase

SEM: Scanning Electron Microscopy

SIBs: Sodium-Ion Batteries

SoH: State of Health

SSBs: Solid-State Batteries

TRL: Technology Readiness Level

U_{an}: Anodic Potential

VC: Vinylene Carbonate

W: Warburg

WD: Working Distance

WLTC: Worldwide Harmonized Light-Duty Vehicles Test Cycles

XRF: X-Ray fluorescence

Bibliography

1. Chen, K., Zhao, F., Hao, H. & Liu, Z. Selection of Lithium-ion Battery Technologies for Electric Vehicles under China's New Energy Vehicle Credit Regulation. *Energy Procedia* **158**, 3038–3044 (2019).
2. https://www.isi.fraunhofer.de/en/blog/themen/batterie-update/lithium-ionen-batteriezellen-entwicklung-batteriezellformate.html
3. Jiang, J. & Zhang, C. *Fundamentals and Applications of Lithium-ion Batteries in Electric Drive Vehicles*. (Wiley, 2015).
4. Megahed, S. & Scrosati, B. Lithium-ion rechargeable batteries. *Journal of Power Sources* **51**, 79–104 (1994).
5. Scrosati, B. & Garche, J. Lithium batteries: Status, prospects and future. *Journal of Power Sources* **195**, 2419–2430 (2010).
6. Pollet, B. G., Staffell, I. & Shang, J. L. Current status of hybrid, battery and fuel cell electric vehicles: From electrochemistry to market prospects. *Electrochimica Acta* **84**, 235–249 (2012).
7. https://battery2030.eu/wp-content/uploads/2022/07/BATTERY-2030-Roadmap_Revision_FINAL
8. Abraham, K. M. How Comparable Are Sodium-Ion Batteries to Lithium-Ion Counterparts? *ACS Energy Lett.* **5**, 3544–3547 (2020).
9. Bachman, J. C. *et al.* Inorganic Solid-State Electrolytes for Lithium Batteries: Mechanisms and Properties Governing Ion Conduction. *Chemical Reviews* **116**, 140–162 (2016).
10. Kwak, W.-J. *et al.* Lithium–Oxygen Batteries and Related Systems: Potential, Status, and Future. *Chem. Rev.* **120**, 6626–6683 (2020).
11. Ahniyaz, A. *et al.* Progress in solid-state high voltage lithium-ion battery electrolytes. *Advances in Applied Energy* **4**, 100070 (2021).

12. Armand, M. *et al.* Lithium-ion batteries – Current state of the art and anticipated developments. *Journal of Power Sources* **479**, 228708 (2020).
13. Li, J. *et al.* Toward Low-Cost, High-Energy Density, and High-Power Density Lithium-Ion Batteries. *JOM* **69**, 1484–1496 (2017).
14. Pelegov, D. V. & Pontes, J. Main Drivers of Battery Industry Changes: Electric Vehicles—A Market Overview. 13 (2018).
15. Ding, Y., Cano, Z. P., Yu, A., Lu, J. & Chen, Z. Automotive Li-Ion Batteries: Current Status and Future Perspectives. *Electrochem. Energ. Rev.* **2**, 1–28 (2019).
16. Opitz, A., Badami, P., Shen, L., Vignarooban, K. & Kannan, A. M. Can Li-Ion batteries be the panacea for automotive applications? *Renewable and Sustainable Energy Reviews* **68**, 685–692 (2017).
17. Pevec, D. *et al.* A survey-based assessment of how existing and potential electric vehicle owners perceive range anxiety. *Journal of Cleaner Production* **276**, 122779 (2020).
18. Manthiram, A. Materials for High-energy Density Batteries. in *Energy Harvesting Technologies* (eds. Priya, S. & Inman, D. J.) 365–385 (Springer US, 2009). doi:10.1007/978-0-387-76464-1_14.
19. Cui, Z., Xie, Q. & Manthiram, A. Zinc-Doped High-Nickel, Low-Cobalt Layered Oxide Cathodes for High-Energy-Density Lithium-Ion Batteries. *ACS Appl. Mater. Interfaces* 9 (2021).
20. Namsar, O. Improved electrochemical performance of anode materials for high energy density lithium-ion batteries through Sn(SnO2)–SiO2/graphene-based nanocomposites prepared by a facile and low-cost approach. *Sustainable Energy Fuels* 12 (2020).
21. Keil, P. Charging protocols for lithium-ion batteries and their impact on cycle life—An experimental study with different 18650 high-power cells. *Journal of Energy Storage* 17 (2016).
22. Tomaszewska, A. *et al.* Lithium-ion battery fast charging: A review. *eTransportation* **1**, 100011 (2019).

23. Dotoli, M. *et al.* Detection of Lithium Plating in Li-Ion Cell Anodes Using Realistic Automotive Fast-Charge Profiles. *Batteries* **7**, 46 (2021).
24. Jiang, J. & Zhang, C. *Fundamentals and Applications of Lithium-ion Batteries in Electric Drive Vehicles*. (Wiley, 2015). doi:10.1002/9781118414798.
25. Silva, F. A. Lithium-Ion Batteries: Fundamentals and Applications [Book News]. *EEE Ind. Electron. Mag.* **10**, 58–59 (2016).
26. Deng, D. Li-ion batteries: basics, progress, and challenges. *Energy Science & Engineering* **3**, 385–418 (2015).
27. Goodenough, J. B. & Park, K.-S. The Li-Ion Rechargeable Battery: A Perspective. *J. Am. Chem. Soc.* **135**, 1167–1176 (2013).
28. Peljo, Pekka, and Hubert H. Girault. Electrochemical Potential Window of Battery Electrolytes: The HOMO–LUMO Misconception. *Electrochemical Potential Window of Battery Electrolytes: The HOMO–LUMO Misconception.* **Energy&Environmental Science**, 2306–309. (2018).
29. Manthiram, A. A reflection on lithium-ion battery cathode chemistry. *Nat Commun* **11**, 1550 (2020).
30. Zhang, R. *et al.* State of the Art of Lithium-Ion Battery SOC Estimation for Electrical Vehicles. *Energies* **11**, (2018).
31. Julien, C. M. & Mauger, A. NCA, NCM811, and the Route to Ni-Richer Lithium-Ion Batteries. *Energies* **13**, (2020).
32. Liang, G., Peterson, V. K., See, K. W., Guo, Z. & Pang, W. K. Developing high-voltage spinel LiNi0.5Mn1.5O4 cathodes for high-energy-density lithium-ion batteries: current achievements and future prospects. *J. Mater. Chem. A* **8**, 15373–15398 (2020).
33. Nie, L., Chen, S. & Liu, W. Challenges and strategies of lithium-rich layered oxides for Li-ion batteries. *Nano Research* **16**, 391–402 (2023).
34. Nzereogu, P. U., Omah, A. D., Ezema, F. I., Iwuoha, E. I. & Nwanya, A. C. Anode materials for lithium-ion batteries: A review. *Applied Surface Science Advances* **9**, 100233 (2022).

35. Zhang, L. *et al.* The typical structural evolution of silicon anode. *Cell Reports Physical Science* **3**, 100811 (2022).
36. Li, P. *et al.* Recent progress on silicon-based anode materials for practical lithium-ion battery applications. *Energy Storage Materials* **15**, 422–446 (2018).
37. Wang, R., Cui, W., Chu, F. & Wu, F. Lithium metal anodes: Present and future. *Journal of Energy Chemistry* **48**, 145–159 (2020).
38. Yuan, H. *et al.* A review of concepts and contributions in lithium metal anode development. *Materials Today* **53**, 173–196 (2022).
39. Al Hassan, M. R., Sen, A., Zaman, T. & Mostari, M. S. Emergence of graphene as a promising anode material for rechargeable batteries: a review. *Materials Today Chemistry* **11**, 225–243 (2019).
40. Yang, Y. *et al.* A review on silicon nanowire-based anodes for next-generation high-performance lithium-ion batteries from a material-based perspective. *Sustainable Energy Fuels* **4**, 1577–1594 (2020).
41. Li, Q., Chen, J., Fan, L., Kong, X. & Lu, Y. Progress in electrolytes for rechargeable Li-based batteries and beyond. *Green Energy & Environment* **1**, 18–42 (2016).
42. Marcinek, M. *et al.* Electrolytes for Li-ion transport – Review. *Solid State Ionics* **276**, 107–126 (2015).
43. Guo, K. *et al.* High-Voltage Electrolyte Chemistry for Lithium Batteries. *Small Science* **2**, 2100107 (2022).
44. Gond, R., van Ekeren, W., Mogensen, R., Naylor, A. J. & Younesi, R. Non-flammable liquid electrolytes for safe batteries. *Mater. Horiz.* **8**, 2913–2928 (2021).
45. Lewandowski, A. & Świderska-Mocek, A. Ionic liquids as electrolytes for Li-ion batteries—An overview of electrochemical studies. *Journal of Power Sources* **194**, 601–609 (2009).
46. Liu, S. *et al.* LiFSI and LiDFBOP Dual-Salt Electrolyte Reinforces the Solid Electrolyte Interphase on a Lithium Metal Anode. *ACS Appl. Mater. Interfaces* **12**, 33719–33728 (2020).

47. Yang, J. *et al.* Dual-Salt Electrolytes to Effectively Reduce Impedance Rise of High-Nickel Lithium-Ion Batteries. *ACS Appl. Mater. Interfaces* **13**, 40502–40512 (2021).
49. Pasta, M. *et al.* 2020 roadmap on solid-state batteries. *J. Phys. Energy* **2**, 032008 (2020).
50. Zhang, J. *et al.* Research Progress of Anode-Free Lithium Metal Batteries. *Crystals* **12**, (2022).
51. Kim, J. G. *et al.* A review of lithium and non-lithium based solid state batteries. *Journal of Power Sources* **282**, 299–322 (2015).
52. Duffner, F. *et al.* Post-lithium-ion battery cell production and its compatibility with lithium-ion cell production infrastructure. *Nat Energy* **6**, 123–134 (2021).
53. Zhang, J. *et al.* Research Progress of Anode-Free Lithium Metal Batteries. *Crystals* **12**, 1241 (2022).
54. https://battery2030.eu/wp-content/uploads/2022/07/BATTERY-2030-Roadmap_Revision_FINAL
55. Ma, J. *et al.* The 2021 battery technology roadmap. *Journal of Physics D: Applied Physics* **54**, 183001 (2021).
56. Lin, C., Tang, A., Mu, H., Wang, W. & Wang, C. Aging Mechanisms of Electrode Materials in Lithium-Ion Batteries for Electric Vehicles. *Journal of Chemistry* **2015**, 1–11 (2015).
57. Sarre, G., Blanchard, P. & Broussely, M. Aging of lithium-ion batteries. *Journal of Power Sources* **127**, 65–71 (2004).
58. Barcellona, S. & Piegari, L. Effect of current on cycle aging of lithium ion batteries. *Journal of Energy Storage* **29**, 101310 (2020).
59. Agubra, V. & Fergus, J. Lithium Ion Battery Anode Aging Mechanisms. *Materials* **6**, 1310–1325 (2013).
60. Xiong, R., Pan, Y., Shen, W., Li, H. & Sun, F. Lithium-ion battery aging mechanisms and diagnosis method for automotive applications: Recent advances and perspectives. *Renewable and Sustainable Energy Reviews* **131**, 110048 (2020).

61. Broussely, M. *et al.* Main aging mechanisms in Li ion batteries. *Journal of Power Sources* **146**, 90–96 (2005).
62. Palacín, M. R. Understanding ageing in Li-ion batteries: a chemical issue. *Chem. Soc. Rev.* **47**, 4924–4933 (2018).
63. Keil, P. *et al.* Calendar Aging of Lithium-Ion Batteries. *Journal of The Electrochemical Society* **163**, A1872 (2016).
64. Wright, R. B. *et al.* Power fade and capacity fade resulting from cycle-life testing of Advanced Technology Development Program lithium-ion batteries. *Journal of Power Sources* **119–121**, 865–869 (2003).
65. Pastor-Fernandez, C., Dhammika Widanage, W., Marco, J., Gama-Valdez, M.-A. & Chouchelamane, Gael. H. Identification and quantification of ageing mechanisms in Lithium-ion batteries using the EIS technique. in *2016 IEEE Transportation Electrification Conference and Expo (ITEC)* 1–6 (IEEE, 2016). doi:10.1109/ITEC.2016.7520198.
66. Meda, U. S., Lal, L., M, S. & Garg, P. Solid Electrolyte Interphase (SEI), a boon or a bane for lithium batteries: A review on the recent advances. *Journal of Energy Storage* **47**, 103564 (2022).
67. Heiskanen, S. K., Kim, J. & Lucht, B. L. Generation and Evolution of the Solid Electrolyte Interphase of Lithium-Ion Batteries. *Joule* **3**, 2322–2333 (2019).
68. Pinson, M. B. & Bazant, M. Z. Theory of SEI Formation in Rechargeable Batteries: Capacity Fade, Accelerated Aging and Lifetime Prediction. *J. Electrochem. Soc.* **160**, A243–A250 (2013).
69. Rowden, B. & Garcia-Araez, N. A review of gas evolution in lithium ion batteries. *Energy Reports* **6**, 10–18 (2020).
70. Lemordant, D. *et al.* Artificial SEI for Lithium-Ion Battery Anodes. in *Advanced Fluoride-Based Materials for Energy Conversion* 173–202 (Elsevier, 2015). doi:10.1016/B978-0-12-800679-5.00008-7.

71. Yu, Z., Cui, Y. & Bao, Z. Design Principles of Artificial Solid Electrolyte Interphases for Lithium-Metal Anodes. *Cell Reports Physical Science* **1**, 100119 (2020).
72. Jankowski, P., Wieczorek, W. & Johansson, P. SEI-forming electrolyte additives for lithium-ion batteries: development and benchmarking of computational approaches. *J Mol Model* **23**, 6 (2017).
73. Tokranov, A. *et al.* Control and Optimization of the Electrochemical and Mechanical Properties of the Solid Electrolyte Interphase on Silicon Electrodes in Lithium Ion Batteries. *Adv. Energy Mater.* **6**, 1502302 (2016).
74. Cho, J.-H. & Picraux, S. T. Silicon Nanowire Degradation and Stabilization during Lithium Cycling by SEI Layer Formation. *Nano Lett.* **14**, 3088–3095 (2014).
75. Frankenberger, M. *et al.* SEI Growth Impacts of Lamination, Formation and Cycling in Lithium Ion Batteries. *Batteries* **6**, 21 (2020).
76. Keil, J. *et al.* Linear and Nonlinear Aging of Lithium-Ion Cells Investigated by Electrochemical Analysis and In-Situ Neutron Diffraction. *J. Electrochem. Soc.* **166**, A3908–A3917 (2019).
77. Estevez, M. A. P., Conte, F. V., Tremonti, C. & Renzi, M. Aging estimation of lithium ion cells under real-world conditions through mechanical stress measurements. *Journal of Energy Storage* **64**, 107186 (2023).
78. Diao, W., Saxena, S., Han, B. & Pecht, M. Algorithm to Determine the Knee Point on Capacity Fade Curves of Lithium-Ion Cells. *Energies* **12**, 2910 (2019).
79. Schuster, S. F. *et al.* Nonlinear aging characteristics of lithium-ion cells under different operational conditions. *Journal of Energy Storage* **1**, 44–53 (2015).
80. Attia, P. M. *et al.* Review—"Knees" in Lithium-Ion Battery Aging Trajectories. *J. Electrochem. Soc.* **169**, 060517 (2022).
81. Birkl, C. R., Roberts, M. R., McTurk, E., Bruce, P. G. & Howey, D. A. Degradation diagnostics for lithium ion cells. *Journal of Power Sources* **341**, 373–386 (2017).

82. Sarasketa-Zabala, E. *et al.* Understanding Lithium Inventory Loss and Sudden Performance Fade in Cylindrical Cells during Cycling with Deep-Discharge Steps. *J. Phys. Chem. C* **119**, 896–906 (2015).
83. Schlasza, C., Ostertag, P., Chrenko, D., Kriesten, R. & Bouquain, D. Review on the aging mechanisms in Li-ion batteries for electric vehicles based on the FMEA method. in *2014 IEEE Transportation Electrification Conference and Expo (ITEC)* 1–6 (IEEE, 2014). doi:10.1109/ITEC.2014.6861811.
84. Essl, C., Seifert, L., Rabe, M. & Fuchs, A. Early Detection of Failing Automotive Batteries Using Gas Sensors. *Batteries* **7**, 25 (2021).
85. Zhuo, M., Offer, G. & Marinescu, M. Degradation model of high-nickel positive electrodes: Effects of loss of active material and cyclable lithium on capacity fade. *Journal of Power Sources* **556**, 232461 (2023).
86. Janakiraman, U., Garrick, T. R. & Fortier, M. E. Review—Lithium Plating Detection Methods in Li-Ion Batteries. *J. Electrochem. Soc.* **167**, 160552 (2020).
87. Lin, X., Khosravinia, K., Hu, X., Li, J. & Lu, W. Lithium Plating Mechanism, Detection, and Mitigation in Lithium-Ion Batteries. *Progress in Energy and Combustion Science* **87**, 100953 (2021).
88. Koleti, U. R., Dinh, T. Q. & Marco, J. A new on-line method for lithium plating detection in lithium-ion batteries. *Journal of Power Sources* **451**, 227798 (2020).
89. Petzl, M., Kasper, M. & Danzer, M. A. Lithium plating in a commercial lithium-ion battery – A low-temperature aging study. *Journal of Power Sources* **275**, 799–807 (2015).
90. Liu, Q. *et al.* Understanding undesirable anode lithium plating issues in lithium-ion batteries. *RSC Adv.* **6**, 88683–88700 (2016).
91. Guo, Z., Zhu, J., Feng, J. & Du, S. Direct in situ observation and explanation of lithium dendrite of commercial graphite electrodes. *RSC Adv.* **5**, 69514–69521 (2015).
92. Tian, Y., Lin, C., Li, H., Du, J. & Xiong, R. Detecting undesired lithium plating on anodes for lithium-ion batteries – A review on the in-situ methods. *Applied Energy* **300**, 117386 (2021).

93. Bitzer, B. & Gruhle, A. A new method for detecting lithium plating by measuring the cell thickness. *Journal of Power Sources* **262**, 297–302 (2014).
94. Lüders, C. *et al.* Lithium plating in lithium-ion batteries investigated by voltage relaxation and in situ neutron diffraction. *Journal of Power Sources* **342**, (2017).
95. Campbell, I. D., Marzook, M., Marinescu, M. & Offer, G. J. How Observable Is Lithium Plating? Differential Voltage Analysis to Identify and Quantify Lithium Plating Following Fast Charging of Cold Lithium-Ion Batteries. *J. Electrochem. Soc.* **166**, A725–A739 (2019).
96. Tomaszewska, A. *et al.* Lithium-ion battery fast charging: A review. *eTransportation* **1**, 100011 (2019).
97. Liu, Y.-H. & Luo, Y.-F. Search for an Optimal Rapid-Charging Pattern for Li-Ion Batteries Using the Taguchi Approach. *Industrial Electronics, IEEE Transactions on* **57**, 3963–3971 (2011).
98. Waldmann, T., Kasper, M. & Wohlfahrt-Mehrens, M. Optimization of Charging Strategy by Prevention of Lithium Deposition on Anodes in high-energy Lithium-ion Batteries - Electrochemical Experiments. *Electrochimica Acta* **178**, 525 (2015).
99. Abdel Monem, M. *et al.* Lithium-ion batteries: Evaluation study of different charging methodologies based on aging process. *Applied Energy* **152**, 143–155 (2015).
100. Abdel-Monem, M. *et al.* A comparative study of different fast charging methodologies for lithium-ion batteries based on aging process. in *EVS28 Int Electr Veh Symp Exhib* (2015).
101. Li, J., Murphy, E., Winnick, J. & Kohl, P. A. The effects of pulse charging on cycling characteristics of commercial lithium-ion batteries. *Journal of Power Sources* **102**, 302–309 (2001).
102. Notten, P. H. L., Veld, J. H. G. O. het & Beek, J. R. G. van. Boostcharging Li-ion batteries: A challenging new charging concept. *Journal of Power Sources* **145**, 89–94 (2005).
103. Cho, I.-H., Lee, P.-Y. & Kim, J.-H. Analysis of the Effect of the Variable Charging Current Control Method on Cycle Life of Li-ion Batteries. *Energies* **12**, 3023 (2019).

104. Patnaik, L., Praneeth, A. V. J. S. & Williamson, S. S. A Closed-Loop Constant-Temperature Constant-Voltage Charging Technique to Reduce Charge Time of Lithium-Ion Batteries. *IEEE Trans. Ind. Electron.* **66**, 1059–1067 (2019).
105. Rangarajan, S. P., Barsukov, Y. & Mukherjee, P. P. Anode potential controlled charging prevents lithium plating. *J. Mater. Chem. A* **8**, 13077–13085 (2020).
106. Wu, W. *et al.* Impact of low temperature and charge profile on the aging of lithium-ion battery: Non-invasive and post-mortem analysis. *International Journal of Heat and Mass Transfer* **170**, 121024 (2021).
107. Diao, W., Kulkarni, C. & Pecht, M. Development of an Informative Lithium-Ion Battery Datasheet. *Energies* **14**, 5434 (2021).
108. Waldmann, T. *et al.* Interplay of Operational Parameters on Lithium Deposition in Lithium-Ion Cells: Systematic Measurements with Reconstructed 3-Electrode Pouch Full Cells. *J. Electrochem. Soc.* **163**, A1232–A1238 (2016).
109. Kuntz, P. *et al.* Identification of Degradation Mechanisms by Post-Mortem Analysis for High Power and High Energy Commercial Li-Ion Cells after Electric Vehicle Aging. *Batteries* **7**, 48 (2021).
110. Buchberger, I. *et al.* Aging Analysis of Graphite/LiNi $_{1/3}$ Mn $_{1/3}$ Co $_{1/3}$ O $_{2}$ Cells Using XRD, PGAA, and AC Impedance. *J. Electrochem. Soc.* **162**, A2737–A2746 (2015).
111. Schindler, S., Bauer, M., Petzl, M. & Danzer, M. A. Voltage relaxation and impedance spectroscopy as in-operando methods for the detection of lithium plating on graphitic anodes in commercial lithium-ion cells. *Journal of Power Sources* **304**, 170–180 (2016).
112. Stiaszny, B., Ziegler, J. C., Krauß, E. E., Schmidt, J. P. & Ivers-Tiffée, E. Electrochemical characterization and post-mortem analysis of aged LiMn2O4–Li(Ni0.5Mn0.3Co0.2)O2/graphite lithium ion batteries. Part I: Cycle aging. *Journal of Power Sources* **251**, 439–450 (2014).
113. Zech, C. *et al.* Quantitative manganese dissolution investigation in lithium-ion batteries by means of X-ray spectrometry techniques. *J. Anal. At. Spectrom.* **36**, 2056–2062 (2021).

114. Medic, D., Milic, S., Alagic, S., Djordjevic, I. & Dimitrijevic, S. Classification of spent Li-ion batteries based on ICP-OES/X-ray characterization of the cathode materials. *Hem Ind* **74**, 221–230 (2020).
115. Gantenbein, S., Schönleber, M., Weiss, M. & Ivers-Tiffée, E. Capacity Fade in Lithium-Ion Batteries and Cyclic Aging over Various State-of-Charge Ranges. *Sustainability* **11**, 6697 (2019).
116. Gaberšček, M. Impedance spectroscopy of battery cells: Theory versus experiment. *Current Opinion in Electrochemistry* **32**, 100917 (2022).
117. R-Smith, N. A.-Z. *et al.* Multiplexed 16 × 16 Li-Ion Cell Measurements Including Internal Resistance for Quality Inspection and Classification. *IEEE Trans. Instrum. Meas.* **70**, 1–9 (2021).
118. Schweiger, H.-G. *et al.* Comparison of Several Methods for Determining the Internal Resistance of Lithium Ion Cells. *Sensors* **10**, 5604–5625 (2010).
119. Barai, A., Uddin, K., Widanage, W. D., McGordon, A. & Jennings, P. A study of the influence of measurement timescale on internal resistance characterisation methodologies for lithium-ion cells. *Sci Rep* **8**, 21 (2018).
120. Krupp, A., Ferg, E., Schuldt, F., Derendorf, K. & Agert, C. Incremental Capacity Analysis as a State of Health Estimation Method for Lithium-Ion Battery Modules with Series-Connected Cells. *Batteries* **7**, 2 (2020).
121. Riviere, E., Sari, A., Venet, P., Meniere, F. & Bultel, Y. Innovative Incremental Capacity Analysis Implementation for C/LiFePO4 Cell State-of-Health Estimation in Electrical Vehicles. *Batteries* **5**, 37 (2019).
122. Fly, A. & Chen, R. Rate dependency of incremental capacity analysis (dQ/dV) as a diagnostic tool for lithium-ion batteries. *Journal of Energy Storage* **29**, 101329 (2020).
123. Baddour-Hadjean, R. & Pereira-Ramos, J.-P. Raman Microspectrometry Applied to the Study of Electrode Materials for Lithium Batteries. *Chem. Rev.* **110**, 1278–1319 (2010).
124. Heber, M., Hofmann, K. & Hess, C. Raman Diagnostics of Cathode Materials for Li-Ion Batteries Using Multi-Wavelength Excitation. *Batteries* **8**, 10 (2022).

125. Mulvaney, S. P. & Keating, C. D. Raman Spectroscopy. *Anal. Chem.* **72**, 145–158 (2000).
126. Meddings, N. *et al.* Application of electrochemical impedance spectroscopy to commercial Li-ion cells: A review. *Journal of Power Sources* **480**, 228742 (2020).
127. Cioroianu, C. C., Marinescu, D. G., Iorga, A. & Sibiceanu, A. R. Simulation of an electric vehicle model on the new WLTC test cycle using AVL CRUISE software. *IOP Conf. Ser.: Mater. Sci. Eng.* **252**, 012060 (2017).
128. Ruan, H. *et al.* Lithium-ion battery lifetime extension: A review of derating methods. *Journal of Power Sources* **563**, 232805 (2023).
129. Sun, Y., Saxena, S. & Pecht, M. Derating Guidelines for Lithium-Ion Batteries. *Energies* **11**, 3295 (2018).
130. Vetter, J. *et al.* Ageing mechanisms in lithium-ion batteries. *Journal of Power Sources* **147**, 269–281 (2005).
131. Edge, J. S. *et al.* Lithium ion battery degradation: what you need to know. *Phys. Chem. Chem. Phys.* **23**, 8200–8221 (2021).
132. Atalay, S. *et al.* Theory of battery ageing in a lithium-ion battery: Capacity fade, nonlinear ageing and lifetime prediction. *Journal of Power Sources* **478**, 229026 (2020).
133. Ruess, R. *et al.* Influence of NCM Particle Cracking on Kinetics of Lithium-Ion Batteries with Liquid or Solid Electrolyte. *J. Electrochem. Soc.* **167**, 100532 (2020).
134. Pfrang, A. *et al.* Geometrical Inhomogeneities as Cause of Mechanical Failure in Commercial 18650 Lithium Ion Cells. *J. Electrochem. Soc.* **166**, A3745–A3752 (2019).
135. Jung, S.-K. *et al.* Understanding the Degradation Mechanisms of $LiNi_{0.5}Co_{0.2}Mn_{0.3}O_2$ Cathode Material in Lithium Ion Batteries. *Adv. Energy Mater.* **4**, 1300787 (2014).
136. de Biasi, L. *et al.* Phase Transformation Behavior and Stability of $LiNiO_2$ Cathode Material for Li-Ion Batteries Obtained from In Situ Gas Analysis and Operando X-Ray Diffraction. *ChemSusChem* **12**, 2240–2250 (2019).
137. Li, T. *et al.* Degradation Mechanisms and Mitigation Strategies of Nickel-Rich NMC-Based Lithium-Ion Batteries. *Electrochem. Energ. Rev.* **3**, 43–80 (2020).

138. Zhu, J. *et al.* Investigation of capacity fade for 18650-type lithium-ion batteries cycled in different state of charge (SoC) ranges. *Journal of Power Sources* **489**, 229422 (2021).
139. Li, Y., Guo, J., Pedersen, K., Gurevich, L. & Stroe, D.-I. Investigation of multi-step fast charging protocol and aging mechanism for commercial NMC/graphite lithium-ion batteries. *Journal of Energy Chemistry* **80**, 237–246 (2023).
140. Janakiraman, U., Garrick, T. R. & Fortier, M. E. Review—Lithium Plating Detection Methods in Li-Ion Batteries. *J. Electrochem. Soc.* **167**, 160552 (2020).
141. Sieg, J. *et al.* Fast charging of an electric vehicle lithium-ion battery at the limit of the lithium deposition process. *Journal of Power Sources* **427**, 260–270 (2019).
142. F. Rodrigues, M. T. *et al.* How Fast Can a Li-Ion Battery Be Charged? Determination of Limiting Fast Charging Conditions. *ACS Appl. Energy Mater.* **4**, 1063–1068 (2021).
143. Baker, D. R. & Verbrugge, M. W. Modeling Overcharge at Graphite Electrodes: Plating and Dissolution of Lithium. *J. Electrochem. Soc.* **167**, 013504 (2020).
144. Waldmann, T., Scurtu, R.-G., Brändle, D. & Wohlfahrt-Mehrens, M. Effects of Tab Design in 21700 Li-Ion Cells: Improvements of Cell Impedance, Rate Capability, and Cycling Aging. *Energy Technology* **11**, 2200583 (2023).
145. Brailsford, D. F. & Robertson, A. J. B. Calculation of electric field strengths at a sharp edge. *International Journal of Mass Spectrometry and Ion Physics* **1**, 75–85 (1968).
146. Ryu, H.-H. *et al.* Capacity Fading Mechanisms in Ni-Rich Single-Crystal NCM Cathodes. *ACS Energy Lett.* **6**, 2726–2734 (2021).
147. Ahn, Y., Jo, Y. N., Cho, W., Yu, J.-S. & Kim, K. J. Mechanism of Capacity Fading in the LiNi0.8Co0.1Mn0.1O2 Cathode Material for Lithium-Ion Batteries. *Energies* **12**, 1638 (2019).
148. Wang, H. & Whitacre, J. F. Inhomogeneous aging of cathode materials in commercial 18650 lithium ion battery cells. *Journal of Energy Storage* **35**, 102244 (2021).
149. Bach, T. C. *et al.* Nonlinear aging of cylindrical lithium-ion cells linked to heterogeneous compression. *Journal of Energy Storage* **5**, 212–223 (2016).

150. Friedrich, F. *et al.* Editors' Choice—Capacity Fading Mechanisms of NCM-811 Cathodes in Lithium-Ion Batteries Studied by X-ray Diffraction and Other Diagnostics. *J. Electrochem. Soc.* **166**, A3760–A3774 (2019).
151. Wu, X. *et al.* Effects of charging rates on LiNi0.6Mn0.2Co0.2O2 (NMC622)/graphite Li-ion cells. *Journal of Energy Chemistry* **56**, 121–126 (2021).
152. Sun, H. & Zhao, K. Electronic Structure and Comparative Properties of $LiNi_xMn_yCo_zO_2$ Cathode Materials. *J. Phys. Chem. C* **121**, 6002–6010 (2017).
153. Li, J. *et al.* Addressing cation mixing in layered structured cathodes for lithium-ion batteries: A critical review. *Nano Materials Science* S2589965122000496 (2022) doi:10.1016/j.nanoms.2022.09.001.
154. Radziuk, D. & Möhwald, H. Ultrasonically treated liquid interfaces for progress in cleaning and separation processes. *Phys. Chem. Chem. Phys.* **18**, 21–46 (2016).
155. Gupta, H. & Singh, R. K. High-Voltage Nickel-Rich NMC Cathode Material with Ionic-Liquid-Based Polymer Electrolytes for Rechargeable Lithium-Metal Batteries. *ChemElectroChem* **7**, 3597–3605 (2020).
156. https://publica-rest.fraunhofer.de/server/api/core/bitstreams/dee457d4-fd40-44dd-a03b-9feefcda584a/content
157. Cabañero, M. A., Hagen, M. & Quiroga-González, E. In-operando Raman study of lithium plating on graphite electrodes of lithium ion batteries. *Electrochimica Acta* **374**, 137487 (2021).
158. Fonseca Rodrigues, M.-T. *et al.* Lithium Acetylide: A Spectroscopic Marker for Lithium Deposition During Fast Charging of Li-Ion Cells. *ACS Appl. Energy Mater.* **2**, 873–881 (2019).
159. Tuinstra, F. & Koenig, J. L. Raman Spectrum of Graphite. *The Journal of Chemical Physics* **53**, 1126–1130 (1970).
160. Christensen, J. & Newman, J. A Mathematical Model of Stress Generation and Fracture in Lithium Manganese Oxide. *Journal of The Electrochemical Society* **153**, A1019 (2006).

161. Aishova, A., Park, G., Yoon, C. S. & Sun, Y. Cobalt-Free High-Capacity Ni-Rich Layered Li[Ni $_{0.9}$ Mn $_{0.1}$]O $_2$ Cathode. *Adv. Energy Mater.* **10**, 1903179 (2020).
162. Sun, G. *et al.* On the fragmentation of active material secondary particles in lithium ion battery cathodes induced by charge cycling. *Extreme Mechanics Letters* **9**, 449–458 (2016).
163. Lazanas, A. Ch. & Prodromidis, M. I. Electrochemical Impedance Spectroscopy─A Tutorial. *ACS Meas. Sci. Au* **3**, 162–193 (2023).
164. Macdonald, J. R. & Johnson, W. B. Fundamentals of Impedance Spectroscopy. in *Impedance Spectroscopy* 1–20 (2018). doi:10.1002/9781119381860.ch1.
165. Zheng, S. *et al.* Correlation between long range and local structural changes in Ni-rich layered materials during charge and discharge process. *Journal of Power Sources* **412**, 336–343 (2019).
166. Jiang, M., Danilov, D. L., Eichel, R.-A. & Notten, P. H. L. A Review of Degradation Mechanisms and Recent Achievements for Ni-Rich Cathode-Based Li-Ion Batteries. *Advanced Energy Materials* **11**, 2103005 (2021).

Acknowledgements

First, I would like to thank Dr. Mauro Sgroi, for the opportunity to start working in the e-mobility field. The possibility to join a PhD student position at Centro Ricerche Fiat was for me a big opportunity to gain knowledge in a very promising and interesting field. I think we worked very proficiently together, starting from the creation of the lab, it was very challenging but for sure satisfying. Thanks for all the teachings, with the hope to share some projects in the future.

Thanks also to Università degli Studi di Torino, in the figures of Prof. Carlo Nervi and Prof. Marcello Baricco, for the support and supervision during the whole period, from the master degreed thesis ahead.

A big thanks to all my former colleagues at Centro Ricerche Fiat.

Nello, all the colleagues from the Mirafiori and Orbassano labs, thank you for the collaborations and for the funny time at the coffee machine also.

A special thanks to Flavio and Giovanna, the historical pillars of the group, thank you for all your precious advice and constant support…and for having me introduced in the European projects world :).

Thanks also to Mattia, Riccardo and Arianna for having shared the daily work in the lab, it was stressing sometimes but we had a lot of fun, indeed.

Thanks guys, with the hope to collaborate with you.

Thanks also to Georgia Kastrinaki and CERTH colleagues, for helping me in performing Raman.

A big thanks to the guys from the Stellantis engineering department. Emanuele, thank you for having shared a three-years long project with me, I think it was very funny and efficient to merge our competencies.

I want to say thanks also to my present colleagues at Comau S.p.A, thanks for the opportunity given me one year ago and for the chance to improve my experience in the R&D, being part of the Battery Competence Centre on cell manufacturing.
Now, coming to more personal acknowledgments, I want to express my gratitude to all my family for the huge support during all these years.
A special thanks to my father, my mother and my sister for permitting me to go on with my studies without pressure, understanding and indulging my wishes, for the moral support and for the concrete support also.
Thanks to the old and to the new friends, for the funny moments and for having shared bad times with me, together is always easier.
A huge thanks to Denise, half of our lives together, you could be scientifically defined as such a pleasant constant in a world full of variables. I am grateful for your always present support and for your efforts in understanding the difficulties along this journey. After all, who better than you can understand these feelings. I hope to be able to do the same for you and I wish you all the best for your carrier, you deserve.
To conclude a little thanks to myself, for the efforts, for not giving up and for getting me the chance to accept this challenge.
With the hope to spend this experience properly in my future carrier.

Matteo

Appendix

EIS: theoretical hints

Impedance spectroscopy measures the resistance and reactance of the battery cell as a function of frequency, using an AC signal. Often, when this measurement is conducted only at 1 kHz, is called ACIR. This test can provide information about the cell internal resistance, which can increase over time due to aging.

It is known that as a Li-ion cell ages, both electrodes and electrolyte can degrade, leading to significant changes in the internal resistance of the system.

Often researchers[126,163] try to extract information about the phenomena occurring in the cell by fitting the EIS spectra. The most appropriate equivalent circuit for fitting EIS spectra of Li-ion batteries will depend on the specific features of the cell studied, along with experimental conditions.

Usually, among the most used electrical parameters to fit EIS spectra there are[164]:

- **Resistance (R)**: represents electron transfer across an interface.
- **Capacitance (C):** represents (typically but not always) non-faradaic charging at an interface.
- **Constant phase element (CPE)**: often capacitors in EIS experiments do not behave ideally, acting more like a constant phase element. This is described with the use of the exponent α, whose value is between 0.9 and 1.0 ($\alpha = 1$ for ideal capacitors).
- **Warburg (W)**: the diffusion of ions in the electrode can create an impedance called "Warburg impedance". At low frequencies, this phenomenon is predominant, showing a 45° slope diagonal line in the Nyquist plot.

The combination of series and parallel configurations of these electric components can provide quantitative information about the system object of study.

From an operative point of view, experimental parameters are fundamental to be controlled. The electrochemical impedance spectroscopy is strongly influenced by:

- State of charge (SoC);
- Temperature;
- Frequency range: Lower frequencies are more sensitive to the Li ion diffusion, higher frequencies are more sensitive to the electrode-electrolyte interface resistance.

Experimentally, the operator can perform an EIS measurement by choosing potentiostatic EIS (PEIS) and galvanostatic EIS (GEIS) conditions. The choice of technique will depend on the experimental design.

DCIR: theoretical hints

The direct current internal resistance (DCIR) is usually implemented to measure the DC resistance cell behaviour. If with ACIR, the measurement of resistance occurs by applying a signal in alternative current, measuring the voltage response (or vice versa), with DCIR instead, a step of current or pulse is used:

Typically DCIR is measured by applying:

$$V_{beforestep} - V_{afterstep} \Big/ I_{beforestep} - I_{afterstep}$$

Normally, the first measurement (before step) is performed with the cell in pause, at the so-called open circuit voltage (OCV), with I_beforestep = 0. For the second measurement it is then considered to apply a current step which causes a change in current (in charge or in discharge). This operation polarises the cell. The quantification of this polarization is the result of the test, giving back an information in terms of resistance to the applied current at a specific SoC% typically.

Normally, cell internal resistance (DCIR) is measured using a defined current against a time pulse, which is comprised between 1 and 30s, depending on the time constant of the system to be characterized. The internal resistance corresponds to the maximum voltage drop divided by the current demand.

When a current pulse is imposed to a Li ion cell, several phenomena contributing to the voltage drop take place, governed by their respective timescales:

- Pure Ohmic resistance R_0 is the responsible for the first instantaneous voltage drop (it comprises electronic resistances and the bulk electrolyte ionic cell resistance);
- The voltage drop within the first few seconds is related to the cell double layer capacitance (C_{dl}) and charge transfer resistance (R_{ct}), which is attributed to the charge transfer reaction at the electrode/electrolyte interface.
- After the first 2-5 seconds, the quasi-linear voltage drop is attributable to the polarisation resistance (Rp), which is linked to ionic diffusion in the solid phase.

Incremental capacity analysis: theoretical hints

Literature reports Incremental capacity analysis (ICA) as a useful tool to understand phenomena occurring inside the battery cell, even at material level. It consists in the calculation of the derivative dQ/dV, displayed as a function of the cell operative voltage.

When the voltage profile curve (Figure 107) shows a small slope, with a limited increase of the cell potential, a transition phase in one of the electrodes is occurring (i.e., H_1-M, M-H_2 etc.).

Looking at the peaks into a typical ICA plot (Figure 108), we can collect information on the main transition phases during charge and discharge.

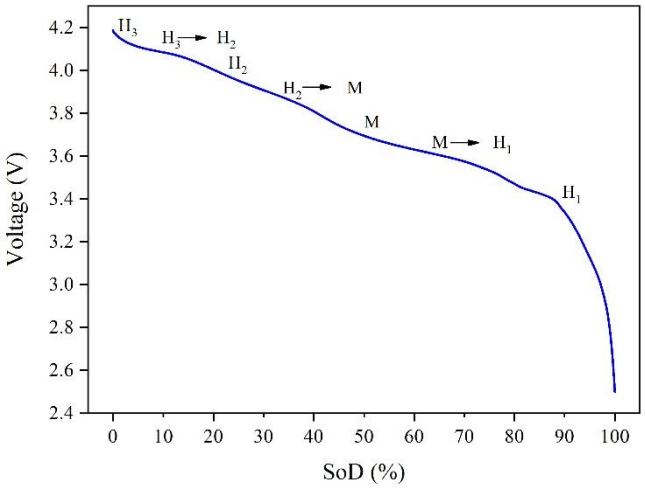

Figure 107 - Voltage vs SoD% curve

From Figure 108 it is possible to notice the first peak around 3.4 V, which indicates the lithiation of the graphite, where the lithium intercalation reaction (C_6 -> LiC_x) occurs.

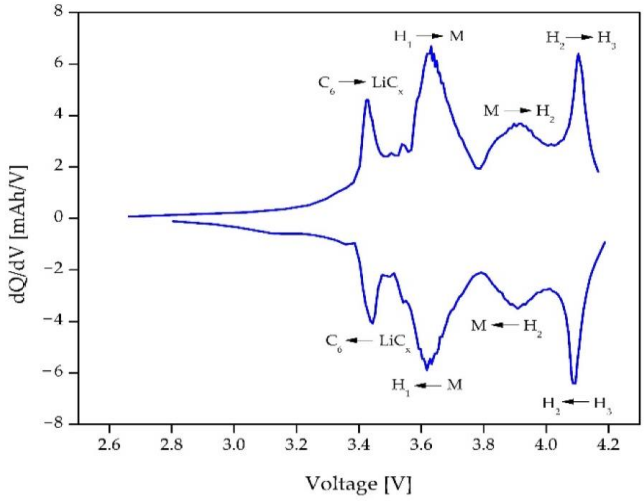

Figure 108 - Incremental capacity analysis curve

Since each single intercalation peak of lithium inside the anode structure is not clearly visible working with full cells, it is necessary to work on single electrodes with half-cell setup, with a Li pseudo-reference electrode, to appreciate all the intercalation phases.

Coming back to full cell analysis, going from 3.6 V to 4.1 V three peaks are present, associated to the phase transitions of the NMC811 structure.

- at 3.6 V: H_1 -> M transition
- at 3.9 V: M -> H_2 transition
- at 4.1 V: H_2 -> H_3 transition

The last two peaks (at 3.9 and 4.1 V) are peculiar of high nickel content (Ni > 80%) NMCs. The first "cathode" transition (3.6 V) indicates the NMC transition from the first hexagonal (H_1) to monoclinic structure (M). The second transition phase (3.9 V) is related to the change from monoclinic (M) to the second hexagonal (H_2) structure. The third transition (4.1 V) is indicative of the second to third hexagonal transition.

As visible in Figure 109, the pristine structure is called H_1. When charging, Li_M (M is indicative of manganese sites) gradually extracts from the material first and finally a Li_M-less H_2 phase forms. In the case of H_3, literature[165] reports two possible crystal structures ($H_{3\text{-}1}$ and $H_{3\text{-}2}$). For $H_{3\text{-}1}$, Li ions tend to be away from Li_N (N is indicative of nickel sites), while for $H_{3\text{-}2}$ a Li re-ordered material is expected.

Literature[166] reports how this transition increases as a symptom for a significant volume contraction, with consequent capacity fade occurrence.

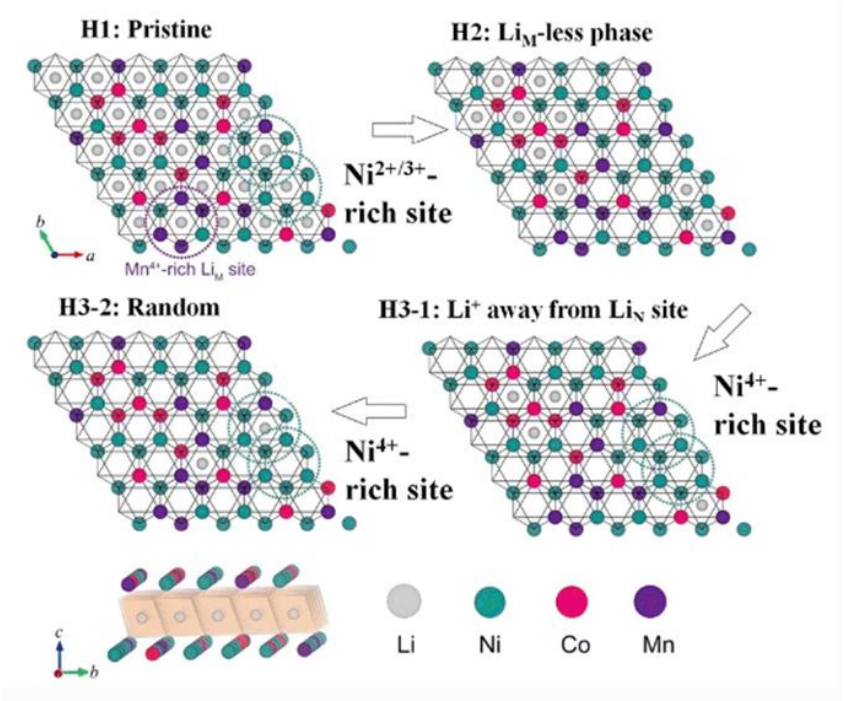

Figure 109 - NMC Transition phases during cycling (Zheng et al. 2019.
Reproduced with permission© 2018 Elsevier B.V. All rights reserved.)

The technique can be potentially applied both for "on board" applications, for instance implementing it in the BMS for continuous check of the battery pack and for ex situ analysis, even at material level. On the other hand, when analysing full Li ion cells there is the risk of peaks overlapping, with hidden contributions coming from anode or cathode side.

Raman spectroscopy: theoretical hints

Raman spectroscopy is a method of non-elastic light scattering when matter is illuminated by monochromatic radiation. The scattered radiation contains new wavelengths (Figure 110).

To perform a Raman spectrum, it is fundamental to have a laser source, as visible in Figure 111, interacting with the sample (gas, liquid, solid-amorphous or crystalline). Once the molecule goes back to the fundamental vibrational state, we have the light scattering (Rayleigh + Raman). The filter between the vibrating molecule and the detector that cut off the Rayleigh scattering only collecting the Raman scattering.

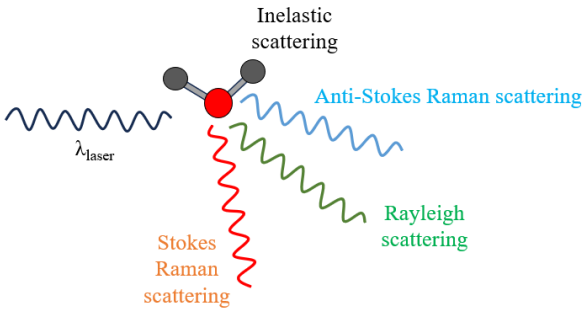

Figure 110 - Radiation - sample interaction

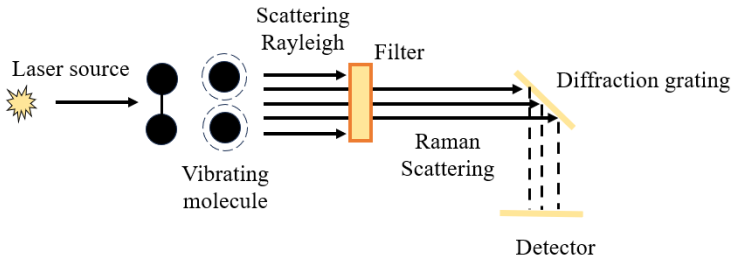

Figure 111 - Raman analysis radiation scheme

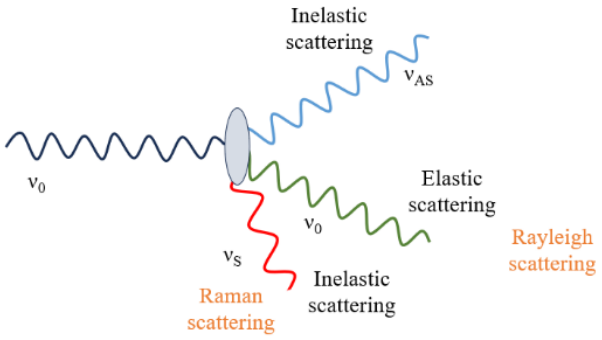

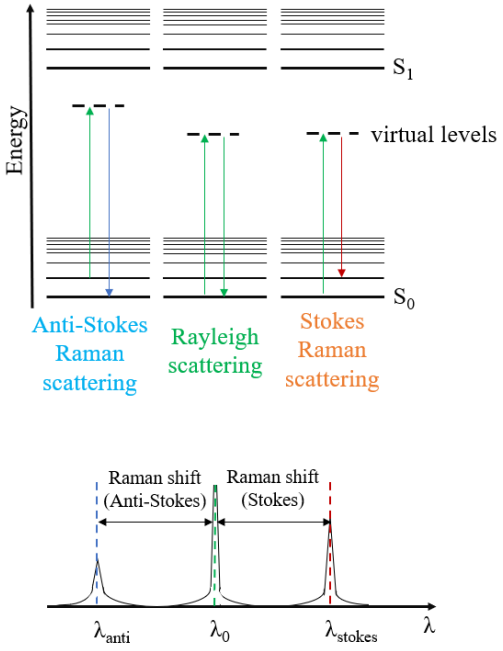

Figure 112 – Energy levels

Going into the energy levels of the vibrating molecule (Figure 112), the initial energy is in a specific frequency and once the molecule absorbs it and then emits it back we can observe the Rayleigh scattering which is exactly at the same energy of the initial one, together with two kind of inelastic scatterings (Raman), the Stokes (at higher wave numbers and the Anti Stokes at lower wave numbers). To get a proper Raman emission a strong laser source is needed, since every 10^7 counts of Rayleigh vibration, just 1 is Raman. As mentioned, the filter cut the very intense frequencies responses, allowing only the Raman signal detection.

The instrument, as visible in Figure 113 is composed by a laser source the generate a beam passing across different mirrors until reaching the sample with a lens to focus the beam. Then,

by backscattering, the Raman portion goes from the source across the holographic filter, towards the detector.

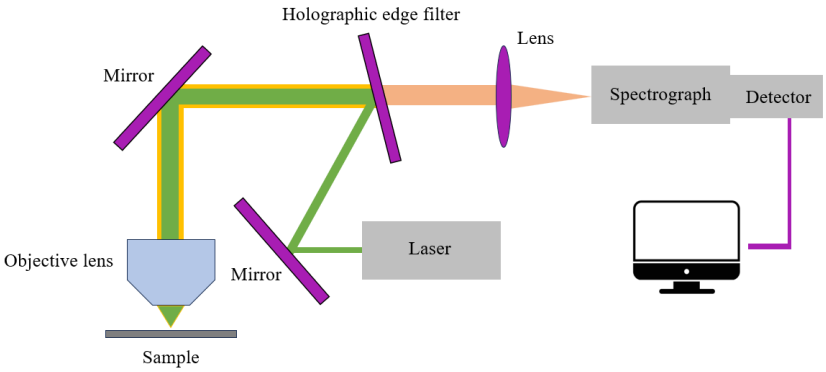

Figure 113 – MicroRaman instrument setup

This technique can provide important structural information, complementary to XRD and microscopy.

When dealing with batteries, Raman spectroscopy can be a valid tool to study structural transformations in electrodes' surface. Because of its high sensitivity to small structural changes, it can provide information about the molecular vibrations and chemical bonding in a sample by a non-destructive approach. It is applicable both for in-situ and ex-situ analysis.

The application of this method is straightforward, with no specific sample preparation requirements.